Distribution Agreement

In presenting this thesis or dissertation as a partial fulfillment of the requirements for an advanced degree from Emory University, I hereby grant to Emory University and its agents the non-exclusive license to archive, make accessible, and display my thesis or dissertation in whole or in part in all forms of media, now or hereafter known, including display on the world wide web. I understand that I may select some access restrictions as part of the online submission of this thesis or dissertation. I retain all ownership rights to the copyright of the thesis or dissertation. I also retain the right to use in future works (such as articles or books) all or part of this thesis or dissertation.

Signature:

_____ _____

Qingyang Zhu Date

Investigating the Association between Air Pollution and Cognitive and Mental Health Outcomes Using Satellite-Driven Exposure Models

By

Qingyang Zhu
Doctor of Philosophy

Environmental Health Sciences

_____

Yang Liu, Ph.D.
Advisor

_____

Howard H. Chang, Ph.D.
Committee Member

_____

Kyle Steenland, Ph.D.
Committee Member

_____

Stefanie Ebelt, Sc.D.
Committee Member

Accepted:

_____

Kimberly Jacob Arriola, Ph.D, MPH
Dean of the James T. Laney School of Graduate Studies

_____

Date

Investigating the Association between Air Pollution and Cognitive and Mental Health Outcomes Using Satellite-Driven Exposure Models

By

Qingyang Zhu

MS, Fudan University, 2019

B.S., Southeast University, 2016

Advisor: Yang Liu, PhD

An abstract of
A dissertation submitted to the Faculty of the
James T. Laney School of Graduate Studies of Emory University
In partial fulfillment of the requirements for the degree of
Doctor of Philosophy in
Environmental Health Sciences
2023

Abstract

Investigating the Association between Air Pollution and Cognitive and Mental Health Outcomes Using Satellite-Driven Exposure Models

By

Qingyang Zhu

Air pollution has been linked to various adverse health outcomes, affecting cardiovascular, respiratory, reproductive, and renal systems. According to the Global Burden of Disease (GBD) study, air pollution was the fourth leading contributor to global attributable deaths for both males and females in 2019. Nevertheless, existing epidemiological studies typically focus on a specific type of air pollutant due to the limited availability of large-scale exposure matrices. Recent advances in satellite remote sensing have provided a promising tool to evaluate the long-term spatiotemporal distribution of air pollution in a large domain.

In this dissertation, we first established a high-performance O_3 prediction model in China using the OMPROFOZ ozone profile. The model considered the two major pathways (i.e., the photochemical reactions between NOx and volatile organic compounds (VOCs) and the stratospheric intrusion) through which ground-level O_3 pollution is produced. Our prediction model achieved a random CV R^2 of 0.87 at a high spatial resolution of 0.05°. The model predictions also agreed well with the TOAR historical ozone monitoring data from 2005-2013.

Combining our ozone model with other satellite-driven exposure datasets, aim 2 of this dissertation examined the association between long-term exposure to air pollution and cognitive impairment among the Chinese elderly population using data from the Chinese Longitudinal Healthy Longevity Survey (CLHLS). We found that annual average exposure to $PM_{2.5}$ and NO_2 were both associated with an increased risk of cognitive impairment. Although the annual average of daily maximum 8-hour average (MDA8) O_3 was not positively associated with cognitive impairment, warm-season (April-September) mean MDA8 O_3 was identified as a significant risk factor.

In addition to anthropogenic emissions, air pollution may also be produced by natural disasters, especially wildfires. Aim 3 of this dissertation evaluated the association between wildfire-related exposures and ED visits for anxiety disorders in the Western US using satellite-driven exposure data. Our results suggested that wildfires are associated with anxiety disorders through two different pathways, i.e., the inhalation of smoke $PM_{2.5}$ and the direct psychological impact of smoke events and active fire points. Furthermore, women and the elderly population are more susceptible to the anxiety disorders associated with wildfires.

Investigating the Association between Air Pollution and Cognitive and Mental Health Outcomes Using Satellite-Driven Exposure Models

By

Qingyang Zhu

MS, Fudan University, 2019

B.S., Southeast University, 2016

Advisor: Yang Liu, PhD

A dissertation submitted to the Faculty of the
James T. Laney School of Graduate Studies of Emory University
In partial fulfillment of the requirements for the degree of
Doctor of Philosophy in
Environmental Health Sciences
2023

Table of Contents

List of Figures

List of Tables

1. Introduction

Exposure to ambient air pollution has been linked to a series of adverse health outcomes, impacting cardiovascular (Lee et al., 2014; Miller & Newby, 2020; Rajagopalan et al., 2018), respiratory (Laeremans et al., 2018; Losacco & Perillo, 2018), nervous (Genc et al., 2012; Kim et al., 2020), reproductive (Selevan et al., 2000; Wu et al., 2016), and renal systems (Afsar et al., 2018; Shubham et al., 2022). According to the global burden of disease (GBD) study 2019, ambient air pollution was the fourth leading risk factor for attributable deaths among both males and females (Murray et al., 2020). An estimated total of 6.67 million deaths, including 2.92 million females and 3.75 males, were attributable to ambient fine particulate matter ($PM_{2.5}$) and O_3 in 2019 (Murray et al., 2020). The global disability-adjusted life-years (DALYs) attributable to ambient $PM_{2.5}$ experienced a significant increase from 3.5 million in 1990 to 4.2 million in 2015 (Cohen et al., 2017). Additionally, O_3 has emerged as a new leading contributor to the global burden of disease that accounted for an extra 254,000 deaths and 4.1 million DALYs from chronic obstructive pulmonary disease in 2015 (Cohen et al., 2017).

The comprehensive health impact of air pollution highlighted the need to study the combined effect of multiple air pollutants. Nevertheless, existing studies typically focused on a specific type of air pollutant (e.g., $PM_{2.5}$, NO_2, or O_3) while neglecting the others. A potential reason for this phenomenon is the limitation in the exposure matrices. There does not exist a 'universal approach' to measure multiple air pollutants simultaneously for large population-based studies. Although a well-established air quality monitoring network would benefit environmental epidemiological studies (Seltzer et al., 2018), its limited availability in developing countries also poses a great challenge to understanding the long-term health impact of air pollution, especially among the underrepresented population.

Satellite-driven technologies have long been used to promote the estimation of ambient air pollution worldwide. For example, the Multi-Angle Implementation of Atmospheric Correction (MAIAC) aerosol optical depth (AOD) data has been used to establish high-resolution $PM_{2.5}$ models in China (Xiao et al., 2020), the United States (Di et al., 2016), and Europe (Schneider et al., 2020; Stafoggia et al., 2019). Unlike $PM_{2.5}$, modeling studies on O_3 are sparse due to the intricate chemical mechanism involved in the production and distribution of this chemical. Although a secondary pollutant per se, ozone naturally exists in multiple vertical layers of the atmosphere. The ozone layer in the stratosphere is known as 'good ozone' because it shields the earth from solar ultraviolet (UV) radiation. On the contrary, 'bad ozone' refers to ground-level ozone pollution that is hazardous to human health (Stenke, 2020). Due to the high abundance of ozone in the stratosphere, current satellite-driven UV-based ozone profiles typically have a higher sensitivity to the stratospheric ozone than to the tropospheric ozone (Huang et al., 2017; Huang et al., 2018). Accordingly, satellite-driven ozone profiles may not be used directly as a proxy of human exposure to ambient ozone pollution. Nevertheless, it may be utilized to establish a prediction model for the spatiotemporal distribution of this air pollutant.

Understanding the mechanisms through which ambient O_3 pollution is produced is vital to construct a high-performance prediction model. The overwhelming majority of surface-level O_3 pollution arises from a set of complex photochemical reactions between volatile organic compounds (VOCs) and nitrogen oxides (NOx) in the presence of heat and solar radiation (Li et al., 2020; Pu et al., 2017). In addition to the aforementioned O_3 precursors, the NOx-to-VOCs ratio also influences the production dynamics of O_3. Specifically, the VOC-limited regime occurs when the abundance of NOx exceeds the abundance of VOCs. Under such a circumstance, reducing the emissions of VOCs is more effective in controlling O_3 pollution. On the contrary, in

the NOx-limited regime, where VOCs greatly exceed NOx, greater focus should be placed on reducing NOx emissions (Ren et al., 2022).

Tropospheric ozone concentrations are primarily influenced by photochemical reactions (Lelieveld & Dentener, 2000; Monks, 2005). However, under certain conditions, stratospheric ozone-rich air can quickly penetrate the lower troposphere, leading to a significant rise in ground-level ozone pollution (Knowland et al., 2017). This phenomenon, known as stratospheric intrusions (SI), typically reaches its peak in the northern hemisphere during spring, particularly in high-altitude regions (Appenzeller et al., 1996; Itahashi et al., 2020; Lin et al., 2012; Lu et al., 2019; Y. Wang et al., 2020). Both mechanisms need to be accounted for to establish a high-performance prediction model for ambient O_3 pollution.

Cognitive impairment and dementia have been major threats to global health. It is estimated that 40-50 million people were living with dementia in 2019 (Nichols et al., 2019). Previous studies have suggested the link between air pollution and cognitive impairment in China using the air pollution index (API) (Zhang et al., 2018). Nevertheless, API is a pooled index for ambient air quality and cannot be used to quantify the risk attributable to a specific air pollutant. A handful of studies have reported the association between $PM_{2.5}$ and cognitive disorders. For example, Shi et al. reported that a five $\mu g/m^3$ increase in annual $PM_{2.5}$ concentrations was associated with first-time hospital admission for Parkinson's disease (HR = 1.13; 95% CI: 1.12-1.14) and Alzheimer's disease (HR =1.13; 95% CI: 1.12-1.14) in the American Medicare population (L. Shi et al., 2020). Wang et al. found that per 10 $\mu g/m^3$ increase in $PM_{2.5}$ was associated with a 5.1% increased risk of poor cognitive function in China (J. Wang et al., 2020). Similarly, previous literature has found that ambient nitrogen dioxide (NO_2) is a potential risk factor for

vascular dementia (Li & Xin, 2013). However, evidence on the association between O_3 and cognitive disorders is still sparse and inconclusive (Zhao et al., 2018).

In addition to anthropogenic air pollution, natural disasters, especially wildfires, are also significantly associated with worsened air quality (O'Dell et al., 2019). Over the past two decades, the consequences of climate change have substantially increased global wildfire potential (Ellis et al., 2022), leading to expanded burned areas and prolonged fire seasons (Jolly et al., 2015; Richardson et al., 2022). Due to the frequent occurrence of fire weather conditions, droughts, and the abundance of fuel resources, the Western US has been identified as a major fire-prone region (Gannon & Steinberg, 2021; Jones et al., 2022; Zhang et al., 2020). The widespread prevalence of wildfires in the Western US has prompted a marked increase in smoke emissions. It has been estimated that, in recent years, wildfire smoke accounted for around 40% of the total $PM_{2.5}$ across the whole Western US and even 50% in the Northwestern region, escalated substantially from the 15-20% contribution in the early 2000s (Burke et al., 2021).

Mental health disorders, including anxiety disorders, have been another growing threat to global public health in the past decades. According to the GBD study, anxiety disorders were the most prevalent mental health condition that affected 970.1 per million individuals in 2019 (GBD Collaborators, 2022). Regions with high socio-demographic indices, including Western Europe, Australia, and high-income North America, exhibited the highest age-standardized incidence rates of anxiety disorders (Yang et al., 2021). It has been estimated that living with anxiety is associated with a 2.17-fold increase in personal healthcare expenses, contributing to an average 2.08% increase in healthcare costs at the population level (Konnopka & König, 2020).

The high-prevalence of both wildfires and anxiety disorders in the Western US has highlighted the need to investigate the mental health impacts of wildfires. However, current studies typically

focus on the impact of a specific mega-fire event, such as the Fort McMurray wildfire in 2016, on a small group of nearby residents. The absence of evidence from large population studies has hindered the potential to establish the causal relationship between wildfires and anxiety disorders. Additionally, the mechanisms through which wildfires are associated with anxiety disorders are still unclear. Although previous studies have identified ambient $PM_{2.5}$ as a potential risk factor for anxiety disorders in the US (Power et al., 2015; Pun et al., 2017), China (W. Shi et al., 2020; Zhao et al., 2022), and the UK (Hao et al., 2022), evidence about wildfire smoke exposure remains inconclusive (Eisenman & Galway, 2022). Furthermore, some case studies suggest that wildfires have a direct psychological impact on the nearby population (Agyapong et al., 2018), but the magnitude of this association remains unclear. There is an urgent need of large population studies to explore the association between wildfire-related exposures and anxiety disorders through all potential pathways.

Accordingly, this study aimed to establish a high-resolution model to predict the long-term ground-level ozone concentrations in China and use the model predictions to investigate the long-term cognitive health impact of ozone with a multi-pollutant approach. Furthermore, we also examined whether wildfire-related exposures are associated with anxiety disorders in the Western United States. Specifically,

Aim 1: Establish a high-resolution model to predict the long-term spatiotemporal distribution of ground-level ozone pollution in China. We used a satellite-driven ozone profile to provide direct information on surface-level ozone concentrations. Meteorological factors, land-use information, digital population, and elevation were also utilized to improve the model performance. The prediction model comprised two independent random forest models. Specifically, the first model aimed to impute the missing values of the ozone profile, and the second one was used to predict

the spatiotemporal distribution of ozone in China. The ozone model had a spatial resolution of 0.05 ° and covered the period of 2005-2019.

Aim 2: Investigate the association between long-term exposure to air pollution and cognitive impairment among the elderly population. We used the Chinese Longitudinal Healthy Longevity Survey (CLHLS) database to study the long-term health impact of air pollution on the Chinese elderly population. A localized Mini-Mental Statement Examination (MMSE) scale was used to measure cognitive function. $PM_{2.5}$ and NO_2 concentrations in China were obtained from previous satellite-driven models that cover the period of 2005-2018.

Aim 3: Examine the association between wildfire-related exposures and ED visits for anxiety disorders in the Western United States. The exposures of interest included: 1) wildfire smoke $PM_{2.5}$, wildfire smoke events (defined as wildfire smoke $PM_{2.5}$ contributed to ≥ 25% of the total $PM_{2.5}$), major wildfire smoke events (defined as wildfire smoke $PM_{2.5}$ contributed to ≥ 75% of the total $PM_{2.5}$), 4) the number of active wildfire points, and 5) the cumulative fire radiative power (FRP) of all the active wildfire points. We also explored whether the association between wildfire-related exposures varied across different sex, ethnicity, and age groups.

1.1. References

Afsar, B., Elsurer Afsar, R., Kanbay, A., Covic, A., Ortiz, A., & Kanbay, M. (2018). Air pollution and kidney disease: review of current evidence. Clinical Kidney Journal, 12(1), 19-32. https://doi.org/10.1093/ckj/sfy111.

Agyapong, V. I. O., Hrabok, M., Juhas, M., Omeje, J., Denga, E., Nwaka, B., Akinjise, I., Corbett, S. E., Moosavi, S., Brown, M., Chue, P., Greenshaw, A. J., & Li, X. M. (2018). Prevalence Rates and Predictors of Generalized Anxiety Disorder Symptoms in Residents of Fort McMurray Six Months After a Wildfire. Front Psychiatry, 9, 345. https://doi.org/10.3389/fpsyt.2018.00345

Appenzeller, C., Holton, J. R., & Rosenlof, K. H. (1996). Seasonal variation of mass transport across the tropopause. Journal of Geophysical Research: Atmospheres, 101(D10), 15071-15078. https://doi.org/https://doi.org/10.1029/96JD00821

Burke, M., Driscoll, A., Heft-Neal, S., Xue, J., Burney, J., & Wara, M. (2021). The changing risk and burden of wildfire in the United States. Proceedings of the National Academy of Sciences, 118(2), e2011048118. https://doi.org/10.1073/pnas.2011048118

Cohen, A. J., Brauer, M., Burnett, R., Anderson, H. R., Frostad, J., Estep, K., Balakrishnan, K., Brunekreef, B., Dandona, L., Dandona, R., Feigin, V., Freedman, G., Hubbell, B., Jobling, A., Kan, H., Knibbs, L., Liu, Y., Martin, R., Morawska, L., Pope, C. A., III, Shin, H., Straif, K., Shaddick, G., Thomas, M., van Dingenen, R., van Donkelaar, A., Vos, T., Murray, C. J. L., & Forouzanfar, M. H. (2017). Estimates and 25-year trends of the global burden of disease attributable to ambient air pollution: an analysis of data from the Global Burden of Diseases Study 2015. The Lancet, 389(10082), 1907-1918. https://doi.org/10.1016/S0140-6736(17)30505-6

Collaborators, G. M. D. (2022). Global, regional, and national burden of 12 mental disorders in 204 countries and territories, 1990-2019: a systematic analysis for the Global Burden of Disease Study 2019. The Lancet Psychiatry, 9(2), 137-150. https://doi.org/10.1016/S2215-0366(21)00395-3

Di, Q., Kloog, I., Koutrakis, P., Lyapustin, A., Wang, Y., & Schwartz, J. (2016). Assessing PM2.5 Exposures with High Spatiotemporal Resolution across the Continental United States. Environmental Science & Technology, 50(9), 4712-4721. https://doi.org/10.1021/acs.est.5b06121

Eisenman, D. P., & Galway, L. P. (2022). The mental health and well-being effects of wildfire smoke: a scoping review. BMC Public Health, 22(1), 2274. https://doi.org/10.1186/s12889-022-14662-z

Ellis, T. M., Bowman, D. M. J. S., Jain, P., Flannigan, M. D., & Williamson, G. J. (2022). Global increase in wildfire risk due to climate-driven declines in fuel moisture [https://doi.org/10.1111/gcb.16006]. Global Change Biology, 28(4), 1544-1559. https://doi.org/https://doi.org/10.1111/gcb.16006

Gannon, C. S., & Steinberg, N. C. (2021). A global assessment of wildfire potential under climate change utilizing Keetch-Byram drought index and land cover classifications. Environmental Research Communications, 3(3), 035002. https://doi.org/10.1088/2515-7620/abd836

Genc, S., Zadeoglulari, Z., Fuss, S. H., & Genc, K. (2012). The Adverse Effects of Air Pollution on the Nervous System. Journal of Toxicology, 2012, 782462. https://doi.org/10.1155/2012/782462

Hao, G., Zuo, L., Xiong, P., Chen, L., Liang, X., & Jing, C. (2022). Associations of PM2.5 and road traffic noise with mental health: Evidence from UK Biobank. Environmental Research, 207, 112221. https://doi.org/https://doi.org/10.1016/j.envres.2021.112221

Huang, G., Liu, X., Chance, K., Yang, K., Bhartia, P. K., Cai, Z., Allaart, M., Ancellet, G., Calpini, B., Coetzee, G. J. R., Cuevas-Agulló, E., Cupeiro, M., De Backer, H., Dubey, M. K., Fuelberg, H. E., Fujiwara, M., Godin-Beekmann, S., Hall, T. J., Johnson, B., Joseph, E., Kivi, R., Kois, B., Komala, N., König-Langlo, G., Laneve, G., Leblanc, T., Marchand, M., Minschwaner, K. R., Morris, G., Newchurch, M. J., Ogino, S. Y., Ohkawara, N., Piters, A. J. M., Posny, F., Querel, R., Scheele, R., Schmidlin, F. J., Schnell, R. C., Schrems, O., Selkirk, H., Shiotani, M., Skrivánková, P., Stübi, R., Taha, G., Tarasick, D. W., Thompson, A. M., Thouret, V., Tully, M. B., Van Malderen, R., Vömel, H., von der Gathen, P., Witte, J. C., & Yela, M. (2017). Validation of 10-year SAO OMI Ozone

Profile (PROFOZ) product using ozonesonde observations. Atmos. Meas. Tech., 10(7), 2455-2475. https://doi.org/10.5194/amt-10-2455-2017
Huang, G., Liu, X., Chance, K., Yang, K., & Cai, Z. (2018). Validation of 10-year SAO OMI ozone profile (PROFOZ) product using Aura MLS measurements. Atmos. Meas. Tech., 11(1), 17-32. https://doi.org/10.5194/amt-11-17-2018
Itahashi, S., Mathur, R., Hogrefe, C., & Zhang, Y. (2020). Modeling stratospheric intrusion and trans-Pacific transport on tropospheric ozone using hemispheric CMAQ during April 2010 – Part 1: Model evaluation and air mass characterization for stratosphere–troposphere transport. Atmos. Chem. Phys., 20(6), 3373-3396. https://doi.org/10.5194/acp-20-3373-2020
Jolly, W. M., Cochrane, M. A., Freeborn, P. H., Holden, Z. A., Brown, T. J., Williamson, G. J., & Bowman, D. M. J. S. (2015). Climate-induced variations in global wildfire danger from 1979 to 2013. Nature Communications, 6(1), 7537. https://doi.org/10.1038/ncomms8537
Jones, M. W., Abatzoglou, J. T., Veraverbeke, S., Andela, N., Lasslop, G., Forkel, M., Smith, A. J. P., Burton, C., Betts, R. A., van der Werf, G. R., Sitch, S., Canadell, J. G., Santín, C., Kolden, C., Doerr, S. H., & Le Quéré, C. (2022). Global and Regional Trends and Drivers of Fire Under Climate Change [https://doi.org/10.1029/2020RG000726]. Reviews of Geophysics, 60(3), e2020RG000726. https://doi.org/https://doi.org/10.1029/2020RG000726
Kim, H., Kim, W.-H., Kim, Y.-Y., & Park, H.-Y. (2020). Air Pollution and Central Nervous System Disease: A Review of the Impact of Fine Particulate Matter on Neurological Disorders [Review]. Frontiers in Public Health, 8. https://doi.org/10.3389/fpubh.2020.575330
Knowland, K. E., Ott, L. E., Duncan, B. N., & Wargan, K. (2017). Stratospheric Intrusion-Influenced Ozone Air Quality Exceedances Investigated in the NASA MERRA-2 Reanalysis. Geophysical Research Letters, 44(20), 10,691-610,701. https://doi.org/10.1002/2017gl074532
Konnopka, A., & König, H. (2020). Economic Burden of Anxiety Disorders: A Systematic Review and Meta-Analysis. PharmacoEconomics, 38(1), 25-37. https://doi.org/10.1007/s40273-019-00849-7
Laeremans, M., Dons, E., Avila-Palencia, I., Carrasco-Turigas, G., Orjuela, J. P., Anaya, E., Cole-Hunter, T., de Nazelle, A., Nieuwenhuijsen, M., Standaert, A., Van Poppel, M., De Boever, P., & Int Panis, L. (2018). Short-term effects of physical activity, air pollution and their interaction on the cardiovascular and respiratory system. Environment International, 117, 82-90. https://doi.org/https://doi.org/10.1016/j.envint.2018.04.040
Lee, B.-J., Kim, B., & Lee, K. (2014). Air pollution exposure and cardiovascular disease. Toxicological research, 30(2), 71-75. https://doi.org/10.5487/TR.2014.30.2.071
Lelieveld, J., & Dentener, F. J. (2000). What controls tropospheric ozone? Journal of Geophysical Research: Atmospheres, 105(D3), 3531-3551. https://doi.org/https://doi.org/10.1029/1999JD901011
Li, H., & Xin, X. (2013). Nitrogen dioxide (NO2) pollution as a potential risk factor for developing vascular dementia and its synaptic mechanisms. Chemosphere, 92(1), 52-58. https://doi.org/https://doi.org/10.1016/j.chemosphere.2013.02.061

Li, K., Jacob, D. J., Shen, L., Lu, X., De Smedt, I., & Liao, H. (2020). Increases in surface ozone pollution in China from 2013 to 2019: anthropogenic and meteorological influences. Atmos. Chem. Phys., 20(19), 11423-11433. https://doi.org/10.5194/acp-20-11423-2020

Lin, M., Fiore, A. M., Cooper, O. R., Horowitz, L. W., Langford, A. O., Levy II, H., Johnson, B. J., Naik, V., Oltmans, S. J., & Senff, C. J. (2012). Springtime high surface ozone events over the western United States: Quantifying the role of stratospheric intrusions. Journal of Geophysical Research: Atmospheres, 117(D21). https://doi.org/https://doi.org/10.1029/2012JD018151

Losacco, C., & Perillo, A. (2018). Particulate matter air pollution and respiratory impact on humans and animals. Environmental Science and Pollution Research, 25(34), 33901-33910. https://doi.org/10.1007/s11356-018-3344-9

Lu, X., Zhang, L., Chen, Y., Zhou, M., Zheng, B., Li, K., Liu, Y., Lin, J., Fu, T. M., & Zhang, Q. (2019). Exploring 2016–2017 surface ozone pollution over China: source contributions and meteorological influences. Atmos. Chem. Phys., 19(12), 8339-8361. https://doi.org/10.5194/acp-19-8339-2019

Miller, M. R., & Newby, D. E. (2020). Air pollution and cardiovascular disease: car sick. Cardiovascular Research, 116(2), 279-294. https://doi.org/10.1093/cvr/cvz228

Monks, P. S. (2005). Gas-phase radical chemistry in the troposphere [10.1039/B307982C]. Chemical Society Reviews, 34(5), 376-395. https://doi.org/10.1039/B307982C

Murray, C. J. L., Aravkin, A. Y., Zheng, P., Abbafati, C., Abbas, K. M., Abbasi-Kangevari, M., Abd-Allah, F., Abdelalim, A., Abdollahi, M., Abdollahpour, I., Abegaz, K. H., Abolhassani, H., Aboyans, V., Abreu, L. G., Abrigo, M. R. M., Abualhasan, A., Abu-Raddad, L. J., Abushouk, A. I., Adabi, M., Adekanmbi, V., Adeoye, A. M., Adetokunboh, O. O., Adham, D., Advani, S. M., Agarwal, G., Aghamir, S. M. K., Agrawal, A., Ahmad, T., Ahmadi, K., Ahmadi, M., Ahmadieh, H., Ahmed, M. B., Akalu, T. Y., Akinyemi, R. O., Akinyemiju, T., Akombi, B., Akunna, C. J., Alahdab, F., Al-Aly, Z., Alam, K., Alam, S., Alam, T., Alanezi, F. M., Alanzi, T. M., Alemu, B. w., Alhabib, K. F., Ali, M., Ali, S., Alicandro, G., Alinia, C., Alipour, V., Alizade, H., Aljunid, S. M., Alla, F., Allebeck, P., Almasi-Hashiani, A., Al-Mekhlafi, H. M., Alonso, J., Altirkawi, K. A., Amini-Rarani, M., Amiri, F., Amugsi, D. A., Ancuceanu, R., Anderlini, D., Anderson, J. A., Andrei, C. L., Andrei, T., Angus, C., Anjomshoa, M., Ansari, F., Ansari-Moghaddam, A., Antonazzo, I. C., Antonio, C. A. T., Antony, C. M., Antriyandarti, E., Anvari, D., Anwer, R., Appiah, S. C. Y., Arabloo, J., Arab-Zozani, M., Ariani, F., Armoon, B., Ärnlöv, J., Arzani, A., Asadi-Aliabadi, M., Asadi-Pooya, A. A., Ashbaugh, C., Assmus, M., Atafar, Z., Atnafu, D. D., Atout, M. M. d. W., Ausloos, F., Ausloos, M., Ayala Quintanilla, B. P., Ayano, G., Ayanore, M. A., Azari, S., Azarian, G., Azene, Z. N., Badawi, A., Badiye, A. D., Bahrami, M. A., Bakhshaei, M. H., Bakhtiari, A., Bakkannavar, S. M., Baldasseroni, A., Ball, K., Ballew, S. H., Balzi, D., Banach, M., Banerjee, S. K., Bante, A. B., Baraki, A. G., Barker-Collo, S. L., Bärnighausen, T. W., Barrero, L. H., Barthelemy, C. M., Barua, L., Basu, S., Baune, B. T., Bayati, M., Becker, J. S., Bedi, N., Beghi, E., Béjot, Y., Bell, M. L., Bennitt, F. B., Bensenor, I. M., Berhe, K., Berman, A. E., Bhagavathula, A. S., Bhageerathy, R., Bhala, N., Bhandari, D., Bhattacharyya, K., Bhutta, Z. A., Bijani, A., Bikbov, B., Bin Sayeed, M. S., Biondi, A., Birihane, B. M., Bisignano, C., Biswas, R. K., Bitew, H., Bohlouli, S., Bohluli, M., Boon-Dooley, A. S., Borges, G., Borzì, A. M., Borzouei, S., Bosetti, C., Boufous, S., Braithwaite, D., Breitborde, N. J. K., Breitner, S., Brenner, H., Briant, P. S., Briko, A. N.,

Briko, N. I., Britton, G. B., Bryazka, D., Bumgarner, B. R., Burkart, K., Burnett, R. T., Burugina Nagaraja, S., Butt, Z. A., Caetano dos Santos, F. L., Cahill, L. E., Cámera, L. L. A. A., Campos-Nonato, I. R., Cárdenas, R., Carreras, G., Carrero, J. J., Carvalho, F., Castaldelli-Maia, J. M., Castañeda-Orjuela, C. A., Castelpietra, G., Castro, F., Causey, K., Cederroth, C. R., Cercy, K. M., Cerin, E., Chandan, J. S., Chang, K.-L., Charlson, F. J., Chattu, V. K., Chaturvedi, S., Cherbuin, N., Chimed-Ochir, O., Cho, D. Y., Choi, J.-Y. J., Christensen, H., Chu, D.-T., Chung, M. T., Chung, S.-C., Cicuttini, F. M., Ciobanu, L. G., Cirillo, M., Classen, T. K. D., Cohen, A. J., Compton, K., Cooper, O. R., Costa, V. M., Cousin, E., Cowden, R. G., Cross, D. H., Cruz, J. A., Dahlawi, S. M. A., Damasceno, A. A. M., Damiani, G., Dandona, L., Dandona, R., Dangel, W. J., Danielsson, A.-K., Dargan, P. I., Darwesh, A. M., Daryani, A., Das, J. K., Das Gupta, R., das Neves, J., Dávila-Cervantes, C. A., Davitoiu, D. V., De Leo, D., Degenhardt, L., DeLang, M., Dellavalle, R. P., Demeke, F. M., Demoz, G. T., Demsie, D. G., Denova-Gutiérrez, E., Dervenis, N., Dhungana, G. P., Dianatinasab, M., Dias da Silva, D., Diaz, D., Dibaji Forooshani, Z. S., Djalalinia, S., Do, H. T., Dokova, K., Dorostkar, F., Doshmangir, L., Driscoll, T. R., Duncan, B. B., Duraes, A. R., Eagan, A. W., Edvardsson, D., El Nahas, N., El Sayed, I., El Tantawi, M., Elbarazi, I., Elgendy, I. Y., El-Jaafary, S. I., Elyazar, I. R. F., Emmons-Bell, S., Erskine, H. E., Eskandarieh, S., Esmaeilnejad, S., Esteghamati, A., Estep, K., Etemadi, A., Etisso, A. E., Fanzo, J., Farahmand, M., Fareed, M., Faridnia, R., Farioli, A., Faro, A., Faruque, M., Farzadfar, F., Fattahi, N., Fazlzadeh, M., Feigin, V. L., Feldman, R., Fereshtehnejad, S.-M., Fernandes, E., Ferrara, G., Ferrari, A. J., Ferreira, M. L., Filip, I., Fischer, F., Fisher, J. L., Flor, L. S., Foigt, N. A., Folayan, M. O., Fomenkov, A. A., Force, L. M., Foroutan, M., Franklin, R. C., Freitas, M., Fu, W., Fukumoto, T., Furtado, J. M., Gad, M. M., Gakidou, E., Gallus, S., Garcia-Basteiro, A. L., Gardner, W. M., Geberemariyam, B. S., Gebreslassie, A. A. A. A., Geremew, A., Gershberg Hayoon, A., Gething, P. W., Ghadimi, M., Ghadiri, K., Ghaffarifar, F., Ghafourifard, M., Ghamari, F., Ghashghaee, A., Ghiasvand, H., Ghith, N., Gholamian, A., Ghosh, R., Gill, P. S., Ginindza, T. G. G., Giussani, G., Gnedovskaya, E. V., Goharinezhad, S., Gopalani, S. V., Gorini, G., Goudarzi, H., Goulart, A. C., Greaves, F., Grivna, M., Grosso, G., Gubari, M. I. M., Gugnani, H. C., Guimarães, R. A., Guled, R. A., Guo, G., Guo, Y., Gupta, R., Gupta, T., Haddock, B., Hafezi-Nejad, N., Hafiz, A., Haj-Mirzaian, A., Haj-Mirzaian, A., Hall, B. J., Halvaei, I., Hamadeh, R. R., Hamidi, S., Hammer, M. S., Hankey, G. J., Haririan, H., Haro, J. M., Hasaballah, A. I., Hasan, M. M., Hasanpoor, E., Hashi, A., Hassanipour, S., Hassankhani, H., Havmoeller, R. J., Hay, S. I., Hayat, K., Heidari, G., Heidari-Soureshjani, R., Henrikson, H. J., Herbert, M. E., Herteliu, C., Heydarpour, F., Hird, T. R., Hoek, H. W., Holla, R., Hoogar, P., Hosgood, H. D., Hossain, N., Hosseini, M., Hosseinzadeh, M., Hostiuc, M., Hostiuc, S., Househ, M., Hsairi, M., Hsieh, V. C.-r., Hu, G., Hu, K., Huda, T. M., Humayun, A., Huynh, C. K., Hwang, B.-F., Iannucci, V. C., Ibitoye, S. E., Ikeda, N., Ikuta, K. S., Ilesanmi, O. S., Ilic, I. M., Ilic, M. D., Inbaraj, L. R., Ippolito, H., Iqbal, U., Irvani, S. S. N., Irvine, C. M. S., Islam, M. M., Islam, S. M. S., Iso, H., Ivers, R. Q., Iwu, C. C. D., Iwu, C. J., Iyamu, I. O., Jaafari, J., Jacobsen, K. H., Jafari, H., Jafarinia, M., Jahani, M. A., Jakovljevic, M., Jalilian, F., James, S. L., Janjani, H., Javaheri, T., Javidnia, J., Jeemon, P., Jenabi, E., Jha, R. P., Jha, V., Ji, J. S., Johansson, L., John, O., John-Akinola, Y. O., Johnson, C. O., Jonas, J. B., Joukar, F., Jozwiak, J. J., Jürisson, M., Kabir, A., Kabir, Z., Kalani, H., Kalani, R., Kalankesh, L. R., Kalhor, R., Kanchan, T., Kapoor, N., Karami Matin, B.,

Karch, A., Karim, M. A., Kassa, G. M., Katikireddi, S. V., Kayode, G. A., Kazemi Karyani, A., Keiyoro, P. N., Keller, C., Kemmer, L., Kendrick, P. J., Khalid, N., Khammarnia, M., Khan, E. A., Khan, M., Khatab, K., Khater, M. M., Khatib, M. N., Khayamzadeh, M., Khazaei, S., Kieling, C., Kim, Y. J., Kimokoti, R. W., Kisa, A., Kisa, S., Kivimäki, M., Knibbs, L. D., Knudsen, A. K. S., Kocarnik, J. M., Kochhar, S., Kopec, J. A., Korshunov, V. A., Koul, P. A., Koyanagi, A., Kraemer, M. U. G., Krishan, K., Krohn, K. J., Kromhout, H., Kuate Defo, B., Kumar, G. A., Kumar, V., Kurmi, O. P., Kusuma, D., La Vecchia, C., Lacey, B., Lal, D. K., Lalloo, R., Lallukka, T., Lami, F. H., Landires, I., Lang, J. J., Langan, S. M., Larsson, A. O., Lasrado, S., Lauriola, P., Lazarus, J. V., Lee, P. H., Lee, S. W. H., LeGrand, K. E., Leigh, J., Leonardi, M., Lescinsky, H., Leung, J., Levi, M., Li, S., Lim, L.-L., Linn, S., Liu, S., Liu, S., Liu, Y., Lo, J., Lopez, A. D., Lopez, J. C. F., Lopukhov, P. D., Lorkowski, S., Lotufo, P. A., Lu, A., Lugo, A., Maddison, E. R., Mahasha, P. W., Mahdavi, M. M., Mahmoudi, M., Majeed, A., Maleki, A., Maleki, S., Malekzadeh, R., Malta, D. C., Mamun, A. A., Manda, A. L., Manguerra, H., Mansour-Ghanaei, F., Mansouri, B., Mansournia, M. A., Mantilla Herrera, A. M., Maravilla, J. C., Marks, A., Martin, R. V., Martini, S., Martins-Melo, F. R., Masaka, A., Masoumi, S. Z., Mathur, M. R., Matsushita, K., Maulik, P. K., McAlinden, C., McGrath, J. J., McKee, M., Mehndiratta, M. M., Mehri, F., Mehta, K. M., Memish, Z. A., Mendoza, W., Menezes, R. G., Mengesha, E. W., Mereke, A., Mereta, S. T., Meretoja, A., Meretoja, T. J., Mestrovic, T., Miazgowski, B., Miazgowski, T., Michalek, I. M., Miller, T. R., Mills, E. J., Mini, G. K., Miri, M., Mirica, A., Mirrakhimov, E. M., Mirzaei, H., Mirzaei, M., Mirzaei, R., Mirzaei-Alavijeh, M., Misganaw, A. T., Mithra, P., Moazen, B., Mohammad, D. K., Mohammad, Y., Mohammad Gholi Mezerji, N., Mohammadian-Hafshejani, A., Mohammadifard, N., Mohammadpourhodki, R., Mohammed, A. S., Mohammed, H., Mohammed, J. A., Mohammed, S., Mokdad, A. H., Molokhia, M., Monasta, L., Mooney, M. D., Moradi, G., Moradi, M., Moradi-Lakeh, M., Moradzadeh, R., Moraga, P., Morawska, L., Morgado-da-Costa, J., Morrison, S. D., Mosapour, A., Mosser, J. F., Mouodi, S., Mousavi, S. M., Mousavi Khaneghah, A., Mueller, U. O., Mukhopadhyay, S., Mullany, E. C., Musa, K. I., Muthupandian, S., Nabhan, A. F., Naderi, M., Nagarajan, A. J., Nagel, G., Naghavi, M., Naghshtabrizi, B., Naimzada, M. D., Najafi, F., Nangia, V., Nansseu, J. R., Naserbakht, M., Nayak, V. C., Negoi, I., Ngunjiri, J. W., Nguyen, C. T., Nguyen, H. L. T., Nguyen, M., Nigatu, Y. T., Nikbakhsh, R., Nixon, M. R., Nnaji, C. A., Nomura, S., Norrving, B., Noubiap, J. J., Nowak, C., Nunez-Samudio, V., Oţoiu, A., Oancea, B., Odell, C. M., Ogbo, F. A., Oh, I.-H., Okunga, E. W., Oladnabi, M., Olagunju, A. T., Olusanya, B. O., Olusanya, J. O., Omer, M. O., Ong, K. L., Onwujekwe, O. E., Orpana, H. M., Ortiz, A., Osarenotor, O., Osei, F. B., Ostroff, S. M., Otstavnov, N., Otstavnov, S. S., Øverland, S., Owolabi, M. O., P A, M., Padubidri, J. R., Palladino, R., Panda-Jonas, S., Pandey, A., Parry, C. D. H., Pasovic, M., Pasupula, D. K., Patel, S. K., Pathak, M., Patten, S. B., Patton, G. C., Pazoki Toroudi, H., Peden, A. E., Pennini, A., Pepito, V. C. F., Peprah, E. K., Pereira, D. M., Pesudovs, K., Pham, H. Q., Phillips, M. R., Piccinelli, C., Pilz, T. M., Piradov, M. A., Pirsaheb, M., Plass, D., Polinder, S., Polkinghorne, K. R., Pond, C. D., Postma, M. J., Pourjafar, H., Pourmalek, F., Poznańska, A., Prada, S. I., Prakash, V., Pribadi, D. R. A., Pupillo, E., Quazi Syed, Z., Rabiee, M., Rabiee, N., Radfar, A., Rafiee, A., Raggi, A., Rahman, M. A., Rajabpour-Sanati, A., Rajati, F., Rakovac, I., Ram, P., Ramezanzadeh, K., Ranabhat, C. L., Rao, P. C., Rao, S. J., Rashedi, V., Rathi, P., Rawaf, D. L., Rawaf,

S., Rawal, L., Rawassizadeh, R., Rawat, R., Razo, C., Redford, S. B., Reiner, R. C., Jr., Reitsma, M. B., Remuzzi, G., Renjith, V., Renzaho, A. M. N., Resnikoff, S., Rezaei, N., Rezaei, N., Rezapour, A., Rhinehart, P.-A., Riahi, S. M., Ribeiro, D. C., Ribeiro, D., Rickard, J., Rivera, J. A., Roberts, N. L. S., Rodríguez-Ramírez, S., Roever, L., Ronfani, L., Room, R., Roshandel, G., Roth, G. A., Rothenbacher, D., Rubagotti, E., Rwegerera, G. M., Sabour, S., Sachdev, P. S., Saddik, B., Sadeghi, E., Sadeghi, M., Saeedi, R., Saeedi Moghaddam, S., Safari, Y., Safi, S., Safiri, S., Sagar, R., Sahebkar, A., Sajadi, S. M., Salam, N., Salamati, P., Salem, H., Salem, M. R. R., Salimzadeh, H., Salman, O. M., Salomon, J. A., Samad, Z., Samadi Kafil, H., Sambala, E. Z., Samy, A. M., Sanabria, J., Sánchez-Pimienta, T. G., Santomauro, D. F., Santos, I. S., Santos, J. V., Santric-Milicevic, M. M., Saraswathy, S. Y. I., Sarmiento-Suárez, R., Sarrafzadegan, N., Sartorius, B., Sarveazad, A., Sathian, B., Sathish, T., Sattin, D., Saxena, S., Schaeffer, L. E., Schiavolin, S., Schlaich, M. P., Schmidt, M. I., Schutte, A. E., Schwebel, D. C., Schwendicke, F., Senbeta, A. M., Senthilkumaran, S., Sepanlou, S. G., Serdar, B., Serre, M. L., Shadid, J., Shafaat, O., Shahabi, S., Shaheen, A. A., Shaikh, M. A., Shalash, A. S., Shams-Beyranvand, M., Shamsizadeh, M., Sharafi, K., Sheikh, A., Sheikhtaheri, A., Shibuya, K., Shield, K. D., Shigematsu, M., Shin, J. I., Shin, M.-J., Shiri, R., Shirkoohi, R., Shuval, K., Siabani, S., Sierpinski, R., Sigfusdottir, I. D., Sigurvinsdottir, R., Silva, J. P., Simpson, K. E., Singh, J. A., Singh, P., Skiadaresi, E., Skou, S. T., Skryabin, V. Y., Smith, E. U. R., Soheili, A., Soltani, S., Soofi, M., Sorensen, R. J. D., Soriano, J. B., Sorrie, M. B., Soshnikov, S., Soyiri, I. N., Spencer, C. N., Spotin, A., Sreeramareddy, C. T., Srinivasan, V., Stanaway, J. D., Stein, C., Stein, D. J., Steiner, C., Stockfelt, L., Stokes, M. A., Straif, K., Stubbs, J. L., Sufiyan, M. a. B., Suleria, H. A. R., Suliankatchi Abdulkader, R., Sulo, G., Sultan, I., Szumowski, Ł., Tabarés-Seisdedos, R., Tabb, K. M., Tabuchi, T., Taherkhani, A., Tajdini, M., Takahashi, K., Takala, J. S., Tamiru, A. T., Taveira, N., Tehrani-Banihashemi, A., Temsah, M.-H., Tesema, G. A., Tessema, Z. T., Thurston, G. D., Titova, M. V., Tohidinik, H. R., Tonelli, M., Topor-Madry, R., Topouzis, F., Torre, A. E., Touvier, M., Tovani-Palone, M. R. R., Tran, B. X., Travillian, R., Tsatsakis, A., Tudor Car, L., Tyrovolas, S., Uddin, R., Umeokonkwo, C. D., Unnikrishnan, B., Upadhyay, E., Vacante, M., Valdez, P. R., van Donkelaar, A., Vasankari, T. J., Vasseghian, Y., Veisani, Y., Venketasubramanian, N., Violante, F. S., Vlassov, V., Vollset, S. E., Vos, T., Vukovic, R., Waheed, Y., Wallin, M. T., Wang, Y., Wang, Y.-P., Watson, A., Wei, J., Wei, M. Y. W., Weintraub, R. G., Weiss, J., Werdecker, A., West, J. J., Westerman, R., Whisnant, J. L., Whiteford, H. A., Wiens, K. E., Wolfe, C. D. A., Wozniak, S. S., Wu, A.-M., Wu, J., Wulf Hanson, S., Xu, G., Xu, R., Yadgir, S., Yahyazadeh Jabbari, S. H., Yamagishi, K., Yaminfirooz, M., Yano, Y., Yaya, S., Yazdi-Feyzabadi, V., Yeheyis, T. Y., Yilgwan, C. S., Yilma, M. T., Yip, P., Yonemoto, N., Younis, M. Z., Younker, T. P., Yousefi, B., Yousefi, Z., Yousefinezhadi, T., Yousuf, A. Y., Yu, C., Yusefzadeh, H., Zahirian Moghadam, T., Zamani, M., Zamanian, M., Zandian, H., Zastrozhin, M. S., Zhang, Y., Zhang, Z.-J., Zhao, J. T., Zhao, X.-J. G., Zhao, Y., Zhou, M., Ziapour, A., Zimsen, S. R. M., Brauer, M., Afshin, A., & Lim, S. S. (2020). Global burden of 87 risk factors in 204 countries and territories, 1990-2013;2019: a systematic analysis for the Global Burden of Disease Study 2019. The Lancet, 396(10258), 1223-1249. https://doi.org/10.1016/S0140-6736(20)30752-2

Nichols, E., Szoeke, C. E. I., Vollset, S. E., Abbasi, N., Abd-Allah, F., Abdela, J., Aichour, M. T. E., Akinyemi, R. O., Alahdab, F., Asgedom, S. W., Awasthi, A., Barker-Collo, S. L.,

Baune, B. T., Béjot, Y., Belachew, A. B., Bennett, D. A., Biadgo, B., Bijani, A., Bin Sayeed, M. S., Brayne, C., Carpenter, D. O., Carvalho, F., Catalá-López, F., Cerin, E., Choi, J.-Y. J., Dang, A. K., Degefa, M. G., Djalalinia, S., Dubey, M., Duken, E. E., Edvardsson, D., Endres, M., Eskandarieh, S., Faro, A., Farzadfar, F., Fereshtehnejad, S.-M., Fernandes, E., Filip, I., Fischer, F., Gebre, A. K., Geremew, D., Ghasemi-Kasman, M., Gnedovskaya, E. V., Gupta, R., Hachinski, V., Hagos, T. B., Hamidi, S., Hankey, G. J., Haro, J. M., Hay, S. I., Irvani, S. S. N., Jha, R. P., Jonas, J. B., Kalani, R., Karch, A., Kasaeian, A., Khader, Y. S., Khalil, I. A., Khan, E. A., Khanna, T., Khoja, T. A. M., Khubchandani, J., Kisa, A., Kissimova-Skarbek, K., Kivimäki, M., Koyanagi, A., Krohn, K. J., Logroscino, G., Lorkowski, S., Majdan, M., Malekzadeh, R., März, W., Massano, J., Mengistu, G., Meretoja, A., Mohammadi, M., Mohammadi-Khanaposhtani, M., Mokdad, A. H., Mondello, S., Moradi, G., Nagel, G., Naghavi, M., Naik, G., Nguyen, L. H., Nguyen, T. H., Nirayo, Y. L., Nixon, M. R., Ofori-Asenso, R., Ogbo, F. A., Olagunju, A. T., Owolabi, M. O., Panda-Jonas, S., Passos, V. M. d. A., Pereira, D. M., Pinilla-Monsalve, G. D., Piradov, M. A., Pond, C. D., Poustchi, H., Qorbani, M., Radfar, A., Reiner, R. C., Jr., Robinson, S. R., Roshandel, G., Rostami, A., Russ, T. C., Sachdev, P. S., Safari, H., Safiri, S., Sahathevan, R., Salimi, Y., Satpathy, M., Sawhney, M., Saylan, M., Sepanlou, S. G., Shafieesabet, A., Shaikh, M. A., Sahraian, M. A., Shigematsu, M., Shiri, R., Shiue, I., Silva, J. P., Smith, M., Sobhani, S., Stein, D. J., Tabarés-Seisdedos, R., Tovani-Palone, M. R., Tran, B. X., Tran, T. T., Tsegay, A. T., Ullah, I., Venketasubramanian, N., Vlassov, V., Wang, Y.-P., Weiss, J., Westerman, R., Wijeratne, T., Wyper, G. M. A., Yano, Y., Yimer, E. M., Yonemoto, N., Yousefifard, M., Zaidi, Z., Zare, Z., Vos, T., Feigin, V. L., & Murray, C. J. L. (2019). Global, regional, and national burden of Alzheimer's disease and other dementias, 1990-2013;2016: a systematic analysis for the Global Burden of Disease Study 2016. The Lancet Neurology, 18(1), 88-106. https://doi.org/10.1016/S1474-4422(18)30403-4

O'Dell, K., Ford, B., Fischer, E. V., & Pierce, J. R. (2019). Contribution of Wildland-Fire Smoke to US PM2.5 and Its Influence on Recent Trends. Environmental Science & Technology, 53(4), 1797-1804. https://doi.org/10.1021/acs.est.8b05430

Power, M. C., Kioumourtzoglou, M.-A., Hart, J. E., Okereke, O. I., Laden, F., & Weisskopf, M. G. (2015). The relation between past exposure to fine particulate air pollution and prevalent anxiety: observational cohort study. BMJ : British Medical Journal, 350, h1111. https://doi.org/10.1136/bmj.h1111

Pu, X., Wang, T. J., Huang, X., Melas, D., Zanis, P., Papanastasiou, D. K., & Poupkou, A. (2017). Enhanced surface ozone during the heat wave of 2013 in Yangtze River Delta region, China. Science of The Total Environment, 603-604, 807-816. https://doi.org/https://doi.org/10.1016/j.scitotenv.2017.03.056

Pun, V. C., Manjourides, J., & Suh, H. (2017). Association of Ambient Air Pollution with Depressive and Anxiety Symptoms in Older Adults: Results from the NSHAP Study. Environmental Health Perspectives, 125(3), 342-348. https://doi.org/doi:10.1289/EHP494

Rajagopalan, S., Al-Kindi Sadeer, G., & Brook Robert, D. (2018). Air Pollution and Cardiovascular Disease. Journal of the American College of Cardiology, 72(17), 2054-2070. https://doi.org/10.1016/j.jacc.2018.07.099

Ren, J., Guo, F., & Xie, S. (2022). Diagnosing ozone–NOx–VOC sensitivity and revealing causes of ozone increases in China based on 2013–2021 satellite retrievals. Atmos. Chem. Phys., 22(22), 15035-15047. https://doi.org/10.5194/acp-22-15035-2022

Richardson, D., Black, A. S., Irving, D., Matear, R. J., Monselesan, D. P., Risbey, J. S., Squire, D. T., & Tozer, C. R. (2022). Global increase in wildfire potential from compound fire weather and drought. npj Climate and Atmospheric Science, 5(1), 23. https://doi.org/10.1038/s41612-022-00248-4

Schneider, R., Vicedo-Cabrera, A. M., Sera, F., Masselot, P., Stafoggia, M., de Hoogh, K., Kloog, I., Reis, S., Vieno, M., & Gasparrini, A. (2020). A Satellite-Based Spatio-Temporal Machine Learning Model to Reconstruct Daily PM(2.5) Concentrations across Great Britain. Remote sensing, 12(22), 3803-3803. https://doi.org/10.3390/rs12223803

Selevan, S. G., Borkovec, L., Slott, V. L., Zudová, Z., Rubes, J., Evenson, D. P., & Perreault, S. D. (2000). Semen quality and reproductive health of young Czech men exposed to seasonal air pollution. Environmental Health Perspectives, 108(9), 887-894. https://doi.org/10.1289/ehp.00108887

Seltzer, K. M., Shindell, D. T., & Malley, C. S. (2018). Measurement-based assessment of health burdens from long-term ozone exposure in the United States, Europe, and China. Environmental Research Letters, 13(10), 104018. https://doi.org/10.1088/1748-9326/aae29d

Shi, L., Wu, X., Danesh Yazdi, M., Braun, D., Abu Awad, Y., Wei, Y., Liu, P., Di, Q., Wang, Y., Schwartz, J., Dominici, F., Kioumourtzoglou, M.-A., & Zanobetti, A. (2020). Long-term effects of PM2.5 on neurological disorders in the American Medicare population: a longitudinal cohort study. The Lancet Planetary Health, 4(12), e557-e565. https://doi.org/10.1016/S2542-5196(20)30227-8

Shi, W., Li, T., Zhang, Y., Sun, Q., Chen, C., Wang, J., Fang, J., Zhao, F., Du, P., & Shi, X. (2020). Depression and Anxiety Associated with Exposure to Fine Particulate Matter Constituents: A Cross-Sectional Study in North China. Environmental Science & Technology, 54(24), 16006-16016. https://doi.org/10.1021/acs.est.0c05331

Shubham, S., Kumar, M., Sarma, D. K., Kumawat, M., Verma, V., Samartha, R. M., & Tiwari, R. R. (2022). Role of air pollution in chronic kidney disease: an update on evidence, mechanisms and mitigation strategies. International Archives of Occupational and Environmental Health, 95(5), 897-908. https://doi.org/10.1007/s00420-021-01808-6

Stafoggia, M., Bellander, T., Bucci, S., Davoli, M., de Hoogh, K., de' Donato, F., Gariazzo, C., Lyapustin, A., Michelozzi, P., Renzi, M., Scortichini, M., Shtein, A., Viegi, G., Kloog, I., & Schwartz, J. (2019). Estimation of daily PM10 and PM2.5 concentrations in Italy, 2013–2015, using a spatiotemporal land-use random-forest model. Environment International, 124, 170-179. https://doi.org/https://doi.org/10.1016/j.envint.2019.01.016

Stenke, A. (2020). Natural control on ozone pollution. Nature Climate Change, 10(2), 101-102. https://doi.org/10.1038/s41558-019-0686-3

Wang, J., Li, T., Lv, Y., Kraus Virginia, B., Zhang, Y., Mao, C., Yin, Z., Shi, W., Zhou, J., Zheng, T., Kinney Patrick, L., Ji, J., Tang, S., & Shi, X. (2020). Fine Particulate Matter and Poor Cognitive Function among Chinese Older Adults: Evidence from a Community-Based, 12-Year Prospective Cohort Study. Environmental Health Perspectives, 128(6), 067013. https://doi.org/10.1289/EHP5304

Wang, Y., Wang, H., & Wang, W. (2020). A Stratospheric Intrusion-Influenced Ozone Pollution Episode Associated with an Intense Horizontal-Trough Event. Atmosphere, 11(2), 164. https://www.mdpi.com/2073-4433/11/2/164

Wu, J., Laurent, O., Li, L., Hu, J., & Kleeman, M. (2016). Adverse Reproductive Health Outcomes and Exposure to Gaseous and Particulate-Matter Air Pollution in Pregnant Women. Res Rep Health Eff Inst, 2016(188), 1-58.

Xiao, Q., Geng, G., Liang, F., Wang, X., Lv, Z., Lei, Y., Huang, X., Zhang, Q., Liu, Y., & He, K. (2020). Changes in spatial patterns of PM2.5 pollution in China 2000–2018: Impact of clean air policies. Environment International, 141, 105776. https://doi.org/https://doi.org/10.1016/j.envint.2020.105776

Yang, X., Fang, Y., Chen, H., Zhang, T., Yin, X., Man, J., Yang, L., & Lu, M. (2021). Global, regional and national burden of anxiety disorders from 1990 to 2019: results from the Global Burden of Disease Study 2019. Epidemiol Psychiatr Sci, 30, e36. https://doi.org/10.1017/s2045796021000275

Zhang, L., Lau, W., Tao, W., & Li, Z. (2020). Large Wildfires in the Western United States Exacerbated by Tropospheric Drying Linked to a Multi-Decadal Trend in the Expansion of the Hadley Circulation [https://doi.org/10.1029/2020GL087911]. Geophysical Research Letters, 47(16), e2020GL087911. https://doi.org/https://doi.org/10.1029/2020GL087911

Zhang, X., Chen, X., & Zhang, X. (2018). The impact of exposure to air pollution on cognitive performance. Proceedings of the National Academy of Sciences, 115(37), 9193-9197. https://doi.org/10.1073/pnas.1809474115

Zhao, T., Markevych, I., Romanos, M., Nowak, D., & Heinrich, J. (2018). Ambient ozone exposure and mental health: A systematic review of epidemiological studies. Environ Res, 165, 459-472. https://doi.org/10.1016/j.envres.2018.04.015

Zhao, W., Zhao, Y., Wang, P., Zhou, Y., Meng, X., Ma, W., Li, J., & Zhang, Y. (2022). PM2.5 exposure associated with prenatal anxiety and depression in pregnant women. Ecotoxicology and Environmental Safety, 248, 114284. https://doi.org/https://doi.org/10.1016/j.ecoenv.2022.114284

2. Satellite-based long-term spatiotemporal patterns of surface ozone concentrations in China: 2005-2019

[Manuscript 1]

Qingyang Zhu, Jianzhao Bi, Xiong Liu, Shenshen Li, Wenhao Wang, Yu Zhao, and Yang Liu

2.1. Abstract

Background: While short-term ozone exposure has been associated with a series of adverse health outcomes, research on the health effects of chronic ozone exposure is still limited, especially in developing countries due to the lack of long-term exposure estimates.

Objectives: The present study aimed to estimate the spatiotemporal distribution of monthly mean daily maximum 8-hour average (MDA8) ozone concentrations in China from 2005-2019 at 0.05° spatial resolution.

Methods: We developed a machine learning model with satellite-derived boundary layer ozone column, ozone precursors, meteorological conditions, land-use information, and proxies of anthropogenic emissions as predictors.

Results: The random, spatial, and temporal cross-validation R^2 of our model were 0.87, 0.86, and 0.76, respectively. Model-predicted spatial distribution of ground-level ozone concentrations showed significant differences across seasons. The highest summer peak of ozone occurred in the North China Plain (NCP), while southern regions were the most polluted in winter. Most large urban centers showed elevated ozone levels, but their surrounding suburban areas may have even higher ozone concentrations due to NOx titration. The annual trend of ozone concentrations fluctuated over 2005-2013, but a significant nationwide increase was observed afterward.

Discussion: The present model had enhanced performance in predicting ground-level ozone concentrations in China. This national dataset of ozone concentrations would facilitate epidemiological studies to investigate the long-term health effect of ozone in China. Our results also highlighted the importance of controlling ozone in China's next round of the Air Pollution Prevention and Control Action Plan.

2.2. Introduction

Numerous epidemiological studies have shown that short-term ozone exposure is associated with a series of adverse health outcomes, including all-cause non-accidental mortality (Yin et al. 2017) and respiratory morbidity (Barry et al. 2019). In 2015, ozone pollution contributed to an estimated 9-23 million asthma emergency room visits globally (Anenberg et al. 2018). A handful of studies have also investigated the chronic health effects of ozone, but their conclusions differed, as reviewed by Nuvolone et al. (Nuvolone et al. 2018). For example, Turner et al. reported a positive association between long-term ozone exposure and all-cause mortality in a large prospective study in the US (Turner et al. 2016). However, a meta-analysis reported that this association only existed in the warm season rather than the whole year (Atkinson et al. 2016). One potential reason for this inconsistency was the bias in the exposure matrices, especially in large long-term studies. Seltzer et al. highlighted the value of a dense monitoring network in measuring long-term ozone exposure (Seltzer et al. 2018), but such a network is unavailable in most developing countries. As the world's most populous nation, China began to establish its national air quality monitoring network in 2013. To date, this network covers most Chinese cities, but the rural and suburban areas remain largely unmonitored (Xiao et al. 2020). The insufficient spatiotemporal coverage of ozone measurements presents a major hurdle to retrospective epidemiological studies in China, especially those established before the 2010s (Wang et al. 2017).

Satellite remote sensing has become a promising tool to extend the records of ozone measurements in space and time. For example, the Ozone Monitoring Instrument (OMI) is a nadir-viewing ultraviolet-visible (270-550 nm) solar backscatter spectrometer aboard the NASA Aura satellite designed to measure total ozone column and other trace gases (Levelt et al. 2006).

Since its launch in July 2004, researchers have been exploring ways to estimate boundary layer ozone levels using OMI and other satellite data. Based on OMI's measurements, Liu et al. developed an optimal estimation technique to retrieve the ozone profile from the surface to approximately 60 km to produce the OMPROFOZ product (Liu et al. 2010). It has been shown to capture enhancements of lower tropospheric ozone over China (Shen et al. 2019) and East Asia (Hayashida et al. 2015), but its performance varies in space and by season due to various factors affecting the horizontal and vertical distribution of tropospheric ozone (Huang et al. 2017). In China, the daily correlation between the OMPROFOZ tropospheric column and ground-level ozone measurements varies from less than 0.1 in high-latitude regions to over 0.6 in low-latitude regions (Shen et al. 2019).

Surface-level ozone is formed by complex photochemical reactions between volatile organic compounds (VOCs) and nitrogen oxides (NOx) in the presence of heat and solar radiation (Li et al. 2020; Pu et al. 2017). In addition to the abundance of precursors, the production of surface ozone can be strongly influenced by meteorology. For example, high temperature boosts ozone chemistry by increasing the decomposition rate of Peroxyacytyl nitrate (PAN), thus preventing the sinkage of NOx and peroxyl radicals (Fischer et al. 2014; Lu et al. 2019a). Water vapor may affect surface ozone production by modulating the hydrogen oxide radicals (HOx) essential to ozone production from oxygen (Lu et al. 2016). Besides these persistent effects, lightning would result in a surge in NOx emission, thus significantly elevate short-term ground-level ozone (DeCaria et al. 2005; Kang et al. 2020).

While photochemical reactions predominantly determine tropospheric ozone concentrations (Lelieveld and Dentener 2000; Monks 2005), in some circumstances, the stratospheric ozone-rich air may penetrate rapidly into the lower troposphere and cause a sharp increase in ground-

level ozone pollution (Knowland et al. 2017). The peak of this cross-tropopause mass transport known as stratospheric intrusions (SI) in the northern hemisphere usually occurs in springtime, especially in the high-altitude regions such as the Qinghai-Tibet plateau (Appenzeller et al. 1996; Itahashi et al. 2020; Lin et al. 2012; Lu et al. 2019b; Yiping Wang et al. 2020). Changes in large-scale climate patterns such as El Niño are associated with increased SI and surface ozone concentrations (Shen and Mickley 2017; Xie et al. 2014). Additionally, vegetation has complicated effects on surface ozone. On the one hand, it can remove surface ozone through dry deposition (Clifton et al. 2020). On the other hand, plants may emit VOCs to the atmosphere and affect ozone pollution (Kigathi et al. 2019). Therefore, land cover types are also important in determining ambient ozone concentrations.

In this study, we developed a national-scale machine learning model to estimate historical ambient ground-level ozone concentrations in China at a monthly level from 2005 to 2019 at 0.05 ° spatial resolution. In addition to the OMPROFOZ ozone profile, we included meteorological factors, land-use information, ozone precursors, and indicators of anthropogenic emissions to account for the complicated formation and removal processes of surface ozone. We first present our model development strategy, then evaluate model performance using statistical techniques as well as ground measurements not included in model training. Finally, we investigate the spatiotemporal trend of ozone and discuss the drivers of these patterns.

2.3. Data and Methods

2.3.1. Model Development

We used a random forest framework to estimate monthly mean daily maximum 8-hour average (MDA8) ozone concentrations in China from 2005 to 2019. The overall study workflow is illustrated in figure S1-1. Briefly, we first extracted the fraction of the boundary layer ozone column from the OMPROFOZ ozone profile. The depth of this layer for each grid cell was determined dynamically by the tropopause pressure (Liu et al. 2010). Missing fraction values were imputed with daily random forest models incorporating the Modern-Era Retrospective Analysis for Research and Applications (MERRA-2) meteorological fields and surface flux. The gap-filled boundary-layer ozone fractions were then used to calculate the full coverage boundary-layer ozone column (in Dobson unit). The surface-level monthly average MDA8 ozone concentration was generated by a separate random forest model trained with the gap-filled boundary-layer ozone column, meteorological fields, land-use terms, elevation, and population density. The details of these predictors are described below.

2.3.2. Ground ozone measurements

Ground-level monitoring data from 2013 to 2019 were obtained from the China National Environmental Monitoring Centre (CNEMC, http://www.cnemc.cn/). China's national air quality monitoring network measures hourly ozone concentration with either ultraviolet absorption (for point analyzers) or differential optical absorption spectroscopy (for open-path analyzers). MDA8 ozone concentration was defined as the maximum eight-hour moving average ozone concentration (contains at least six valid hourly values) within a calendar day. We chose to use

MDA8 rather than MDA1 or 24-hr average because MDA8 has been widely used in ozone health effects research (Lu et al. 2020; Lyu et al. 2019).

The quality assurance of the CNEMC data was conducted primarily based on its official standard (CNEMC 2012). Briefly, a valid 8-hour moving average ozone concentration must contain at least six hourly measurements. No regulatory standard has yet been set up for MDA8 ozone, but twenty hourly measurements were generally required for daily air pollutant concentrations. Therefore, we also removed all the observations during a given day from the stations with less than 15 hourly measurements to balance data abundance and data quality. A total of 2443 (3%) monthly MDA8 ozone concentrations were removed from the dataset.

We further separated rural stations from urban stations to test our model performance in different settings. In compliance with China's official regulations (NBS 2008), we define areas with a population density less than 1,500 per km^2 (approximately 37,500 per grid cell) as rural. Consequently, 406 monitoring stations out of 1532 (27%) were identified as rural stations, contributing to a total of 24,405 (31%) data points. Note that population density is not the only determinant of rural/urban status listed in China's official standards. We used population to identify rural/urban stations primarily because other economic and political determinants are less quantifiable in this modeling study.

Ozone monitoring data before 2014 was obtained from the Tropospheric Ozone Assessment Report (TOAR) (Xu et al. 2020). This dataset contains MDA8 ozone concentrations from eight different stations, including Mt. Waliguan (WLG, locates at 36.30°N, 100.9°E); Shangdianzi (SDZ, locates at 40.39°N, 117.00°E); Lin'an (LAN, locates at 30.30°N, 119.73°E); Longfengshan (LFS, locates at 44.73°N, 127.60°E); Xianggelila (XGLL, locates at 28.01°N, 99.68°E); Akedala (AKDL, locates at 47.10°N, 87.93°E); Gucheng (GCH, locates at 39.13°N,

115.67°E); and China Meteorological Administration (CMA, locates at 39.95°N, 116.32°E). The locations of the TOAR sites can be found in Fig. S1-2. The TOAR historical monitoring data was not used to train the final model but served as an independent external validation dataset.

2.3.3. OMI data

In this study, we used the OMI OMPROFOZ product developed at the Harvard Smithsonian Astrophysical Observatory (SAO), publicly available at NASA Aura Validation Data Center (AVDC). Ozone profile is retrieved at 24 layers (~2.5 km per layer) from the surface to ~65 km from the spectral range 270-330 nm using the optimal estimation approach. It is based on the initial retrieval algorithm (Liu et al. 2010) with modifications described in Kim et al. (Kim et al. 2013). The layers between surface and the tropopause were defined on a daily basis. That is to say, the layers' pressure boundaries were initially set at $P_i = 2^{-i/2}$ atm for i = 0 to 23, and $P_{24} = 0$. For each individual day, the National Centers for Environmental Prediction (NCEP) tropopause pressure is used to replace the pressure level closest to it. The layers between surface and the tropopause are then re-assigned based on equal logarithmic pressure intervals (Liu et al. 2010). OMPROFOZ's retrieval errors due to precision (instrument random-noise) and smoothing errors (insufficient vertical resolution) ranged from 1–6% in the stratosphere to 6–35% in the troposphere. The retrieval is performed at a spatial resolution of 52 x 48 km^2 at nadir and gridded to 0.5° resolution for easy use.

For more intuitive interpretations, we define OMPROFOZ's boundary layer (from surface pressure to ~ 700 hPa) as Layer 24 (L24). Correspondingly, L23-L1 represents the second-lowest layer to the top layer. Our model initially used the boundary layer (L24) partial column ozone from the OMPROFOZ ozone profile. To better understand OMPROFOZ's role in modeling long-term ozone pollution, we also tested if using additional tropospheric columns (i.e., the

summation of L22-L24) or replacing the retrievals with a priori ozone profile (both L24 and the summation of L22-L24) would influence the model performance.

Tropospheric column NO_2 concentration from 2005 to 2019 was extracted from the OMI global nitrogen dioxide product named OMNO2d (Krotkov et al. 2017). It provides global daily tropospheric column NO_2 at 0.25° resolution. We extracted the tropospheric column NO_2 concentration with cloud screening (i.e., pixels with a cloud fraction higher than 30% were removed for quality assurance) as a measurement of ozone precursor in the present study.

2.3.4. MERRA-2 assimilated data

We used the MERRA-2 meteorological data in the present study. MERRA-2 provides the latest NASA atmospheric reanalysis data starting from 1980. It has a native resolution of 0.5 ° x 0.625 ° and 72 vertical layers (Gelaro et al. 2017). We extracted surface-level meteorological fields as well as those between surface and 150 hPa to account for the effects of stratospheric intrusion (Knowland et al. 2017). The detailed list of MERRA-2 meteorological and chemistry fields we used is provided in Table S1-1.

2.3.5. Lightning flash density

Previous studies have shown that lightning flash is an important enhancer of tropospheric ozone because of its considerable contribution to NOx (DeCaria et al. 2005; Finney et al. 2016), especially in springtime (Lu et al. 2019b). We obtained global monthly lightning flash density data from the Harvard-NASA Emissions Component (HEMCO) at 0.5° x 0.625° resolution, which adopted an optimal regional scaling algorithm to reduce the bias of satellite-driven tropical lightning data (Murray et al. 2012).

2.3.6. South and Southeast Asia wildfire

The massive human-initiated biomass burning in South and Southeast Asia would greatly enhance springtime ozone pollution over China, especially in the southwest (Ni et al. 2018; Wang et al. 2011). To test if incorporating foreign wildfire data would increase model performance, we obtained the Moderate Resolution Imaging Spectrometer (MODIS) daily active fire data from 2005 to 2019 via the Fire Information for Resource Management System (FIRMS) data achieve (MODIS Collection 6)**.** Fire points from ten South and Southeast Asian countries, namely Bangladesh, Bhutan, Cambodia, India, Laos, Myanmar, Nepal, Pakistan, Thailand, and Vietnam were selected to capture most fire points in China's southern neighbors. Fire radiative power (FRP) was used as a quantitative proxy of fire-related emissions (F Li et al. 2019; Wooster et al. 2003).

2.3.7. Land use, population, road length, and digital elevation

Annual land cover maps were obtained from the European Space Agency (ESA) Climate Change Initiative (CCI) (ESA 2017) for 2005-2015 and the Copernicus Climate Change Service (C3S) Climate Data Store (CDS) for 2016-2019 (CDS 2021). The C3S land-use product used the same methodology as the ESA CCI land cover maps to guarantee long-term continuity, according to the product manual (C3S 2021). Both products provide 23 types of land cover at a spatial resolution of 300 m.

LandScan global population data were obtained from the Oak Ridge National Laboratory (https://landscan.ornl.gov/). This dataset provides annual population density from 2005 to 2019 at 1 km resolution. Road networks were obtained from the Global Roads Open Access Data Set (gROADs) (CIESIN and ITOS 2013). This dataset was compiled from sources before 2010

(specific date unavailable). Total road length is included in our model as a proxy of traffic emissions. We also used 30 m elevation data from the Advanced Spaceborne Thermal Emission and Reflection Radiometer (ASTER) Global Digital Elevation Model (GDEM), version 3 (NASA/METI/AIST/Japan Spacesystems and U.S./Japan ASTER Science Team 2019). This latest version of ASTER GDEM has an increased accuracy compared to previous versions.

2.3.8. Missing value imputation

Eq. 2-1 Illustrates the relationship between the total column ozone and the boundary layer (L24) column ozone.

$$\boldsymbol{C_{PBL} = f_{PBL} \times C_{total}} \qquad \text{(Eq. 2-1)}$$

Where C_{PBL} denotes the boundary layer column ozone (in Dobson unit); C_{total} is the total column ozone; f_{PBL} is the boundary layer fraction of total column ozone. The OMPROFOZ product has a nonnegligible portion of missing values that will reduce the spatial coverage of f_{PBL} and affect predicted ground-level ozone concentrations. We first filled the data gap of OMI f_{PBL}, then multiplied it with MERRA-2 C_{total} to get the final C_{PBL}. We chose this approach over directly imputing the OMPROFOZ product because OMI total ozone column and MLS stratospheric ozone profiles have been assimilated into MERRA-2 data after 2004 (Wargan et al. 2017). The correlation coefficient between MERRA-2 column ozone and OMI column ozone was 0.97 in the present study. The missing values of OMI f_{PBL} were imputed with random forest models incorporating MERRA-2 meteorological fields and surface flux measurements. These models were trained on a daily basis at the native resolution of the OMPROFOZ product.

Other OMI-derived partial column ozone amounts were processed similarly. To specify, missing values in other retrieved partial column ozone were imputed independently with the same

process to the boundary layer, but with different meteorological fields corresponding to their pressure levels (i.e., 500-700 hPa for L23, 350-500 hPa for L22). The a priori ozone profile (L22, L23, and L24) was processed independently but with the same methodology as the retrieved ozone profile.

2.3.9. Data integration

We created a 0.05° resolution modeling grid across China for data integration and model construction (Fig. 2-1). A 50 km buffer region was added to China's national boundaries to ensure data sensitivity at the border area. The total number of grid cells was 399,513. Three megacity clusters were selected to study the regional patterns of ozone pollution, i.e., the North China Plain (NCP), the Yangtze River Delta (YRD), and the Pearl River Delta (PRD). We used an inverse distance weighting (IDW) method to resample data at a spatial resolution coarser than 0.05°, including all OMI-derived column ozone amounts, tropospheric column NO_2, MERRA-2 meteorological fields, and lightning flash density. In addition, we calculated the percentage coverage of different land-use categories, average elevation, total road length, and total population for each pixel. Daily data were then aggregated to the monthly level. Population and land use were processed at the annual level, while elevation and road length were fixed during the entire study period. After data integration, we selected grid cells that contain air quality monitoring stations to generate the training dataset. All valid ground-level MDA8 O_3 observations within each grid cell were averaged on a monthly basis to match with other model parameters.

The foreign wildfire data was processed in a different way as our study domain did not extend to China's neighboring countries other than the buffer area. We assumed that the foreign fire points have an additive and distance-dependent influence on China's ozone concentrations. Therefore,

the contributions of the South and Southeast Asian countries were quantified with the equation below (Eq. 2-2).

$$FFE_{it} = \sum FRP_{jt} * (dist_{ij})^{-2} \qquad \text{(Eq. 2-2)}$$

Where FFE_{it} denotes the influence of foreign fire emissions on grid cell i at day t; FRP_{jt} represents the FRP for fire point j at day t; $dist_{ij}$ is the distance between fire point j and grid cell i.

2.3.10. Model training, validation, and parameter comparison

We divided the study period into the training period (2014-2019) and the hindcast period (2005-2013). The year 2013 was excluded from model training due to fewer numbers of ozone monitors and unstable data quality at the onset of the Chinese national monitoring network. We trained two separate random forest models with the same set of predictors for springtime (March-April-May) and the rest of the year due to the significantly different pattern of springtime ozone in the northern hemisphere (Lin et al. 2012; Ni et al. 2018). To specify, the aforementioned 'rest of the year' includes summer (June-July-August), autumn (September-October-November), and winter (December-January-February). The detailed list of predictors included in our random forest models could be found in Table S1-1.

Note that some parameters were not included in the initial model. To specify, our original model was established with the boundary layer (L24) column ozone from the OMPROFOZ retrieved ozone profile. The OMI L22-24 retrieval and the a priori partial columns were used separately to compare model performance with different OMI-derived ozone fields. In addition, MODIS FRP was not initially used because it was completely generated outside of the study domain.

Therefore, the original model hereafter represents the model with the retrieved ozone profile L24 and without foreign fire emissions.

All models were validated with 10-fold random cross-validation (CV), i.e., we randomly divided the original dataset into ten equal-sized subsets, used nine of them to train a model, and made predictions on the left-out subset. This process was repeated 10 times so that each monthly mean MDA8 measurement would have a corresponding predicted value. Model performance metrics including R^2 and root-mean-square error (RMSE) were calculated using the measurement-prediction pairs. Similarly, we conducted a 10-fold spatial CV to test whether our model can make reliable predictions at locations without ground monitors. In the spatial CV, the original dataset was randomly divided based on each data point's location. Model predictions at a given location were generated by a model trained with data elsewhere. Finally, temporal CV was conducted where models trained for a given year would be validated with data from other years in the training period to test the reliability of model predictions in the hindcast period.

Since each variable has a different contribution to the overall model performance, the predictors' importance was evaluated with a permutation method (Altmann et al. 2010). Briefly, a variable's importance represents the percentage increase in the model's total mean squared error if this variable is replaced by its random permutation.

We used R (version 3.6.3) to process data and perform statistical analyses. Package *ranger* was utilized for training the random forest models.

2.3.11. Coupled trend evaluation between ozone and $PM_{2.5}$

To reduce severe air pollution, the State Council of China enacted the Air Pollution Prevention and Control Action Plan (APPCAP) in 2013. This policy has resulted in a substantial reduction

in ambient $PM_{2.5}$, but the contemporary ozone concentrations increased unexpectedly (Huang et al. 2018; Yonghong Wang et al. 2020). We obtained model-estimated nationwide $PM_{2.5}$ concentrations at 1 km resolution (Liang et al. 2020; Xiao et al. 2021) to evaluate the nationwide long-term coupled change between ozone and $PM_{2.5}$ under the APPCAP. The correlation between $PM_{2.5}$ and ozone was examined with a partial correlation analysis controlling for temperature, relative humidity, and total precipitation from MERRA-2.

2.4. Results

2.4.1. Model performance and parameter comparison

The performance of the original model is illustrated in Fig. 2-2. The predicted monthly average MDA8 ozone concentrations from the combined springtime and non-spring model were in good agreement with the ground-based observations, with a random CV R^2 of 0.87 and an RMSE of 13.03 $\mu g/m^3$. The spatial CV had an almost identical performance with the random CV (R^2 = 0.86, RMSE = 13.56 $\mu g/m^3$). The temporal CV had a slightly lower R^2 of 0.76 and a higher RMSE of 17.71 $\mu g/m^3$. The regression lines between the predicted and observed ozone concentrations were close to the 1:1 line for all three types of CV.

As shown in Fig. S1-3, replacing OMI L24 retrieval with the summation of L22-24 retrievals would not substantially impact the model performance. The R^2 and RMSE were almost identical with the original model for all three CV types. Similarly, using the a priori ozone profile (L24 or L22-L24) also had a minimum influence on the overall performance. Although using a priori L22-L24 would increase the temporal CV R^2 by 0.6%, such an attempt also had a negative impact on the predicted spatial distribution of ozone. Fig. S1-4, panel A shows an example of the spatial artifact (horizontal gap in the predicted ozone concentrations) from the model with a

priori ozone profile L22-24. This kind of artifact was not seen in the original model (Figure S1-4, panel B). Given that using alternative partial column ozone amount would not improve the model performance, all results presented hereafter used the model with OMI L24 retrieval unless otherwise specified.

The season-specific model performance showed that our model had a lower performance in spring than in other seasons (Fig. S1-5). To specify, the springtime R^2 were 0.72, 0.71, and 0.53 for random, spatial, and temporal CV, respectively. In addition, the RMSE for all types of CV in spring was around 3 $\mu g/m^3$ higher than in autumn, but the overall ozone concentrations were comparable in these two seasons.

In addition, our model had a better performance in urban regions than in rural regions (Fig. S1-6). The random, spatial, and temporal CV R^2 were 0.88, 0.87, 0.76 in urban regions and 0.83, 0.81, 0.72 in rural regions. The prediction errors (RMSE) were also higher in rural regions than urban areas (1-2 $\mu g/m^3$ for all CV types).

Our predicted MDA8 ozone concentrations also agreed well with the TOAR historical data monitoring data before 2014 (overall $R^2 = 0.73$, RMSE = 20.68 $\mu g/m^3$), except for the XGLL station. Site-specific time series comparison (Fig. S1-7) showed that the predicted ozone trends were mostly identical with the observations at stations CMA, GCH, and LFS. Although our model may underestimate ozone concentrations at the stations LAN, SDZ, WLG, especially in springtime, it still captured most of the ozone's temporal variation over these locations. The worst agreement was observed at XGLL, where our model almost had no sensitivity to the springtime peak ozone concentrations. The monitoring data was mostly incomplete at the AKDL station, but it may also indicate some springtime underestimations in that region. Incorporating the MODIS FRP data would neither significantly improve the springtime nor the overall

agreement with the TOAR historical data (Fig. S1-8). Therefore, we excluded MODIS FRP from the model since introducing data fields external to the study domain may incur unexpected uncertainty.

Although the OMI L24 retrieval had a low raw correlation with the CNEMC data (R^2 = 0.34, as presented in Fig. S1-9), removing this parameter would result in a slight decrease in the model performance compared to the original model (~1% decrease in R^2 for all three types of CV, as shown in Figs. 2-2 and S1-10). Besides, the agreement between model predictions and the TOAR historical ozone monitoring data would also be worse if OMI L24 retrieval is removed from the model (overall R^2 dropped from 0.73 to 0.70, RMSE increased from 20.68 $\mu g/m^3$ to 22.38 $\mu g/m^3$), although the predicted temporal trends were generally similar (Figs. S1-7 and S1-11).

2.4.2. Predictor importance ranking

Most of the top predictors in both the spring and non-spring models were meteorological factors, but their relative orders differed (Fig. S1-12). Non-meteorological variables were more important in the non-spring model. For example, the five most important non-meteorological variables in the spring-excluded model were OMI NO_2; population; the proportion of rainfed cropland; irrigated or post-flooding cropland; and elevation. However, their importance ranking all dropped in spring. The gap-filled OMI boundary layer ozone was one of the most important variables in the spring model, and those that gained the most importance were associated with stratospheric intrusion (e.g., tropopause pressure and vertical wind columns) and lightning flash activity.

2.4.3. Seasonality and spatial heterogeneity of ozone levels in China

As shown in Fig.2-3, the spatial distribution and severity of surface ozone pollution in China varied by season. The mean springtime MDA8 ozone concentrations over 2005-2019 were mostly around 80-90 $\mu g/m^3$. Moderate ozone pollution (around 100 $\mu g/m^3$) was observed in Central-East China, especially around the boundary region between the NCP and the YRD. Southwest China, including the Sichuan Basin and Yunnan Province, was also moderately polluted in this season. In summer, heavy ozone pollution was widespread in China, except for the southwest. The NCP had the worst ozone pollution with the highest 15-yr mean MDA8 ozone concentrations around Beijing approaching the national level-2 air quality standard (160 $\mu g/m^3$). In autumn, the PRD region became the most polluted area after a sharp decrease in ozone concentrations in North China. Winter has the lowest ozone level, especially around the NCP region and only the low-latitude regions may have an ozone concentration approaching 100 $\mu g/m^3$.

Different regions appeared to have different seasonal patterns (Fig. 2-4). For example, ozone concentrations in the NCP and nearby northern regions started to rise in spring and peaked in summer. After a sharp decrease in autumn, these regions would have the lowest ozone level in winter. In contrast, high ozone concentrations could persist from spring to autumn in southern China without a clear peak in summer. Sporadic ozone hot spots may even be found in winter (Fig. 2-3). The ozone concentration in the YRD is a mixture of the two patterns above, i.e., it had a flatter summer high and a winter low, but high ozone concentrations also persisted in spring and autumn. Most regions in China followed the aforementioned patterns with a few exceptions. For example, Yunnan province saw ozone levels peak in spring and then drop substantially in summer. Ozone concentrations on the Qinghai-Tibet plateau were relatively stable throughout the year, with only a mild peak occurring in summer.

Ozone's spatial heterogeneity was not only observed nationwide but also at the city level. Fig. 2-5 shows the model-estimated ozone concentrations in the YRD region in August 2019, while the right map shows population densities. Some population centers, such as the sub-regions A (Bengbu and Huainan City) and B (Nanjing Metropolitan Area), had lower ozone levels than their surrounding areas. On the contrary, the subregions C (Anqing City) and D (Quzhou and Jinhua City) were more polluted than their surrounding area. As shown in Fig. S1-13, the tropospheric column NO_2 concentrations were higher in sub-regions A and B than in C and D.

2.4.4. The long-term trend of ozone in China

Fig. 2-6 showed the long-term trend of ozone concentrations in the ozone season (defined as March-November) in China. Before 2014, mean ozone concentrations during the ozone season fluctuated from year to year but generally stayed at the same level nationally at approximately 90 $\mu g/m^3$. Ozone levels in the NCP, YRD, and PRD regions were higher than the national average but were also stable around their respective long-term averages. A sharp decrease was observed in the YRD and PRD from 2014 to 2016. After 2016, ozone levels nationwide started to rise at various paces. For example, seasonal mean ozone concentrations were almost identical for the YRD and NCP before 2014, but the former experienced a sharper increase from 2015 to 2019 due to the significant drop from 2014 to 2015. After 2018, the mean MDA8 ozone concentrations in the ozone season exceeded 100 $\mu g/m^3$ in all these regions.

The summertime (June-July-August) mean MDA8 ozone concentrations showed an overall increasing trend during 2005-2019 in the whole of China (0.27 $\mu g/m^3 * yr^{-1}$, $p = 0.004$), the NCP (1.10 $\mu g/m^3 * yr^{-1}$, $p = 0.002$), and the YRD (0.85 $\mu g/m^3 * yr^{-1}$, $p = 0.010$) (Fig. S1-14). However, similar to the ozone season averages, no significant trend was observed for summertime mean MDA8 ozone concentrations over 2005-2013 (0.04 $\mu g/m^3 * yr^{-1}$, $p = 0.789$; -

0.00 μg/m^3 * yr^{-1}, p = 0.990; 0.15 μg/m^3 * yr^{-1}, p = 0.700; and 0.17 μg/m^3 * yr^{-1}, p = 0.711 for entire China, the NCP, the YRD, and the PRD, respectively) (Fig. S1-15). The NCP was the only region that had an overall increasing springtime ozone pollution over 2005-2019 (0.31 μg/m^3 * yr^{-1}, p = 0.047) (Fig. S1-16) while no significant trend was found for 2005-2013 across China (-0.04 μg/m^3 * yr^{-1}, p = 0.772; -0.21 μg/m^3 * yr^{-1}, p = 0.400; -0.51 μg/m^3 * yr^{-1}, p = 0.354; and 0.02 μg/m^3 * yr^{-1}, p = 0.967 for entire China, the NCP, the YRD, and the PRD, respectively) (Fig. S1-17). As shown in Table S1-2, the TOAR monitoring data also did not exhibit significant increasing trend in ozone pollution during 2005-2013, except for the summertime pollution at the station SDZ (5.79 μg/m^3 * yr^{-1}, p = 0.033).

The predicted temporal trend was similar to the CNEMC observations over the grid cells with monitoring sites (Fig. S1-18). Though our model may slightly underestimate the overall ozone season MDA8 ozone concentrations in China, the predicted summer peak ozone was almost identical with the CNEMC observations in China as a whole as well as the NCP, YRD, and PRD (Fig. S1-19). Unlike our model predictions, the 2018-2019 increase in the ozone-season mean MDA8 ozone concentrations was not seen from the CNEMC data except for the PRD. However, there was a substantial increase in some sub-regions, including Central-East China and the Shandong Peninsula (locations listed on Fig. S1-20), as observed by both the CNEMC data and our predictions (Fig. 2-7).

2.4.5. Couple trend between $PM_{2.5}$ and ozone in China

The temporal trends of population-weighted ozone and $PM_{2.5}$ concentrations in China and three major regions are shown in Fig. 2-8. Despite the visible inverse correlation between $PM_{2.5}$ and ozone levels, partial correlation analyses controlling for temperature, relative humidity, and precipitation indicated that their association varied by region. A statistically significant negative

correlation was observed in the YRD region ($r = -0.31$, $p < 0.001$), while in the PRD region, this correlation turned positive ($r = 0.34$, $p < 0.001$). No significant association was observed in China as a whole ($r = 0.03$, $p = 0.385$) and the NCP ($r = -0.07$, $p = 0.358$) after we controlled for temperature, relative humidity and precipitation.

2.5. Discussion

In the present study, we trained a random forest model to predict long-term ground-level MDA8 ozone concentrations in China. To our best knowledge, our model's performance was the highest among similar studies in China. For example, the 0.1° model established in Liu et al. had a spatial CV R^2 of 0.68 and a temporal CV R^2 of 0.69 for monthly mean MDA8 ozone concentrations (Liu et al. 2020). Compared to their study, our model had a finer spatial resolution (0.05°) and higher spatial and temporal CV R^2 values (0.86 and 0.76, respectively). Despite a coarser spatiotemporal resolution, our model generally had a comparable performance with those established in regions with sufficient historical ozone monitoring data. For instance, the R^2 for daily MDA8 ozone in Di et al. ranged from 0.7-0.8 across the US over 2000-2012 (Di et al. 2017); the land-use regression model in Adam-Poupart et al. had an R^2 of 0.65 for daytime 8-hour average ozone concentrations in Quebec, Canada (Adam-Poupart et al. 2014). One reason for the improved performance was the inclusion of the OMPROFOZ ozone profile instead of the total ozone column. The latter is a noisy proxy of surface-level ozone because approximately 90% of the atmospheric ozone exists in the stratosphere (Fishman and Larsen 1987). Though the gap-filled boundary layer ozone column was not among the top predictors for the non-spring model, it was an important predictor in springtime when ground-level ozone pollution is greatly influenced by SI and foreign transport (Fig. S1-12). Another reason for the higher performance of our model is that the two primary sources of ground-level ozone (i.e., photochemical reactions

and SI) were both accounted for in our study, while previous studies typically focused on the impact of photochemical reactions on ozone patterns.

With the improved spatial resolution, we were able to observe the complex relationship between human activities and ozone concentrations, as presented in Fig. 2-5. These regions have been reported to have a high NOx/VOC ratio so that the abundance of VOCs controls ambient ozone concentrations (X-H Liu et al. 2010). Under the VOC-limited regime, the excessive NOx concentrations would quench ozone molecules through NOx titration (Jhun et al. 2015). On the other hand, ozone concentration in regions C (Anqing City) and D (Quzhou and Jinhua City) with moderate NOx concentrations (Fig. S1-13) fall under the NOx-limited regime with a positive association between ozone and NOx concentrations.

Our modeling results indicated that the seasonality of ozone concentrations in China varied across different regions and was more distinct in northern China than in the south (Fig.2-3 and 2-4). This phenomenon could be explained by three reasons. First, the absolute and relative abundance of ozone precursors have a major impact on ozone concentration. The observed regional and national ozone hot spots occurred predominantly in the megacity clusters (NCP, YRD, PRD, and Sichuan Basin), which was partially attributed to the high anthropogenic emissions of NOx and VOCs (K Li et al. 2019). Second, meteorological conditions such as temperature and solar radiation significantly affect surface ozone formation (Coates et al. 2016; Schnell et al. 2009), making summer the most polluted season in most regions. However, the active monsoon activities in summer, especially in the PRD, may increase cloud cover and weaken solar radiation. Ozone formation would be restrained under such a condition (Qu et al. 2021). The heavy rainfall during the monsoon season may also lead to a reduction in surface

ozone pollution. This may help explain the absence of summer ozone peaks in the low-latitude areas, including the PRD. The stronger seasonal variation of solar radiation in high latitude regions may have contributed to a shorter but more distinct ozone season in the NCP. Finally, the intensity of the SI events varies by region. Deep SI events occur more frequently in the high-altitude regions, with some even reaching the ground (Lin et al. 2012; Lin et al. 2016). Consequently, high ozone concentrations could be observed on the Qinghai-Tibetan plateau in spring despite lower levels of ozone precursors and relatively low temperatures.

Although our model generally captured the seasonal variation of ozone in China, we still found a substantial underestimation of high springtime ozone concentrations, especially at the XGLL station (Fig. S1-7). A potential reason for this underestimation is that foreign ozone transport was not well accounted for in our model. According to Ni et al., foreign regions contribute 40%-60% to China's springtime ozone below the height of 2 km (Ni et al. 2018). This enhancement is very prominent in Southwest China due to the massive biomass burning in South and Southeast Asia (Wang et al. 2011), which peaked in spring (Yin 2020). However, incorporating wildfire emissions from South and Southeast Asia by assuming a distance-dependent influence did not address this underestimation (Fig. S1-8). According to Wang et al., the prevailing westerly wind and active cyclonic activity in spring facilitate ozone transport from South Asia to China (Wang et al. 2011). Therefore, foreign wildfire's impact on China's ozone pollution is not determined by distance itself but follows a certain trajectory. We are unable to address this trajectory in the current model because the grid cells did not extend outside China's boundary except for the 50 km buffer.

China experienced rapid economic growth over the past decades. Nevertheless, the contemporary increase in anthropogenic emissions also greatly exacerbated air pollution over the nation.

According to Lin et al., the 95th percentile summer (June-July-August) MDA8 ozone increased by 1-2 ppb per year in China over 1995-2014 and the springtime (March-April-May) median ozone increased by ~0.5 ppb/yr concurrently (Lin et al. 2017). We also observed an overall increasing trend in summertime ozone pollution during 2005-2019 in the whole of China, the NCP, and the YRD as well as an increase in springtime ozone pollution in the NCP (Figs. S1-14 and S16). However, the increasing trend was not constant from year to year. As seen from our model predictions, neither the springtime nor the summer surface ozone concentrations in China exhibited a significant increasing trend over 2005-2013 (Figs. S1-15 and S1-17). These findings were mostly consistent with the TOAR monitoring data (Table S1-2). SDZ was the only TOAR station that observed an increasing trend in summertime ozone pollution over 2005-2013. The increasing trend at SDZ was primarily driven by an increase from 2005-2007 while no significant trend was observed for 2008-2013 (1.30 $\mu g/m^3 * yr^{-1}$, $p = 0.735$). Xu et al. also showed that both the annual highest MDA8 ozone and the annual 4th highest MDA8 ozone exhibited no significant long-term increasing trend for most TOAR stations, except for SDZ (Xu et al. 2020). Although historical monitoring data were lacking back to the early 2000s, it can be inferred that the overall increasing trend of China's ozone pollution during 1995-2014 was primarily driven by an increase before 2005. Tang et al. also reported that the ozone concentrations in Beijing increased at a rate of 1.1 ppbv/yr during 2001-2006 (Tang et al. 2009). The differential trends of ozone pollution between 1995-2004 and 2005-2013 were possibly attributable to meteorological conditions. According to Sun and Wang., the surface temperature in Northern and Northeastern China increased during the 1990s but stabilized during 2005-2014 (Sun and Wang, 2017).

A sharp decrease in ozone concentration was observed in China during 2014-2016, especially in the PRD region. This was not an isolated event in China as the US EPA also reported the second-lowest ozone concentrations on record during the 2014-2016 average period (U.S. EPA 2017). The significant reduction in ozone concentration in the northern hemisphere was attributable to El Niño during this period. Olsen et al. reported that the anomalous cyclonic circulation induced by El Niño events coincided with decreased tropospheric ozone (Olsen et al. 2016). Shen et al. found a negative association between the El Niño-Southern Oscillation (ENSO) and summertime ozone air quality in the south-central states of the US (Shen and Mickley 2017). Although the effect of ENSO on ozone pollution in China has yet to be fully understood, indirect evidence supported the strong impact of climate factors between 2014 and 2016. Yang et al. reported that meteorological conditions contributed to a 10 $\mu g/m^3$ decrease of surface ozone in 2016 and a 3-5 $\mu g/m^3$ decrease in 2014-2015 in the PRD region. (Yang et al. 2019).

The ozone levels in China increased rapidly after 2016 (Fig. 2-6). This may have to do with both China's emission control policies and meteorological conditions. The issuance of APPCAP in 2013 resulted in a dramatic nationwide decrease in NOx emissions and $PM_{2.5}$ levels near the end of this 5-yr plan (Zheng et al. 2018). However, ozone formation falls under the VOC-limited regime in most Chinese urban centers. Reducing NOx emissions became an enhancer of ozone formation in populous areas, which were then transported to other regions (Liu and Wang 2020). In addition, lower $PM_{2.5}$ levels would modify ozone pollution because the photolysis rates were less attenuated by aerosol light scattering and absorption (Liu and Wang 2020). Decreased $PM_{2.5}$ concentrations could also slow down the sink of hydroperoxyl radicals (HO_2), resulting in enhanced ozone production (K Li et al. 2019). Such complex interactions among ozone

formation, $PM_{2.5}$ levels, and meteorological conditions are reflected in the spatially varying associations between ozone and $PM_{2.5}$ concentrations revealed by our partial correlation analysis. The mild weather and year-round intensive human activities cause a long ozone season (March - November) in the YRD. During this period, $PM_{2.5}$ levels can vary from 25 $\mu g/m^3$ to above 60 $\mu g/m^3$, allowing it to affect ozone production negatively. The PRD region was the cleanest affluent city cluster in China in terms of both $PM_{2.5}$ and ozone. The effect of $PM_{2.5}$ on ozone production was less notable, and $PM_{2.5}$ and ozone concentrations were both positively correlated to the emissions of their precursors (Liu and Wang 2020). While $PM_{2.5}$ levels in the NCP are high in winter, its cold winter strongly suppresses ozone formation, and no significant correlation was found between ozone and $PM_{2.5}$ levels after controlling for meteorological conditions. The 2018-2019 increase in surface ozone pollution in China was more likely to be driven by climatological factors, particularly the increased foehn wind frequency and the subsequent changes in temperature and relative humidity (Li et al. 2020). That explained why this round of increase was only seen in several regions by the CNEMC monitoring data (Fig. 2-7). Again, although ozone pollution in China is not consistently worsening from year to year due to the modulation of climatological factors, it generally exhibited a prominent long-term increasing trend (Lin et al. 2017; Xu et al. 2020). Controlling ozone pollution in China remains a challenging task that requires a better understanding of this air pollutant.

Our study has a few limitations. First, the road network data was fixed over the study period. This may result in an underestimation of China's road density, especially after 2010. Although there are alternative road length data, we prefer not to mix multiple datasets with different methodologies to avoid introducing systematic errors. Second, the ozone precursors included in

our model were limited to NOx. Satellite retrievals of VOCs are limited and often have weak signal-to-noise ratios in the boundary layer (Zhu et al. 2020). While our current model was able to identify regions under the VOC-limited regime of ozone production, we will continue to explore effective indicators of ground-level VOC to improve our ozone exposure model. Finally, the present study focused on domestic determinants of ambient ozone. The present model may underestimate ozone pollution attributable to foreign transport. Future users of our dataset should be cautious with the springtime underestimations, especially in Southwest China. The roles of long-range ozone transport from outside China warrants further investigation.

2.6. Conclusions

We used a data-driven modeling framework to estimate long-term, high-resolution ozone concentrations in China. Predictors that capture the influence of ozone photochemical reactions and SI were included in our model. This model produced reliable historical monthly mean MDA8 ozone concentrations for China at 0.05° resolution with little bias. This 15-yr long, full-coverage national dataset of ambient ozone concentrations includes nine years before China's regulatory air quality monitoring network existed. It could accelerate research on the long-term ozone health effects in China by enabling the use of large general population cohorts established in the 2000s, such as the Chinese Longitudinal Healthy Longevity Survey (Kuang et al. 2020) and the China Health and Retirement Longitudinal Study (Zhao et al. 2014).

2.7. Acknowledgments

This work was supported by the National Institute of Environmental Health Sciences of the National Institutes of Health (Award # R01-ES027892). The content is solely the responsibility of the authors and does not necessarily represent the official views of NIH.

2.8. References

Adam-Poupart A, Brand A, Fournier M, Jerrett M, Smargiassi A. 2014. Spatiotemporal modeling of ozone levels in Quebec (Canada): a comparison of kriging, land-use regression (LUR), and combined Bayesian maximum entropy-LUR approaches. Environ Health Perspect 122:970-976, PMID: 24879650,https://doi.org/10.1289/ehp.1306566.

Altmann A, Toloşi L, Sander O, Lengauer T. 2010. Permutation importance: a corrected feature importance measure. Bioinformatics 26:1340-1347, PMID: 20385727,https://doi.org/10.1093/bioinformatics/btq134.

Anenberg S, C., Henze Daven K, Tinney V, Kinney Patrick L, Raich W, Fann N, et al. 2018. Estimates of the global burden of ambient PM2.5, ozone, and NO2 on asthma incidence and emergency room visits. Environ Health Perspect 126:107004, PMID: 30392403, https://doi.org/10.1289/EHP3766.

Appenzeller C, Holton JR, Rosenlof KH. 1996. Seasonal variation of mass transport across the tropopause, J Geophys Res 101:15071-15078. https://doi.org/10.1029/96JD00821.

Atkinson RW, Butland BK, Dimitroulopoulou C, Heal MR, Stedman JR, Carslaw N, et al. 2016. Long-term exposure to ambient ozone and mortality: a quantitative systematic review and meta-analysis of evidence from cohort studies, BMJ Open 6:e009493. PMID: 26908518, https://doi.org/10.1136/bmjopen-2015-009493.

Barry V, Klein M, Winquist A, Chang HH, Mulholland JA, Talbott EO, et al. 2019. Characterization of the concentration-response curve for ambient ozone and acute respiratory morbidity in 5 US cities. J Expo Sci Environ Epidemiol 29:267-277, PMID: 2991524, https://doi.org/10.1038/s41370-018-0048-7.

CDS. 2021. Land cover classification gridded maps from 1992 to present derived from satellite observations. https://cds.climate.copernicus.eu/cdsapp#!/dataset/satellite-land-cover?tab=overview. [accessed 21 July 2021].

C3S. 2021. Product user guide and specification for ICDR land cover 2016-2020. https://datastore.copernicus-climate.eu/documents/satellite-land-cover/D5.3.1_PUGS_ICDR_LC_v2.1.x_PRODUCTS_v1.1.pdf. [accessed 4 August 2021].

Center for International Earth Science Information Network - CIESIN - Columbia University, and Information Technology Outreach Services - ITOS - University of Georgia. 2013. Global Roads Open Access Data Set, Version 1 (gROADSv1). Palisades, NY: NASA Socioeconomic Data and Applications Center (SEDAC). https://doi.org/10.7927/H4VD6WCT. [accessed 1 January 2021].

Clifton OE, Fiore AM, Massman WJ, Baublitz CB, Coyle M, Emberson L, et al. 2020. Dry deposition of ozone over land: processes, measurement, and modeling. Rev Geophys 58:e2019RG000670, PMID: 33748825, https://doi.org/10.1029/2019RG000670.

CNEMC. 2012. Ambient air quality standards. http://www.cnemc.cn/jcgf/dqhj/201711/W020181008687883046768.pdf [accessed 1 August 2021].

Coates J, Mar KA, Ojha N, Butler TM. 2016. The influence of temperature on ozone production under varying NOx conditions – a modelling study. Atmos Chem Phys 16:11601-11615, https://doi.org/10.5194/acp-16-11601-2016.

DeCaria AJ, Pickering KE, Stenchikov GL, Ott LE. 2005. Lightning-generated NOx and its impact on tropospheric ozone production: a three-dimensional modeling study of a stratosphere-troposphere experiment: radiation, aerosols and ozone (STERAO-A) thunderstorm. J Geophys Res 110, https://doi.org/10.1029/2004JD005556.

Di Q, Rowland S, Koutrakis P, Schwartz J. 2017. A hybrid model for spatially and temporally resolved ozone exposures in the continental United States. J Air Waste Manag Assoc 67:39-52, PMID: 27332675, https://doi.org/10.1080/10962247.2016.1200159.

ESA. Land Cover CCI Product User Guide Version 2. Tech. Rep. (2017). maps.elie.ucl.ac.be/CCI/viewer/download/ESACCI-LC-Ph2-PUGv2_2.0.pdf. [accessed 1 January 2021].
Finney DL, Doherty RM, Wild O, Young PJ, Butler A. 2016. Response of lightning NOx emissions and ozone production to climate change: insights from the Atmospheric Chemistry and Climate Model Intercomparison Project. Geophys Res Lett 43:5492-5500, https://doi.org/10.1002/2016GL068825.
Fischer EV, Jacob DJ, Yantosca RM, Sulprizio MP, Millet DB, Mao J, et al. 2014. Atmospheric peroxyacetyl nitrate (PAN): a global budget and source attribution. Atmos Chem Phys 14:2679-2698, PMID: 33758588, https://doi.org/10.5194/acp-14-2679-2014.
Fishman J, Larsen JC. 1987. Distribution of total ozone and stratospheric ozone in the tropics: implications for the distribution of tropospheric ozone. J Geophys Res 92:6627-6634, https://doi.org/10.1029/JD092iD06p06627.
Gelaro R, McCarty W, Suárez MJ, Todling R, Molod A, Takacs L, et al. 2017. The Modern-Era Retrospective Analysis for Research and Applications, version 2 (MERRA-2). J Climate 30:5419-5454, https://doi.org/10.1175/JCLI-D-16-0758.1.
Hayashida S, Liu X, Ono A, Yang K, Chance K. 2015. Observation of ozone enhancement in the lower troposphere over East Asia from a space-borne ultraviolet spectrometer. Atmos Chem Phys 15:9865-9881., https://doi.org/10.5194/acp-15-9865-2015.
Huang G, Liu X, Chance K, Yang K, Bhartia PK, Cai Z, et al. 2017. Validation of 10-year SAO Omi ozone profile (PROFOZ) product using ozonesonde observations. Atmos Meas Tech 10:2455-2475, https://doi.org/10.5194/amt-10-2455-2017.
Huang J, Pan X, Guo X, Li G. 2018. Health impact of China's Air Pollution Prevention and Control Action Plan: an analysis of national air quality monitoring and mortality data. Lancet Planet Health 2:e313-e323, PMID: 30074894, https://doi.org/10.1016/S2542-5196(18)30141-4.
Itahashi S, Mathur R, Hogrefe C, Zhang Y. 2020. Modeling stratospheric intrusion and trans-Pacific transport on tropospheric ozone using hemispheric CMAQ during April 2010 – Part 1: model evaluation and air mass characterization for stratosphere–troposphere transport. Atmos Chem Phys 20:3373-3396, https://doi.org/10.5194/acp-20-3373-2020.
Jhun I, Coull BA, Zanobetti A, Koutrakis P. 2015. The impact of nitrogen oxides concentration decreases on ozone trends in the USA. Air Qual Atmos Health 8:283-292, PMID: 27547271, https://doi.org/10.1007/s11869-014-0279-2
Kang D, Mathur R, Pouliot GA, Gilliam RC, Wong DC. 2020. Significant ground-level ozone attributed to lightning-induced nitrogen oxides during summertime over the Mountain West States. npj Clim Atmos Sci 3:6, PMID: 32181370, https://doi.org/10.1038/s41612-020-0108-2
Kigathi RN, Weisser WW, Reichelt M, Gershenzon J, Unsicker SB. 2019. Plant volatile emission depends on the species composition of the neighboring plant community. BMC Plant Biol 19:58, PMID: 30727963, https://doi.org/10.1186/s12870-018-1541-9
Kim PS, Jacob DJ, Liu X, Warner JX, Yang K, Chance K, et al. 2013. Global ozone–CO correlations from OMI and AIRS: constraints on tropospheric ozone sources. Atmos Chem Phys 13:9321-9335, https://doi.org/10.5194/acp-13-9321-2013
Knowland KE, Ott LE, Duncan BN, Wargan K. 2017. Stratospheric intrusion-influenced ozone air quality exceedances investigated in the NASA MERRA-2 Reanalysis. Geophys Res Lett 44:10,691-610,701, PMID: 32692318, https://doi.org/10.1002/2017gl074532
Krotkov NA, Lamsal LN, Celarier EA, Swartz WH, Marchenko SV, Bucsela EJ, et al. 2017. The version 3 OMI NO2 standard product. Atmos Meas Tech 10:3133-3149, https://doi.org/10.5194/amt-10-3133-2017
Kuang W, Gao M, Tian L, Wan Y, Qiu P. 2020. Trends in the prevalence of cognitive impairment in Chinese older adults: Based on the Chinese Longitudinal Healthy Longevity Survey cohorts from 1998 to 2014. Int Health 12:378-387, PMID: 31967316, https://doi.org/10.1093/inthealth/ihz114

Lelieveld J, Dentener FJ. 2000. What controls tropospheric ozone? J Geophys Res 105:3531-3551, https://doi.org/10.1029/1999JD901011
Levelt PF, Oord GHJvd, Dobber MR, Malkki A, Huib V, Johan de V, et al. 2006. The Ozone Monitoring Instrument. IEEE Transactions on Geoscience and Remote Sensing 44:1093-1101, https://doi.org/10.1109/TGRS.2006.872333.
Li F, Zhang X, Roy DP, Kondragunta S. 2019. Estimation of biomass-burning emissions by fusing the fire radiative power retrievals from polar-orbiting and geostationary satellites across the conterminous United States. Atmos Environ 211:274-287, https://doi.org/10.1016/j.atmosenv.2019.05.017.
Li K, Jacob DJ, Liao H, Shen L, Zhang Q, Bates KH. 2019. Anthropogenic drivers of 2013–2017 trends in summer surface ozone in China. P Natl Acad Sci USA 116:422-427, PMID: 30598435, https://doi.org/10.1073/pnas.1812168116.
Li K, Jacob DJ, Shen L, Lu X, De Smedt I, Liao H. 2020. Increases in surface ozone pollution in China from 2013 to 2019: Anthropogenic and meteorological influences. Atmos Chem Phys 20:11423-11433, https://doi.org/10.5194/acp-20-11423-2020.
Liang F, Xiao Q, Huang K, Yang X, Liu F, Li J, et al. 2020. The 17-y spatiotemporal trend of PM2.5 and its mortality burden in China. P Natl Acad Sci USA 117:25601, PMID: 32958653, https://doi.org/10.1073/pnas.1919641117.
Lin M, Fiore AM, Cooper OR, Horowitz LW, Langford AO, Levy II H, et al. 2012. Springtime high surface ozone events over the western United States: quantifying the role of stratospheric intrusions. J Geophys Res 117, https://doi.org/10.1029/2012JD018151.
Lin M, Su L, Shaheen R, Fung JCH, Thiemens MH. 2016. Detection of deep stratospheric intrusions by cosmogenic 35S. P Natl Acad Sci USA 113:11131-11136. PMID: 27655890, https://doi.org/10.1073/pnas.1609919113.
Lin M, Horowitz LW, Payton R, Fiore AM, Tonnesen G. 2017. US surface ozone trends and extremes from 1980 to 2014: Quantifying the roles of rising Asian emissions, domestic controls, wildfires, and climate. Atmos Chem Phys 17:2943-2970, https://doi.org/10.5194/acp-17-2943-2017.
Liu R, Ma Z, Liu Y, Shao Y, Zhao W, Bi J. 2020. Spatiotemporal distributions of surface ozone levels in China from 2005 to 2017: A machine learning approach. Environ Int 142:105823, PMID: 32521347, https://doi.org/10.1016/j.envint.2020.105823.
Liu X-H, Zhang Y, Xing J, Zhang Q, Wang K, Streets DG, et al. 2010. Understanding of regional air pollution over China using CMAQ, part II. Process analysis and sensitivity of ozone and particulate matter to precursor emissions. Atmos Environ 44:3719-3727, https://doi.org/10.1016/j.atmosenv.2010.03.036.
Liu X, Bhartia PK, Chance K, Spurr RJD, Kurosu TP. 2010. Ozone profile retrievals from the Ozone Monitoring Instrument. Atmos Chem Phys 10:2521-2537, https://doi.org/10.1029/2005JD006240.
Liu Y, Wang T. 2020. Worsening urban ozone pollution in China from 2013 to 2017 – part 2: the effects of emission changes and implications for multi-pollutant control. Atmos Chem Phys 20:6323-6337, https://doi.org/10.5194/acp-20-6323-2020.
Lu X, Zhang L, Yue X, Zhang J, Jaffe DA, Stohl A, et al. 2016. Wildfire influences on the variability and trend of summer surface ozone in the mountainous western United States. Atmos Chem Phys 16:14687-14702, https://doi.org/10.5194/acp-16-14687-2016.
Lu X, Zhang L, Chen Y, Zhou M, Zheng B, Li K, et al. 2019a. Exploring 2016–2017 surface ozone pollution over China: source contributions and meteorological influences. Atmos Chem Phys 19:8339-8361, https://doi.org/10.5194/acp-19-8339-2019.
Lu X, Zhang L, Shen L. 2019b. Meteorology and climate influences on tropospheric ozone: a review of natural sources, chemistry, and transport patterns. Current Pollution Reports 5:238-260, https://doi.org/10.1007/s40726-019-00118-3.

Lu X, Zhang L, Wang X, Gao M, Li K, Zhang Y, et al. 2020. Rapid Increases in Warm-Season Surface Ozone and Resulting Health Impact in China Since 2013. Environ Sci Tech Let 7(4), 240-247. https://doi.org/10.1021/acs.estlett.0c00171.

Lyu C, Capps SL, Hakami A, Zhao S, Resler J, Carmichael GR, et al. 2019. Elucidating emissions control strategies for ozone to protect human health and public welfare within the continental United States. Environ Res Lett 14(12), 124093. https://doi.org/10.1088/1748-9326/ab5e05

MODIS Collection 6 Hotspot / Active Fire Detections MCD14ML distributed from NASA FIRMS. https://earthdata.nasa.gov/firms [accessed 15 July 2021],
https://doi.org/10.5067/FIRMS/MODIS/MCD14ML.

Monks PS. 2005. Gas-phase radical chemistry in the troposphere. Chem Soc Rev 34:376-395, PMID: 15852151, https://doi.org/10.1039/b307982c.

Murray LT, Jacob DJ, Logan JA, Hudman RC, Koshak WJ. 2012. Optimized regional and interannual variability of lightning in a global chemical transport model constrained by LIS/OTD satellite data. J Geophys Res-Atmos 117, https://doi.org/10.1029/2012JD017934.

NASA/METI/AIST/Japan Spacesystems and U.S./Japan ASTER Science Team. 2019. ASTER Global Digital Elevation Model V003. NASA EOSDIS Land Processes DAAC. https://doi.org/10.5067/ASTER/ASTGTM.003. [accessed 1 January 2021].

NBS (National Bureau of Statistics). 2008. http://www.stats.gov.cn/tjsj/pcsj/rkpc/5rp/html/append7.htm [accessed 26 July 2021].

Ni R, Lin J, Yan Y, Lin W. 2018. Foreign and domestic contributions to springtime ozone over China. Atmos Chem Phys 18:11447-11469, https://doi.org/10.5194/acp-18-11447-2018

Nuvolone D, Petri D, Voller F. 2018. The effects of ozone on human health. Environ Sci Pollut Res Int 25:8074-8088, PMID: 28547375, https://doi.org/10.1007/s11356-017-9239-3.

Olsen MA, Wargan K, Pawson S. 2016. Tropospheric column ozone response to ENSO in GEOS-5 assimilation of OMI and MSL ozone data. Atmos Chem Phys 16:7091-7103, https://doi.org/10.5194/acp-16-7091-2016

Pu X, Wang TJ, Huang X, Melas D, Zanis P, Papanastasiou DK, et al. 2017. Enhanced surface ozone during the heat wave of 2013 in Yangtze River Delta region, China. Sci Total Environ 603-604:807-816, PMID: 28442137, https://doi.org/10.1016/j.scitotenv.2017.03.056.

Qu K, Wang X, Yan Y, Shen J, Xiao T, Dong H, et al. 2021. A comparative study to reveal the influence of typhoons on the transport, production and accumulation of O3 in the Pearl River Delta, China. Atmos Chem Phys 21:11593-11612, https://doi.org/10.5194/acp-21-11593-2021.

Schnell RC, Oltmans SJ, Neely RR, Endres MS, Molenar JV, White AB. 2009. Rapid photochemical production of ozone at high concentrations in a rural site during winter. Nat Geosci 2:120-122, https://doi.org/10.1038/ngeo415.

Seltzer KM, Shindell DT, Malley CS. 2018. Measurement-based assessment of health burdens from long-term ozone exposure in the United States, Europe, and China. Environ Res Lett 13:104018, https://doi.org/10.1088/1748-9326/aae29d.

Shen L, Mickley LJ. 2017. Effects of El Niño on summertime ozone air quality in the Eastern United States. Geophys Res Lett 44:12,543-512,550, PMID: 29622852, https://doi.org/10.1002/2017GL076150.

Shen L, Jacob DJ, Liu X, Huang G, Li K, Liao H, et al. 2019. An evaluation of the ability of the Ozone Monitoring Instrument (OMI) to observe boundary layer ozone pollution across China: application to 2005–2017 ozone trends. Atmos Chem Phys 19:6551-6560, https://doi.org/10.5194/acp-19-6551-2019.

Sun B, Wang H. 2017. A trend towards a stable warm and windless state of the surface weather conditions in northern and northeastern China during 1961–2014. Adv Atmos Sci 34(6), 713-726, https://doi.org/10.1007/s00376-017-6252-x.

Tang G, Li X, Wang Y, Xin J, Ren X. 2009. Surface ozone trend details and interpretations in Beijing, 2001–2006. Atmos Chem Phys 9(22), 8813-8823, https://doi.org/10.5194/acp-9-8813-2009.

Turner MC, Jerrett M, Pope CA, 3rd, Krewski D, Gapstur SM, Diver WR, et al. 2016. Long-term ozone exposure and mortality in a large prospective study. Am J Respir Crit Care Med 193:1134-1142, PMID: 26680605, https://doi.org/10.1164/rccm.201508-1633OC.
United States Environmental Protection Agency (U.S. EPA). 2017. Ambient Concentrations of Ozone. https://cfpub.epa.gov/roe/indicator.cfm?i=8. [accessed 10 January 2021].
Wang T, Xue L, Brimblecombe P, Lam YF, Li L, Zhang L. 2017. Ozone pollution in China: A review of concentrations, meteorological influences, chemical precursors, and effects. Sci Total Environ 575:1582-1596, PMID: **27789078,** https://doi.org/10.1016/j.scitotenv.2016.10.081.
Wang Y, Zhang Y, Hao J, Luo M. 2011. Seasonal and spatial variability of surface ozone over China: Contributions from background and domestic pollution. Atmos Chem Phys 11:3511-3525, https://doi.org/10.5194/acp-11-3511-2011.
Wang Y, Gao W, Wang S, Song T, Gong Z, Ji D, et al. 2020. Contrasting trends of PM2.5 and surface-ozone concentrations in China from 2013 to 2017. Natl Sci Rev 7:1331-1339, PMID: 34692161, https://doi.org/10.1093/nsr/nwaa032.
Wang Y, Wang H, Wang W. 2020. A stratospheric intrusion-influenced ozone pollution episode associated with an intense horizontal-trough event. Atmosphere 11:164, https://doi.org/10.3390/atmos11020164.
Wargan K, Labow G, Frith S, Pawson S, Livesey N, Partyka G. 2017. Evaluation of the ozone fields in NASA's MERRA-2 reanalysis. Journal of Climate 30:2961-2988, https://doi.org/10.1175/JCLI-D-16-0699.1.
Wooster MJ, Zhukov B, Oertel D. 2003. Fire radiative energy for quantitative study of biomass burning: Derivation from the BIRD experimental satellite and comparison to MODIS fire products. Remote Sens Environ 86:83-107, https://doi.org/10.1016/S0034-4257(03)00070-1.
Xiao Q, Geng G, Liang F, Wang X, Lv Z, Lei Y, et al. 2020. Changes in spatial patterns of PM2.5 pollution in China 2000–2018: impact of clean air policies. Environ int 141:105776, PMID: 32402983, https://doi.org/10.1016/j.envint.2020.105776.
Xiao Q, Liang F, Ning M, Zhang Q, Bi J, He K, et al. 2021. The long-term trend of PM2.5-related mortality in China: the effects of source data selection. Chemosphere 263:127894, PMID: 32814138, https://doi.org/10.1016/j.chemosphere.2020.127894.
Xie F, Li J, Tian W, Zhang J, Shu J. 2014. The impacts of two types of El Niño on global ozone variations in the last three decades. Advances in Atmospheric Sciences 31:1113-1126, https://doi.org/10.1007/s00376-013-3166-0.
Xu X, Lin W, Xu W, Jin J, Wang Y, Zhang G, et al. 2020. Long-term changes of regional ozone in China: implications for human health and ecosystem impacts. Elementa: Science of the Anthropocene 8, https://doi.org/10.1525/elementa.409.
Yang L, Luo H, Yuan Z, Zheng J, Huang Z, Li C, et al. 2019. Quantitative impacts of meteorology and precursor emission changes on the long-term trend of ambient ozone over the Pearl River Delta, China, and implications for ozone control strategy. Atmos Chem Phys 19:12901-12916, https://doi.org/10.5194/acp-19-12901-2019.
Yin P, Chen R, Wang L, Meng X, Liu C, Niu Y, et al. 2017. Ambient ozone pollution and daily mortality: a nationwide study in 272 Chinese cities. Environ Health Perspect 125:117006, PMID: 29212061, https://doi.org/10.1289/EHP1849.
Yin S. 2020. Biomass burning spatiotemporal variations over South and Southeast Asia. Environ Int 145:106153, PMID: 33002702, https://doi.org/10.1016/j.envint.2020.106153.
Zhao Y, Hu Y, Smith JP, Strauss J, Yang G. 2014. Cohort profile: the China Health and Retirement Longitudinal Study (CHARLS). Int J Epidemiol 43:61-68, PMID: 23243115, https://doi.org/10.1093/ije/dys203.
Zheng B, Tong D, Li M, Liu F, Hong C, Geng G, et al. 2018. Trends in China's anthropogenic emissions since 2010 as the consequence of clean air actions. Atmos Chem Phys 18:14095-14111, https://doi.org/10.5194/acp-18-14095-2018.

Zhu L, González Abad G, Nowlan CR, Chan Miller C, Chance K, Apel EC, et al. 2020. Validation of satellite formaldehyde (HCHO) retrievals using observations from 12 aircraft campaigns. Atmos Chem Phys 20:12329-12345, https://doi.org/10.5194/acp-20-12329-2020.

2.9. Figures

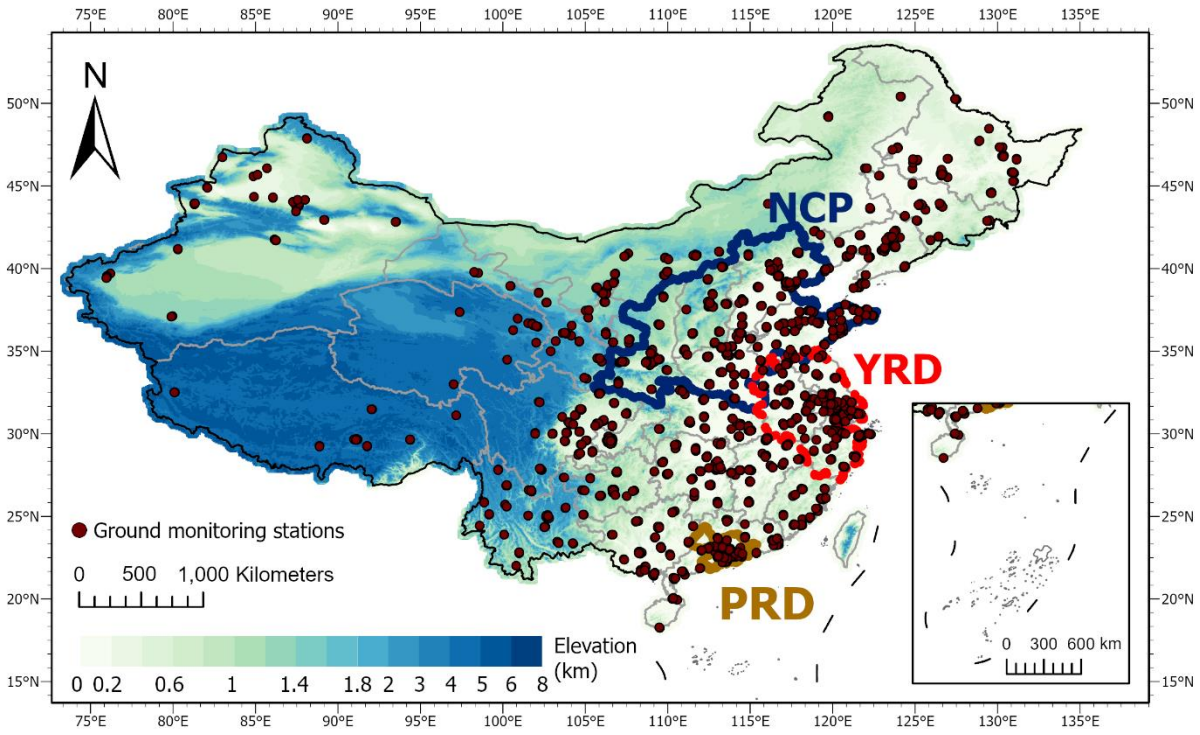

Fig. 2-1. The study domain and three major city clusters. The study domain covered China plus a 50 km buffer region that extends outside the national boundary. NCP: the North China Plain; YRD: the Yangtze River Delta region; PRD: the Pearl River Delta (PRD) region. The points are the location of the China National Environmental Monitoring Centre (CNEMC) monitoring sites. The color scale represents elevation (km).

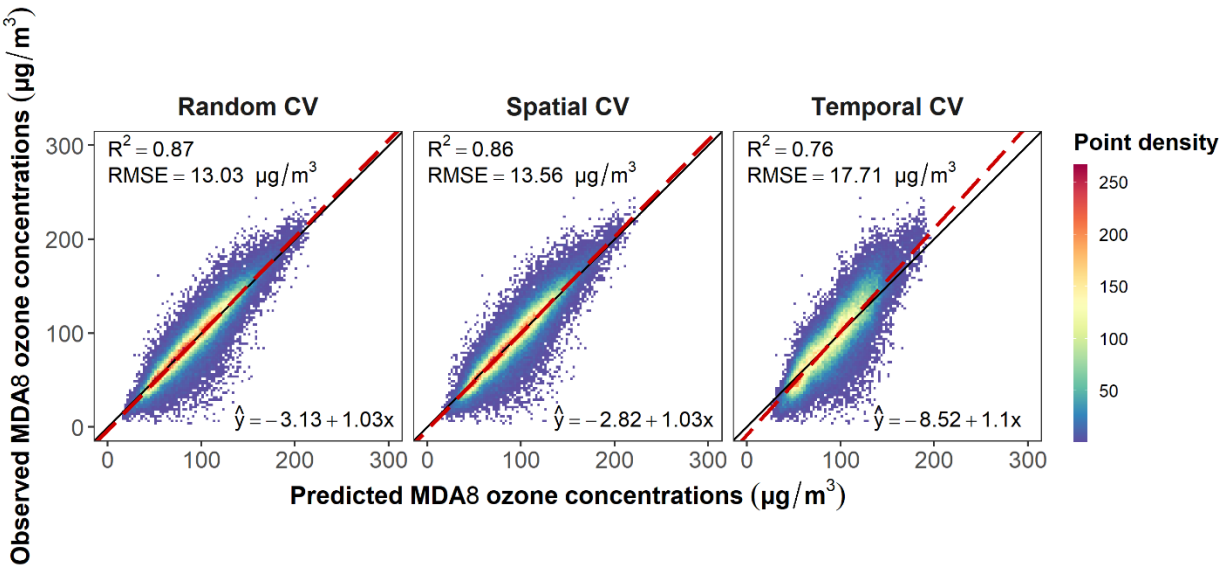

Fig. 2-2. The integrated model performance of the original model with OMI L24 retrieval. Left panel: random CV; middle panel: spatial CV; right panel: temporal CV. The functions on the bottom-right corners are the regression functions between the predicted and observed monthly mean MDA8 ozone concentrations. Red dashed lines: the regression line between the predictions and observations; black solid lines: the x = y line; The color scale represents the density of the points. Abbreviations: CV, cross-validation; MDA8, daily maximum 8-hour average; OMI, Ozone Monitoring Instrument.

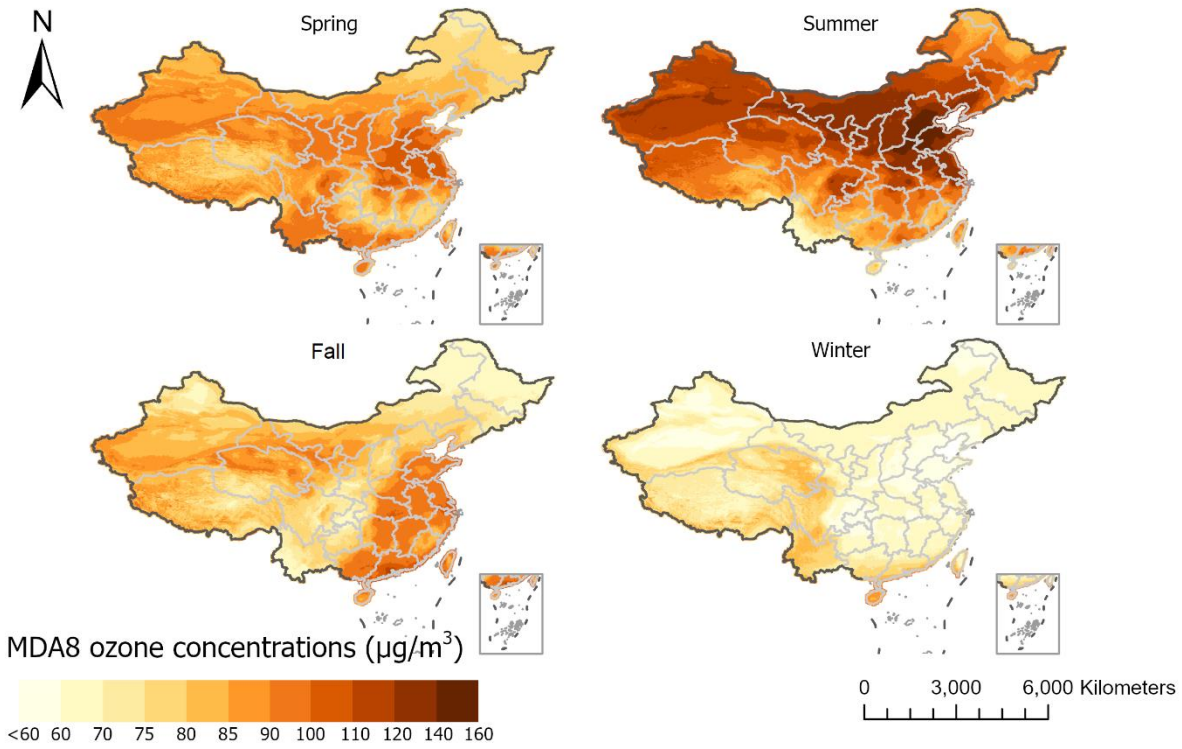

Fig. 2-3. Spatial distribution of seasonal average MDA8 ozone concentrations during 2005-2019. The ozone concentrations were predicted by the original model with OMI L24 retrieval and averaged seasonally over 2005-2019. Spring: March-April-May; summer: June-July-August; autumn: September- October- November; winter: December-January-February. Abbreviations: OMI, Ozone Monitoring Instrument; MDA8, daily maximum 8-hour average.

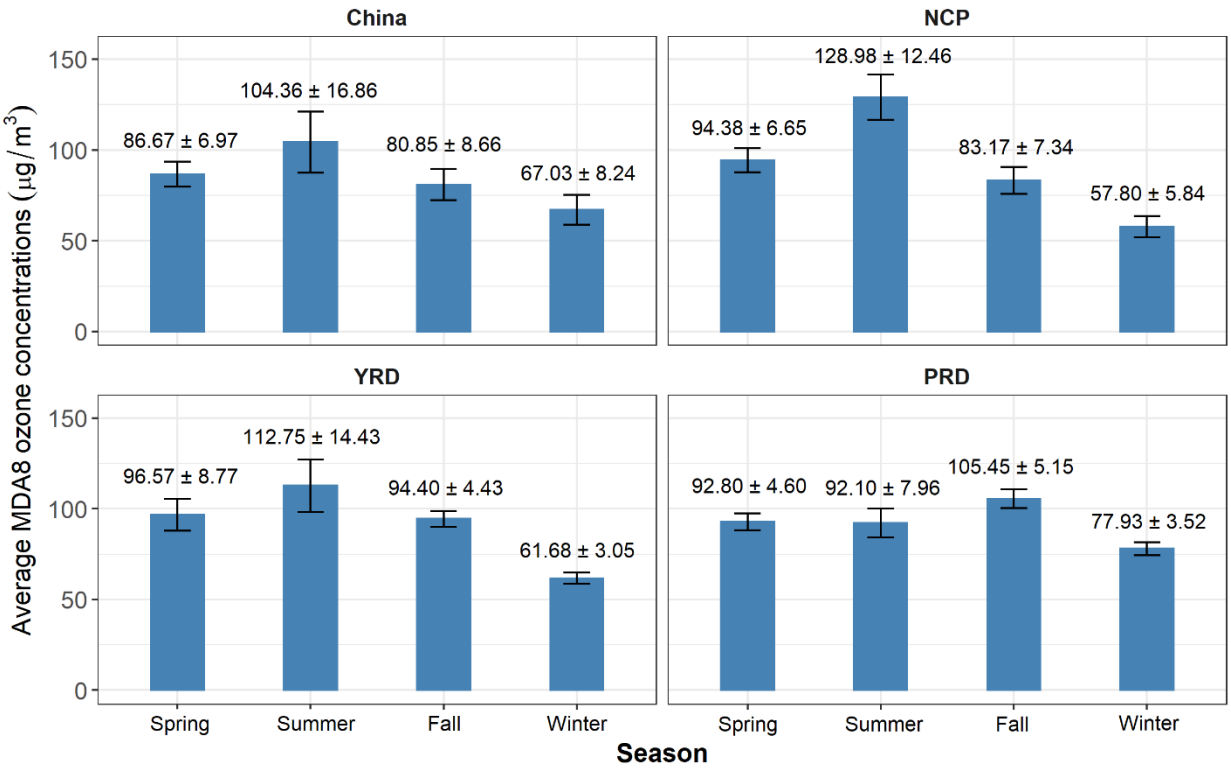

Fig. 2-4. Region-specific seasonal mean MDA8 ozone concentrations during 2005-2019. The ozone concentrations were predicted by the original model with OMI L24 retrievals. The bars and the corresponding numbers represent the season-specific regional mean MDA8 ozone concentrations (± standard deviation) over 2005-2019. Spring: March-April-May; summer: June-July-August; autumn: September- October- November; winter: December-January-February. Abbreviations: OMI, Ozone Monitoring Instrument; MDA8, daily maximum 8-hour average.

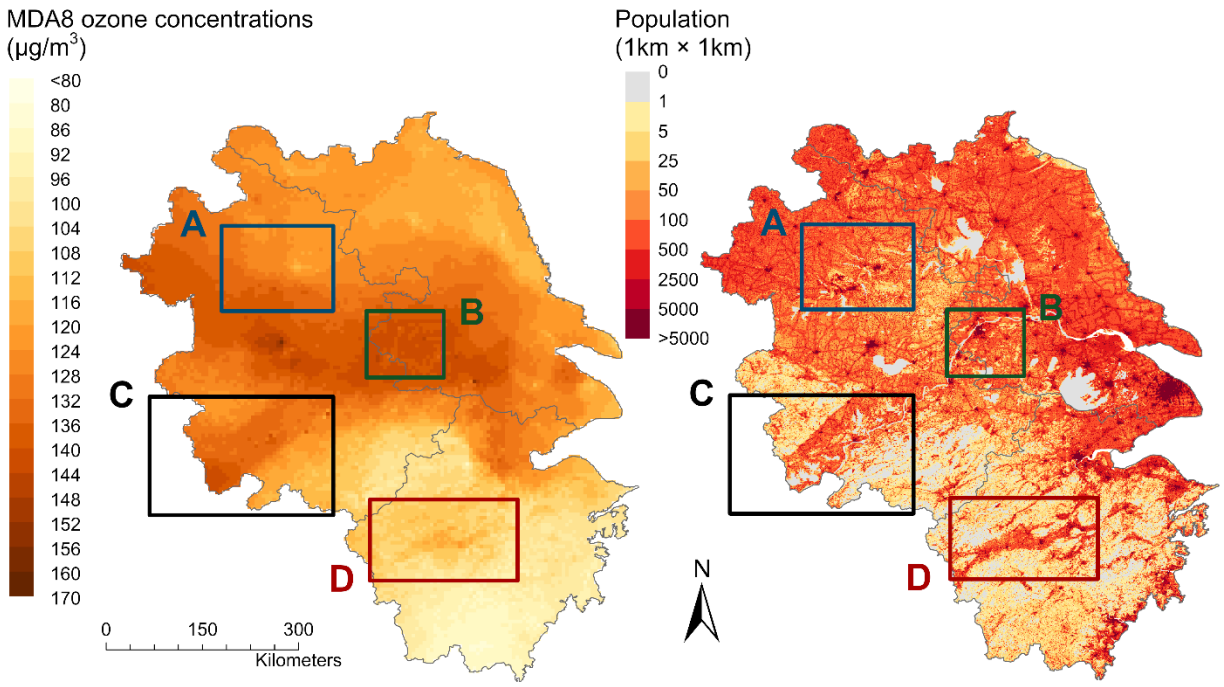

Fig. 2-5. Summer ozone peak (left) and population (right) in the Yangtze River Delta (August 2019). The left panel shows the model predicted monthly mean MDA8 ozone concentrations in August 2019. The right panel shows the 1 km population data for 2019 from LandScan. The boxes represent some YRD cities and their surrounding area; A: Bengbu and Huainan City; B: Nanjing Metropolitan Area; C: Anqing City; D: Quzhou and Jinhua City. Abbreviations: MDA8, daily maximum 8-hour average.

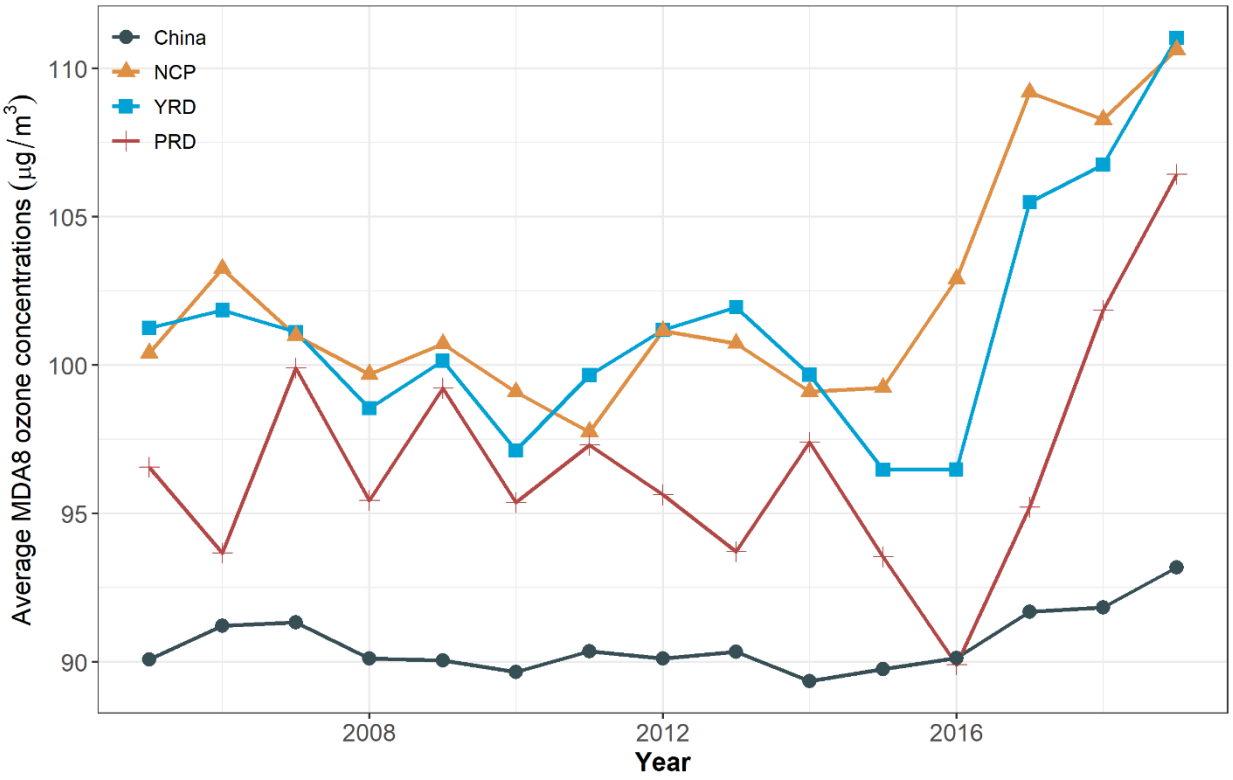

Fig. 2-6. Annual trend of mean ozone season average MDA8 ozone concentrations from 2005 to 2019. Ozone season is defined as March-November. The lines with different colors and marks represent the model-predicted mean MDA8 ozone concentrations in different regions. Grey line with round marks: China; red line with cross marks: the PRD; orange line with triangular marks: the NCP; blue line with square marks: the YRD. Abbreviations: MDA8, daily maximum 8-hour average; NCP: the North China Plain; PRD: the Pearl River Delta; YRD: the Yangtze River Delta.

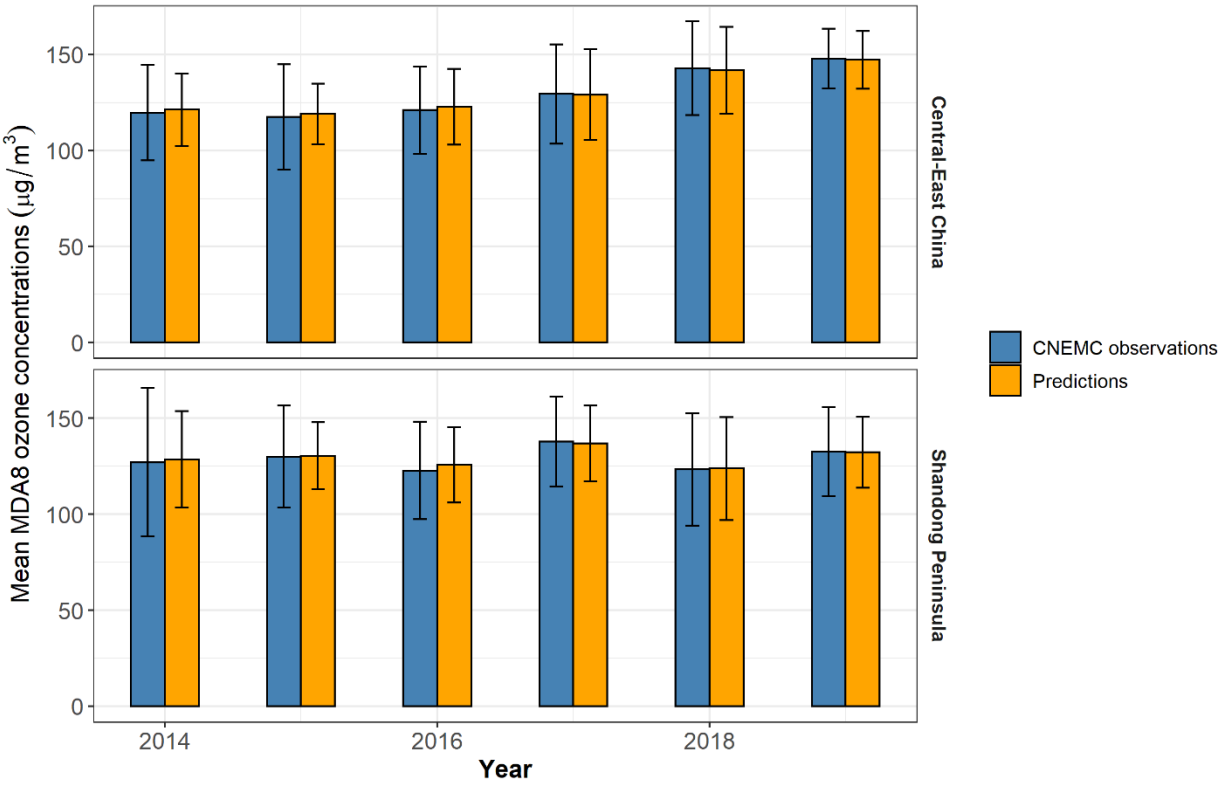

Fig. 2-7. The comparison of the summertime (June-July-August) mean MDA8 ozone concentrations between our model predictions and the CNEMC monitoring data over 2014-2019 for selected regions. Upper panel: Central-East China; Lower panel: the Shandong Peninsula. The blue columns on the left represent the CNEMC observations; the orange column on the right represents our model predictions. The height of the columns and the error bars represent the mean MDA8 ozone concentrations and the standard error. Abbreviations: CNEMC, China National Environmental Monitoring Centre; MDA8, daily maximum 8-hour average; NCP: the North China Plain; PRD: the Pearl River Delta; YRD: the Yangtze River Delta.

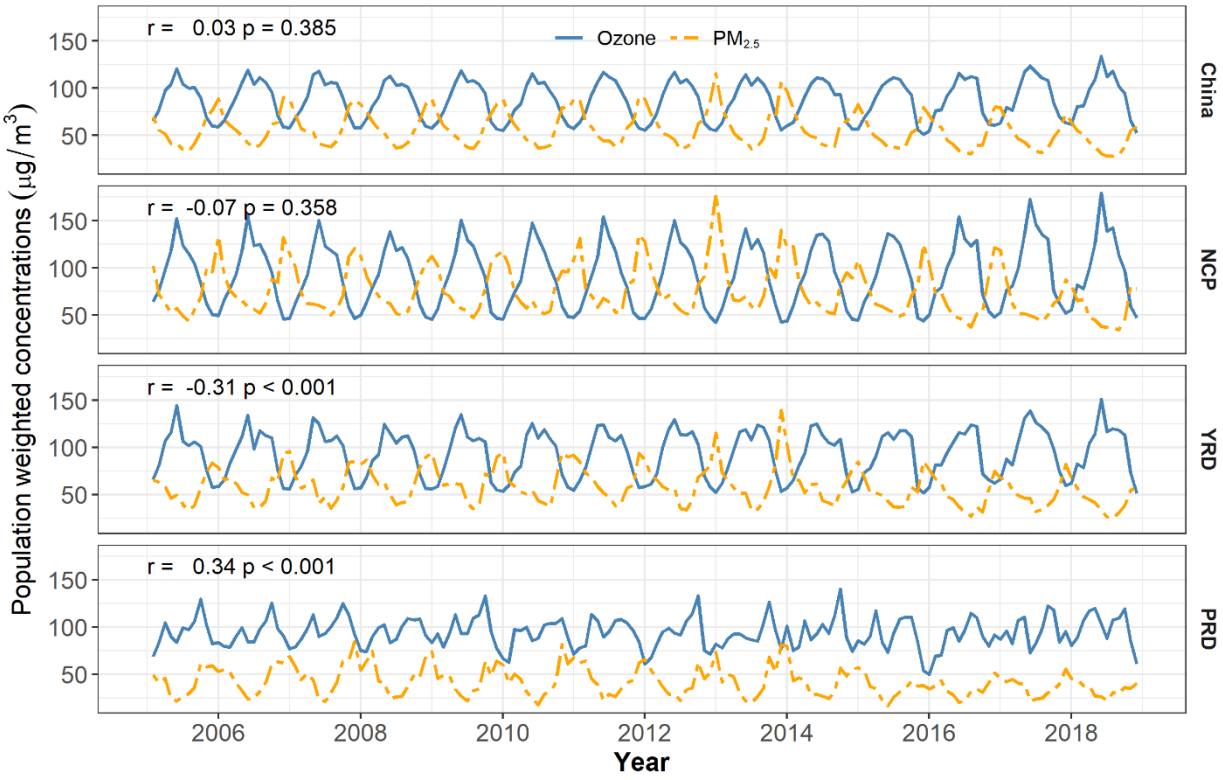

Fig. 2-8. Time-series comparison for population-weighted ambient ozone and $PM_{2.5}$ concentrations in China over 2005-2018. First (from top to bottom) panel: China as a whole; second panel: the NCP; third panel: the YRD; last panel: the PRD; r denotes the partial correlation coefficient controlling for temperature, relative humidity, and total precipitation from MERRA-2. P-values were for the r statistics on the left. Blue lines: population-weighted monthly mean MDA8 ozone predicted by our model; orange lines: population-weighted monthly mean $PM_{2.5}$ concentrations from (Xiao et al. 2021). Abbreviations: MDA8, daily maximum 8-hour average; NCP: the North China Plain; PRD: the Pearl River Delta; YRD: the Yangtze River Delta.

3. Air pollution and cognitive impairment among the Chinese elderly population: A Nationwide cohort study

[Manuscript 2]

Qingyang Zhu, Yuebin Lyu, Keyong Huang, Jinhui Zhou, Wenhao Wang, Kyle Steenland, Howard H. Chang, Stefanie Ebelt, Xiaoming Shi, and Yang Liu

3.1. Abstract

Background: Cognitive decline and dementia have long been recognized as growing public health threats, especially in an aging society. Studies have found that air pollution is a potential risk factor for dementia, but the association between air pollution and cognitive impairment has not been fully understood.

Objectives: This study aimed to evaluate the association between three major air pollutants (i.e., $PM_{2.5}$, O_3, and NO_2) and cognitive impairment among the Chinese elderly population.

Methods: Study participants were selected from the Chinese Longitudinal Health Longevity Survey (CLHLS) after 2005. We define cognitive impairment as a Chinese Mini-Mental-State Exam (CMMSE) score lower than 24. Yearly mean exposure to $PM_{2.5}$, NO_2, and warm-season (April-September) average MDA8 O_3 were evaluated by assigning three high-performance satellite remote sensing models to the participants' residential addresses. The association between air pollution and cognitive impairment was evaluated with a logistic regression model adjusted for time since enrollment, sociodemographic characteristics as well as chronic conditions like high blood pressure, heart disease, and diabetes.

Results: A total of 3,887 participants were enrolled in this study, and 931 (24%) developed cognitive impairment during follow-up visits. In single-pollutant models, we found that per IQR increase in warm-season O_3 (OR per 20.98 $\mu g/m^3$ = 1.011 [1.000, 1.022], p = 0.033), yearly

average $PM_{2.5}$ (OR per 18.34 μg/m^3 = 1.009 [1.001,1.016], p = 0.034), and NO_2 (OR per 18.20 μg/m^3 = 1.019 [1.007, 1.031], p = 0.001) were positively associated with cognitive impairment. Only NO_2 remained positively associated with cognitive impairment (OR per 10 μg/m^3 = 1.018 [1.002, 1.033], p = 0.033) in a multi-pollutant model with $PM_{2.5}$ and O_3.

Conclusion: Our results suggested that cognitive impairment could be positively linked to $PM_{2.5}$, O_3, and NO_2. O_3 is possibly more hazardous in the warm season (April-September).

Keywords: Air pollution, cognitive impairment, CLHLS, concentration-response relationship

3.2. Introduction

Cognitive decline and dementia have long been recognized as growing public health threats, especially in an aging society. The all-age mortality rates attributable to dementia had increased by 100.1% (95% CI: 89.1-117.5) from 1990 to 2019, making it the seventh leading risk factor of excessive deaths globally (Collaborators, 2021). In 2020, the prevalence of dementia among the Chinese population aged 60 and above reached 6.0% (Ren et al., 2022). Meanwhile, the global prevalence of dementia was projected to increase from 57.4 (95% CI: 50.4-65.1) million in 2019 to 152.8 (95% CI: 130.8-175.9) million in 2050 (Nichols et al., 2022), posing a great challenge to the healthy aging of the elderly population.

Air pollution has been identified as a potential risk factor for cognitive decline and dementia. For example, a handful of studies linked $PM_{2.5}$ to poor cognitive performance (Lin et al., 2017), slower reaction time (Cullen et al., 2018), memory loss (Ailshire & Clarke, 2014; Ailshire & Crimmins, 2014), global cognitive decline (Weuve et al., 2012), and Alzheimer's disease (AD) (Jung et al., 2015; Li et al., 2019). Gaseous pollutants, such as ozone (O_3) and nitrogen dioxide (NO_2), were also found to be associated with cognitive decline (Cleary et al., 2018), semantic fluency (Zare Sakhvidi et al., 2022), lower executive function, and impaired logic memory (Gatto et al., 2014). However, as reviewed by Delgado-Saborit et al., current study findings are inconsistent, especially regarding which pollutants have the strongest association with dementia (Delgado-Saborit et al., 2021). This inconsistency is possibly attributable to exposure measurement error, particularly when multiple air pollutants are investigated simultaneously.

Recent advances in satellite remote sensing have offered an opportunity to establish high-performance air pollution models for environmental epidemiological studies. However, satellite retrievals, such as aerosol optical depth (AOD), are typically not direct measurements of ground-

level air pollution per se. A set of machine-learning approaches have been utilized to project the spatiotemporal distribution of multiple air pollutants from satellite-driven data. For example, Liang et al. established a 1-km ensemble learning model for $PM_{2.5}$ in China from 2000-2018. The model had an overall R^2 of 0.79 with a Root-mean-square error (RMSE) of 21 $\mu g/m^3$ (Liang et al., 2020). In addition, we also established 0.05° (approximately 5 km) O_3 (Zhu et al., 2022) and NO_2 prediction models (in submission) covering 2005-2019 from Ozone Measurement Instrument (OMI) retrievals. Certain models not only expanded the spatial coverage of the ground-level monitoring network but also reliably hindcasted historical pollution status for ~10 years before the onset of large-scale environmental monitoring in China (Zhu et al., 2022).

The availability of such long-term air pollution data facilitates epidemiological investigations with large existing cohorts that were established decades ago. The Chinese Longitudinal Health Longevity Survey (CLHLS) is the world's largest survey on centenarians with a compatible group of people aged 65 and above (Zeng et al., 2017). Participants of CLHLS were enrolled in 22 different provinces in China over eight waves of survey data collection that occurred during 1998-2018. Its database includes detailed information on the participants' sociodemographic status as well as medical records. The CLHLS used a Chinese Mini-Mental State Exam (CMMSE, localized from the original MMSE) to evaluate the subjects' cognitive function. To ensure the quality and consistency of the results throughout the whole nation, all the CMMSE tests were conducted face-to-face between trained interviewers and the participants. The CMMSE has proven to be effective for the Chinese elderly population (Ren et al., 2021).

The present study investigated the association between air pollution and cognitive impairment with the CLHLS data. Exposure to $PM_{2.5}$, O_3, and NO_2 was measured with three high-performance satellite-driven machine learning models. The improvement in exposure matrices

could make better use of CLHLS's long temporal coverage and thus benefit our mutual understanding of air pollution as a potential risk factor for dementia.

3.3. Methods

3.3.1. Study population

The CLHLS is a nationwide survey on the healthy aging of the Chinese elderly population covering 22 out of the 31 provinces, namely Beijing, Tianjin, Chongqing, Shanghai, Anhui, Fujian, Guangdong, Guangxi, Hubei, Hunan, Henan, Hebei, Heilongjiang, Liaoning, Jiangxi, Jiangsu, Jilin, Shandong, Shaanxi, Shanxi, Sichuan, and Zhejiang. It comprises eight rounds of data collection that took place in 1998, 2000, 2002, 2005, 2008-2009, 2011-2012, 2014, and 2018, respectively (Zeng et al., 2017). All participants were selected with a targeted random sampling approach to ensure representativeness. The details of CLHLS may also be found at https://cpha.duke.edu/research/chinese-longitudinal-healthy-longevity-survey-clhls.

The present study selected CLHLS participants that were enrolled after 2005 to align with the temporal coverage of the available air pollution exposure dataset. The inclusion criteria covered: 1) free of cognitive impairment (MMSE >= 24) at enrollment; 2) fully completed at least one CMMSE measurement or unable to complete the test only due to significant cognitive impairment; and 3) had clear residential address records. We only tracked participants until they developed a cognitive impairment, if any, assessed via the survey in this study.

The study was approved by the Biomedical Ethics Committee of Peking University (IRB00001052-13074) and the Institutional Review Board of Emory University (STUDY00000950). Signed written consents were obtained from either the participants or their legal representatives for both the baseline and follow-up surveys.

3.3.2. Exposure assessment

We used three satellite-driven machine learning models to estimate the level of exposure to ambient $PM_{2.5}$, O_3, and NO_2. Specifically, the 1-km $PM_{2.5}$ data were developed by Liang et al. using the Multi-Angle Implementation of Atmospheric Correction (MAIAC) aerosol optical depth (AOD) product as the main predictor. This model first used a multiple imputation approach to gap-fill the missing AOD values and then a generalized additive model to synthesize prediction results from two tree-based learning algorithms (i.e., RF and XGBoost). Its final predictions agreed well with the ground-level observations, with a daily R^2 value of 0.79 for 2013-2017 and a monthly R^2 of 0.76 for the hindcast period (2000-2013) (Liang et al., 2020). Surface-level O_3 concentrations were generated with the Smithsonian Astrophysical Observatory (SAO) OMI Ozone Profile (OMPROFOZ) at a 0.05 ° resolution as the main predictor (Zhu et al., 2022). The O_3 model considered surface ozone pollution generated either from the photochemical reactions involving NO_2 and volatile organic species (VOCs) or that came down from the stratosphere through the stratospheric intrusion process. Its monthly R^2 reached 0.86 for 2014-2019 and 0.73 for 2005-2013. The NO_2 model was based on the OMI level-3 tropospheric NO_2 vertical column densities (VCD). It also used an ensemble learning approach to account for the non-linear relationship between model predictors and ground-level NO_2 concentrations. The final monthly NO_2 predictions yielded a random CV R^2 of 0.88. It also showed good performance in spatial ($R^2 = 0.73$) and temporal ($R^2 = 0.82$) cross validation (Huang, Zhu et al. 2023).

Annual average exposure to $PM_{2.5}$, NO_2 as well as annual and warm-season (April-September) average MDA8 (daily maximum 8-hour average) O_3 prior to the cognitive test were assigned to the participants based on their geocoded address. To specify, we first matched all the

participants' addresses to the model grid cells it completely falls into and then identified their exposure levels according to the date when the CMMSE was carried out. For participants whose addresses changed during two consecutive visits, we considered the midpoint of two visits as the date of moving.

3.3.3. Measurement of cognitive impairment

Participants' cognitive function was measured with the CMMSE. This measure was modified from the original MMSE developed by Folstein et al. in 1975 (Folstein et al., 1975) to fit the socioeconomic status of the Chinese elderly population. Given that most participants of the CLHLS are illiterate, the CMMSE simplified questions regarding calculation and verbal skills (Zeng & Vaupel, 2002). The details of the CMMSE and a sample questionnaire can be found at (https://doi.org/10.18170/DVN/WBO7LK). We define cognitive impairment as an MMSE score <24 or unable to complete the test only due to poor cognitive function. Based on previous studies, we treated questions that were marked 'unable to answer' as wrong. Participants who were not able to complete the questionnaire for reasons other than cognitive impairment (e.g., physical disabilities) were removed from the current study.

3.3.4. Covariates

We considered a set of variables as potential confounders. For sociodemographic status, we included age (in years), sex, body mass index (BMI) (kg/m^2), educational level (in years), ethnic group (Han, Zhuang, and others), and living in an urban/rural area.

We also considered the subjects' behavior patterns and chronic disease status as potential sources of confounding, including past or present smoking, drinking, and physical exercise, as well as

currently suffering from high blood pressure, diabetes, or heart disease. All covariates were updated at each round of survey.

3.3.5. Statistical analysis

Since all the surveys of CLHLS were conducted on a cross-sectional basis, we were not able to identify the specific date that a participant developed cognitive impairment. Thus, a typical survival analysis using Cox proportional hazards modeling may be inappropriate (Steenland et al., 2018). As such, we used a logistic regression model that included the follow-up time to analyze the association between air pollution and cognitive impairment. The detailed model is illustrated in Eq. 3-1.

$$Logit(P(Y_{iz})) = \beta_0 + \beta_1 time_{iz} + \sum \beta_j air\ pollutant_{ijz} + \sum \beta_k confounder_{ikz} \quad \text{(Eq. 3-1)}$$

Where Y_i denotes the cognitive impairment status for individual i at z^{th} measurement; $time_{iz}$ denotes the time (in years) since enrollment for individual i; $air\ pollutant_{ijz}$ denotes the average concentration of air air pollutant j for individual i in the previous year of the z^{th} measurement; $confounder_{ikz}$ represents all the confounders that are listed in the previous section.

We first ran single-pollutant models assessing associations of yearly average $PM_{2.5}$, NO_2, warm-season MDA8 O_3, and yearly average MDA8 O_3, with cognitive impairment status. We then conducted a multipollutant model that included yearly average $PM_{2.5}$, NO_2, and warm-season O_3 based on the results of the single-pollutant models. Multiple air pollutants were included based on the temporal range, i.e., the effect of warm season O_3 was adjusted for warm season $PM_{2.5}$ and NO_2, while yearly average air pollutants were evaluated simultaneously in a separate model.

We further used a penalized spline function to study the concentration-response relationship between air pollution and cognitive impairment. The spline function was only applied to pollutants that showed a significant association in their single pollutant model.

All the statistical analyses were conducted with R (v 4.0.5, R core team). A two-sided p-value < 0.05 was considered statistically significant.

3.4. Results

As can be seen in Table 3-1, 3,887 participants at baseline were selected for the present study. Among them, 2,882 (74.1%), 1,362 (35.0%), and 521 (13.4%) completed one, two, and three rounds of the follow-up survey, respectively. At baseline, the average age and BMI were 80.0 ± 11.3 years and 22.0 ± 29.4 kg/m^2. Slightly more than half of the participants (2,088, 53.7%) were male, while 3,480 (89.5%) of them belonged to the Han ethnic group. A total of 2,642 (68.0%) individuals lived in rural areas. The majority of the participants self-identified as never drinkers (2,563, 65.9%) and never smokers (2,401, 61.8%), while 490 (12.6%) and 605 (15.6%) participants identified themselves as former drinkers and former smokers. Thirty-five percent (1,419) of them exercised regularly. Around 10.3% (401), 24.5% (951), and 4.0% (154) of the participants had heart diseases, high blood pressure (HBP), and diabetes at baseline, respectively. At the first follow-up visit, 752 (26.1%) of the remaining participants developed cognitive impairment, while 129 (9.5%) and 50 (9.6%) people developed CI at the second and third follow-up visits.

As illustrated in Table 3-2, a year increase in age was associated with a 0.7% increase in the risk of cognitive impairment (95% CI = [1.004,1.010], p < 0.001). Females (OR = 1.040 [1.004, 1.075], p < 0.001), current smokers (OR = 1.026 [1.006,1.045], p = 0.008), and former drinkers

(OR = 1.024 [1.005,1.042], p = 0.012) were at a higher risk of cognitive impairment. On the contrary, per year increase in education (OR = 0.997 [0.995,0.999], p = 0.003), living in an urban area (OR = 0.980 [0.954,1.012], p = 0.018), and regular exercise (0.966 [0.952,0.980], p < 0.001) were protective factors for cognitive impairment. We did not observe significant association between cognitive impairment and ethnic groups, BMI, high blood pressure, diabetes, heart diseases, past smoking as well as current drinking status.

The baseline annual average exposure levels to $PM_{2.5}$, NO_2, and MDA8 O_3 were 62.5 ± 14.3 $\mu g/m^3$, 29.1 ± 11.7 $\mu g/m^3$, and 89.2 ± 5.82 $\mu g/m^3$, respectively (Table 3-3). Warm season average MDA8 O_3 was significantly higher than the annual average and reached 106 ± 12.2 $\mu g/m^3$. The exposure levels for three follow-up visits were generally comparable to the baseline.

In single-pollutant models (Table 3-4), we found that exposures to O_3, $PM_{2.5}$, and NO_2 were all positively associated with cognitive impairment. Specifically, per IQR (18.34 $\mu g/m^3$) increase in annual average $PM_{2.5}$ was associated with a 1% increased odds of cognitive impairment (OR = 1.009 [1.001-1.016], P = 0.034). The OR values per IRQ increase in annual average NO_2 (18.20 $\mu g/m^3$) and warm season average O_3 (20.98 $\mu g/m^3$) were 1.019 ([1.007, 1.031], p = 0.001) and 1.011 [1.000, 1.022], p = 0.033), respectively. Annual average O_3 exposure was not significantly associated with cognitive impairment (OR per 8.54 $\mu g/m^3$ = 1.001 [0.997,1.014], p = 0.192).

In the multi-pollutant model, only annual average exposure to NO_2 remained positively associated with cognitive impairment (OR = 1.018 [1.002, 1.033] per 18.20 $\mu g/m^3$ increase, p = 0.023). The OR values and 95% CIs per IQR increase in annual average $PM_{2.5}$ and warm season O_3 were 0.965 ([0.919,1.011], p = 0.721), 1.001 ([0.978,1.024], p = 0.452), respectively (Table 3-4).

Fig. 3-1 shows the concentration-response relationship between air pollutants and cognitive impairment. Specifically, the OR of NO_2 increased almost monotonously with higher concentrations (Fig. 3-1A). The lower bound of its 95% CI exceeded 1.00 for 42 $\mu g/m^3$ and above. The concentration-response relationship between warm-season O_3 and cognitive impairment showed a stage-wise increase (Fig. 3-1B). That is to say, the effect of warm season O_3 was generally stable and even protective for the concentration range between 80-110 $\mu g/m^3$. The OR of O_3 increased sharply for 110-130 $\mu g/m^3$ and then stabilized for concentrations higher than 130 $\mu g/m^3$. The OR of $PM_{2.5}$ were greater at both low (< 40 $\mu g/m^3$) and high concentrations (> 100 $\mu g/m^3$), but it was generally around 1.00 for the concentration range 40-100 $\mu g/m^3$ (Fig. 3-1C).

3.5. Discussion

Air pollution has long been considered a potential risk factor for dementia. In the present study, we found that exposure to annual average $PM_{2.5}$ and warm-season O_3 were associated with an increased risk of cognitive impairment in single-pollutant models, annual average NO_2 was associated with cognitive impairment in both the single- and multi-pollutant models. Our findings are in good agreement with studies using the same data source. For example, Wang et al. reported that a 10 $\mu g/m^3$ increase in ambient $PM_{2.5}$ concentrations was associated with a 5.1% increased risk of poor cognitive function (defined as MMSE < 18, HR = 1.05 [1.02,1.08]) using the CLHLS data after 2002 (Wang et al., 2020). Yao et al. found that China's clean air policy significantly decelerated the decline in MMSE score using a quasi-experimental design (Yao et al., 2022). Using CLHLS after 2008, Ma et al. examined the effect of two-year average exposure to $PM_{2.5}$, O_3, and NO_2 on cognitive function. Their findings suggest that $PM_{2.5}$ increased the risk

of cognitive impairment (threshold of MMSE varied from 18-24, HR = 1.10 [1.02,1.18] per 20 $\mu g/m^3$), while O_3 and NO_2 yielded elevated but statistically insignificant risks (Ma et al., 2022). Compared to the studies above, our study improved the assessment of air pollution exposure by using three high-performance satellite-driven air pollution models at fine resolutions. With this advantage, we identified significant positive associations between all three air pollutants and cognitive impairment even under a more sensitive definition (MMSE < 24). The striker definition of cognitive impairment also possibly explained why our magnitudes of association were relatively smaller than the studies mentioned above.

Studies in other countries also examined the association between air pollution and cognitive impairment, but the consistency of results varied across different air pollutants. Specifically, studies in Sweden (Grande et al., 2021), South Korea (Lee et al., 2022), and the US (Grande et al., 2021) reported that $PM_{2.5}$ would escalate the risk of cognitive decline measured by the MMSE. NO_2 has also been positively linked to cognitive decline or dementia in the US (Shi et al., 2021), England (Carey et al., 2018), and Canada (Chen et al., 2017; Smargiassi et al., 2020). However, the findings were more controversial for ozone. For example, Cleary et al. reported that ozone is correlated with faster cognitive decline (Cleary et al., 2018) in the US. On the contrary, Chen et al. found no significant association between O3 and dementia in a Canadian cohort study. Park et al. even reported that O_3 yielded protective effects for cognitive decline in Korea (Park et al., 2022).

A possible reason for this controversy is the time window of ozone exposure. As a secondary pollutant, ground-level ozone is predominantly formed by the photochemical reactions between NOx and VOCs in the presence of heat and solar radiation (Li et al., 2020; Zhu et al., 2022). Consequently, ozone exhibits distinct seasonality in most Chinese regions, where elevated ozone

pollution usually occurs from late spring to early autumn (Zhu et al., 2022). In this study, O_3 posted null or even protective effects at low-medium concentrations (70 – 110 μg/m^3), but its risk surged at concentrations higher than 110 μg/m^3 (Fig. 3-1). Additionally, we found that warm-season exposure to ozone is positively associated with cognitive impairment, but annual averages yielded insignificant effects. This phenomenon has also been spotted for other health outcomes. As reviewed by Atkinson et al., studies that used warm-season exposure to ozone generally reported a positive association with mortality, while no evidence was shown for annual concentrations (Atkinson et al., 2016). These findings suggested that the health effect of ozone is possibly more prominent in the warm seasons with a high pollution level.

The importance of NO_2 needs to be highlighted since it is the only air pollutant that remained positively associated with cognitive impairment in the multi-pollutant model. Previous toxicological studies have also supported the link between NO2 and dementia. For example, Li and Xin found that NO_2 inhalation could induce dose-dependent excitotoxicity and increase the risk of vascular dementia in healthy rats (Li & Xin, 2013). This finding also agreed with the monotonic increasing concentration-response relationship between NO_2 and cognitive impairment in this study (Fig. 3-1). Furthermore, Li et al. also reported that exposure to NO_2 may accelerate neural apoptosis and express neurotoxicity (Li et al., 2012). Nevertheless, current evidence is still controversial regarding which air pollutant is primarily associated with cognitive impairment (Delgado-Saborit et al., 2021), highlighting the need to study air pollution as a mixture rather than individual pollutants.

A major strength of this study is the inclusion of three high-performance satellite-driven air pollution models. To date, China's air quality monitoring network has covered most cities, but rural areas remain largely unmonitored. Given that most participants of the CLHLS lived in rural

areas, using satellite-driven exposure estimates could significantly improve the accuracy of exposure measurement. The extended temporal coverage of our exposure datasets also facilitates the investigations with historical cohort data, especially on chronic health outcomes like cognitive impairment and dementia. Another advantage is that the CLHLS used face-to-face interviews to measure cognitive function and collect other covariates. This process guaranteed the data quality and consistency across the whole nation.

This study also has some limitations. First, we were unable to identify the specific time when a participant developed cognitive impairment, which may lead to exposure misalignment. Accounting for this, we adjusted for the follow-up in the logistic regression model since it could still be an informative predictor of cognitive impairment (Steenland et al., 2018). Second, we could not generate exposure data before 2005 due to the availability of OMI products. Consequently, only four out of the eight waves of the CLHLS were included in the study. Future studies may use a bigger sample size to study the impact of air pollution on healthy aging if the exposure dataset can be further generated to the late 1990s.

3.6. Conclusions

This study used satellite-driven datasets to study the association between air pollution and cognitive impairment among the Chinese elderly population. In the single pollutant models, we found that warm-season mean MDA8 O_3, annual mean $PM_{2.5,}$ and NO_2 were positively associated with cognitive impairment (MMSE < 24). Compared to warm-season O_3, yearly average O_3 yielded similar magnitude but non-significant effect estimates, suggesting that warm-season O_3 is a better exposure metric. Yearly average NO_2 was the only air pollutant that remained a significant risk factor for cognitive impairment in the multi-pollutant model. The

concentration-response relationship showed that NO_2 was associated with a monotonous increasing risk for cognitive impairment and dementia.

3.7. References

Ailshire, J. A., & Clarke, P. (2014). Fine Particulate Matter Air Pollution and Cognitive Function Among U.S. Older Adults. The Journals of Gerontology: Series B, 70(2), 322-328. https://doi.org/10.1093/geronb/gbu064

Ailshire, J. A., & Crimmins, E. M. (2014). Fine particulate matter air pollution and cognitive function among older US adults. Am J Epidemiol, 180(4), 359-366. https://doi.org/10.1093/aje/kwu155

Atkinson, R. W., Butland, B. K., Dimitroulopoulou, C., Heal, M. R., Stedman, J. R., Carslaw, N., Jarvis, D., Heaviside, C., Vardoulakis, S., Walton, H., & Anderson, H. R. (2016). Long-term exposure to ambient ozone and mortality: a quantitative systematic review and meta-analysis of evidence from cohort studies. BMJ Open, 6(2), e009493. https://doi.org/10.1136/bmjopen-2015-009493

Carey, I. M., Anderson, H. R., Atkinson, R. W., Beevers, S. D., Cook, D. G., Strachan, D. P., Dajnak, D., Gulliver, J., & Kelly, F. J. (2018). Are noise and air pollution related to the incidence of dementia? A cohort study in London, England. BMJ Open, 8(9), e022404. https://doi.org/10.1136/bmjopen-2018-022404

Chen, H., Kwong, J. C., Copes, R., Hystad, P., van Donkelaar, A., Tu, K., Brook, J. R., Goldberg, M. S., Martin, R. V., Murray, B. J., Wilton, A. S., Kopp, A., & Burnett, R. T. (2017). Exposure to ambient air pollution and the incidence of dementia: A population-based cohort study. Environment International, 108, 271-277. https://doi.org/https://doi.org/10.1016/j.envint.2017.08.020

Cleary, E. G., Cifuentes, M., Grinstein, G., Brugge, D., & Shea, T. B. (2018). Association of Low-Level Ozone with Cognitive Decline in Older Adults. Journal of Alzheimer's Disease, 61, 67-78. https://doi.org/10.3233/JAD-170658

Collaborators, G. (2021). Global mortality from dementia: Application of a new method and results from the Global Burden of Disease Study 2019. Alzheimer's & Dementia: Translational Research & Clinical Interventions, 7(1), e12200. https://doi.org/https://doi.org/10.1002/trc2.12200

Cullen, B., Newby, D., Lee, D., Lyall, D. M., Nevado-Holgado, A. J., Evans, J. J., Pell, J. P., Lovestone, S., & Cavanagh, J. (2018). Cross-sectional and longitudinal analyses of outdoor air pollution exposure and cognitive function in UK Biobank. Scientific Reports, 8(1), 12089. https://doi.org/10.1038/s41598-018-30568-6

Delgado-Saborit, J. M., Guercio, V., Gowers, A. M., Shaddick, G., Fox, N. C., & Love, S. (2021). A critical review of the epidemiological evidence of effects of air pollution on dementia, cognitive function and cognitive decline in adult population. Sci Total Environ, 757, 143734. https://doi.org/10.1016/j.scitotenv.2020.143734

Folstein, M. F., Folstein, S. E., & McHugh, P. R. (1975). "Mini-mental state". A practical method for grading the cognitive state of patients for the clinician. J Psychiatr Res, 12(3), 189-198. https://doi.org/10.1016/0022-3956(75)90026-6

Gatto, N. M., Henderson, V. W., Hodis, H. N., St. John, J. A., Lurmann, F., Chen, J.-C., & Mack, W. J. (2014). Components of air pollution and cognitive function in middle-aged and older adults in Los Angeles. NeuroToxicology, 40, 1-7. https://doi.org/https://doi.org/10.1016/j.neuro.2013.09.004

Grande, G., Wu, J., Ljungman, P. L. S., Stafoggia, M., Bellander, T., & Rizzuto, D. (2021). Long-Term Exposure to PM 2.5 and Cognitive Decline: A Longitudinal Population-Based Study. Journal of Alzheimer's Disease, 80, 591-599. https://doi.org/10.3233/JAD-200852

Jung, C. R., Lin, Y. T., & Hwang, B. F. (2015). Ozone, particulate matter, and newly diagnosed Alzheimer's disease: a population-based cohort study in Taiwan. J Alzheimers Dis, 44(2), 573-584. https://doi.org/10.3233/jad-140855

Lee, J. J., Kim, J. H., Song, D. S., & Lee, K. (2022). Effect of Short- to Long-Term Exposure to Ambient Particulate Matter on Cognitive Function in a Cohort of Middle-Aged and Older Adults: KoGES. International Journal of Environmental Research and Public Health, 19(16).

Li, C. Y., Li, C. H., Martini, S., & Hou, W. H. (2019). Association between air pollution and risk of vascular dementia: A multipollutant analysis in Taiwan. Environ Int, 133(Pt B), 105233. https://doi.org/10.1016/j.envint.2019.105233

Li, H., Chen, L., Guo, Z., Sang, N., & Li, G. (2012). In vivo screening to determine neurological hazards of nitrogen dioxide (NO2) using Wistar rats. Journal of Hazardous Materials, 225-226, 46-53. https://doi.org/https://doi.org/10.1016/j.jhazmat.2012.04.063

Li, H., & Xin, X. (2013). Nitrogen dioxide (NO2) pollution as a potential risk factor for developing vascular dementia and its synaptic mechanisms. Chemosphere, 92(1), 52-58. https://doi.org/https://doi.org/10.1016/j.chemosphere.2013.02.061

Li, K., Jacob, D. J., Shen, L., Lu, X., De Smedt, I., & Liao, H. (2020). Increases in surface ozone pollution in China from 2013 to 2019: anthropogenic and meteorological influences. Atmos. Chem. Phys., 20(19), 11423-11433. https://doi.org/10.5194/acp-20-11423-2020

Liang, F., Xiao, Q., Huang, K., Yang, X., Liu, F., Li, J., Lu, X., Liu, Y., & Gu, D. (2020). The 17-y spatiotemporal trend of PM(2.5) and its mortality burden in China. Proc Natl Acad Sci U S A, 117(41), 25601-25608. https://doi.org/10.1073/pnas.1919641117

Lin, H., Guo, Y., Zheng, Y., Zhao, X., Cao, Z., Rigdon, S. E., Xian, H., Li, X., Liu, T., Xiao, J., Zeng, W., Weaver, N. L., Qian, Z., Ma, W., & Wu, F. (2017). Exposure to ambient PM(2.5) associated with overall and domain-specific disability among adults in six low- and middle-income countries. Environ Int, 104, 69-75. https://doi.org/10.1016/j.envint.2017.04.004

Ma, Y.-H., Chen, H.-S., Liu, C., Feng, Q.-S., Feng, L., Zhang, Y.-R., Hu, H., Dong, Q., Tan, L., Kan, H.-D., Zhang, C., Suckling, J., Zeng, Y., Chen, R.-J., & Yu, J.-T. (2022). Association of Long-term Exposure to Ambient Air Pollution With Cognitive Decline and Alzheimer's Disease–Related Amyloidosis. Biological Psychiatry. https://doi.org/https://doi.org/10.1016/j.biopsych.2022.05.017

Nichols, E., Steinmetz, J. D., Vollset, S. E., Fukutaki, K., Chalek, J., Abd-Allah, F., Abdoli, A., Abualhasan, A., Abu-Gharbieh, E., Akram, T. T., Al Hamad, H., Alahdab, F., Alanezi, F. M., Alipour, V., Almustanyir, S., Amu, H., Ansari, I., Arabloo, J., Ashraf, T., Astell-Burt, T., Ayano, G., Ayuso-Mateos, J. L., Baig, A. A., Barnett, A., Barrow, A., Baune, B. T., Béjot, Y., Bezabhe, W. M. M., Bezabih, Y. M., Bhagavathula, A. S., Bhaskar, S., Bhattacharyya, K., Bijani, A., Biswas, A., Bolla, S. R., Boloor, A., Brayne, C., Brenner, H., Burkart, K., Burns, R. A., Cámera, L. A., Cao, C., Carvalho, F., Castro-de-Araujo, L. F. S., Catalá-López, F., Cerin, E., Chavan, P. P., Cherbuin, N., Chu, D.-T., Costa, V. M., Couto, R. A. S., Dadras, O., Dai, X., Dandona, L., Dandona, R., De la Cruz-Góngora, V., Dhamnetiya, D., Dias da Silva, D., Diaz, D., Douiri, A., Edvardsson, D., Ekholuenetale, M., El Sayed, I., El-Jaafary, S. I., Eskandari, K., Eskandarieh, S., Esmaeilnejad, S., Fares, J., Faro, A., Farooque, U., Feigin, V. L., Feng, X., Fereshtehnejad, S.-M., Fernandes, E., Ferrara, P., Filip, I., Fillit, H., Fischer, F., Gaidhane, S., Galluzzo, L., Ghashghaee, A., Ghith, N., Gialluisi, A., Gilani, S. A., Glavan, I.-R., Gnedovskaya, E. V., Golechha, M., Gupta, R., Gupta, V. B., Gupta, V. K., Haider, M. R., Hall, B. J., Hamidi, S., Hanif, A., Hankey, G. J., Haque, S., Hartono, R. K., Hasaballah, A. I., Hasan, M. T., Hassan, A., Hay, S. I., Hayat, K., Hegazy, M. I., Heidari, G., Heidari-Soureshjani, R., Herteliu, C., Househ, M., Hussain, R., Hwang, B.-F., Iacoviello, L., Iavicoli, I., Ilesanmi, O. S., Ilic, I. M., Ilic, M. D., Irvani, S. S. N., Iso, H., Iwagami, M., Jabbarinejad, R., Jacob, L., Jain, V., Jayapal, S. K., Jayawardena, R., Jha, R. P., Jonas, J. B., Joseph, N., Kalani, R., Kandel, A., Kandel, H., Karch, A., Kasa, A. S., Kassie, G. M., Keshavarz, P., Khan, M. A. B., Khatib, M. N., Khoja, T. A. M., Khubchandani, J., Kim, M. S., Kim, Y. J., Kisa, A., Kisa, S., Kivimäki, M., Koroshetz, W. J., Koyanagi, A., Kumar, G.

A., Kumar, M., Lak, H. M., Leonardi, M., Li, B., Lim, S. S., Liu, X., Liu, Y., Logroscino, G., Lorkowski, S., Lucchetti, G., Lutzky Saute, R., Magnani, F. G., Malik, A. A., Massano, J., Mehndiratta, M. M., Menezes, R. G., Meretoja, A., Mohajer, B., Mohamed Ibrahim, N., Mohammad, Y., Mohammed, A., Mokdad, A. H., Mondello, S., Moni, M. A. A., Moniruzzaman, M., Mossie, T. B., Nagel, G., Naveed, M., Nayak, V. C., Neupane Kandel, S., Nguyen, T. H., Oancea, B., Otstavnov, N., Otstavnov, S. S., Owolabi, M. O., Panda-Jonas, S., Pashazadeh Kan, F., Pasovic, M., Patel, U. K., Pathak, M., Peres, M. F. P., Perianayagam, A., Peterson, C. B., Phillips, M. R., Pinheiro, M., Piradov, M. A., Pond, C. D., Potashman, M. H., Pottoo, F. H., Prada, S. I., Radfar, A., Raggi, A., Rahim, F., Rahman, M., Ram, P., Ranasinghe, P., Rawaf, D. L., Rawaf, S., Rezaei, N., Rezapour, A., Robinson, S. R., Romoli, M., Roshandel, G., Sahathevan, R., Sahebkar, A., Sahraian, M. A., Sathian, B., Sattin, D., Sawhney, M., Saylan, M., Schiavolin, S., Seylani, A., Sha, F., Shaikh, M. A., Shaji, K. S., Shannawaz, M., Shetty, J. K., Shigematsu, M., Shin, J. I., Shiri, R., Silva, D. A. S., Silva, J. P., Silva, R., Singh, J. A., Skryabin, V. Y., Skryabina, A. A., Smith, A. E., Soshnikov, S., Spurlock, E. E., Stein, D. J., Sun, J., Tabarés-Seisdedos, R., Thakur, B., Timalsina, B., Tovani-Palone, M. R., Tran, B. X., Tsegaye, G. W., Valadan Tahbaz, S., Valdez, P. R., Venketasubramanian, N., Vlassov, V., Vu, G. T., Vu, L. G., Wang, Y.-P., Wimo, A., Winkler, A. S., Yadav, L., Yahyazadeh Jabbari, S. H., Yamagishi, K., Yang, L., Yano, Y., Yonemoto, N., Yu, C., Yunusa, I., Zadey, S., Zastrozhin, M. S., Zastrozhina, A., Zhang, Z.-J., Murray, C. J. L., & Vos, T. (2022). Estimation of the global prevalence of dementia in 2019 and forecasted prevalence in 2050: an analysis for the Global Burden of Disease Study 2019. The Lancet Public Health, 7(2), e105-e125. https://doi.org/https://doi.org/10.1016/S2468-2667(21)00249-8

Park, S. Y., Han, J., Kim, S. H., Suk, H. W., Park, J. E., & Lee, D. Y. (2022). Impact of Long-Term Exposure to Air Pollution on Cognitive Decline in Older Adults Without Dementia. Journal of Alzheimer's Disease, 86, 553-563. https://doi.org/10.3233/JAD-215120

Ren, R., Qi, J., Lin, S., Liu, X., Yin, P., Wang, Z., Tang, R., Wang, J., Huang, Q., Li, J., Xie, X., Hu, Y., Cui, S., Zhu, Y., Yu, X., Wang, P., Zhu, Y., Wang, Y., Huang, Y., Hu, Y., Wang, Y., Li, C., Zhou, M., & Wang, G. (2022). The China Alzheimer Report 2022. General Psychiatry, 35(1), e100751. https://doi.org/10.1136/gpsych-2022-100751

Ren, Z., Li, Y., Li, X., Shi, H., Zhao, H., He, M., Zha, S., Qiao, S., Pu, Y., Liu, H., & Zhang, X. (2021). Associations of body mass index, waist circumference and waist-to-height ratio with cognitive impairment among Chinese older adults: Based on the CLHLS. Journal of Affective Disorders, 295, 463-470. https://doi.org/https://doi.org/10.1016/j.jad.2021.08.093

Shi, L., Steenland, K., Li, H., Liu, P., Zhang, Y., Lyles, R. H., Requia, W. J., Ilango, S. D., Chang, H. H., Wingo, T., Weber, R. J., & Schwartz, J. (2021). A national cohort study (2000–2018) of long-term air pollution exposure and incident dementia in older adults in the United States. Nature Communications, 12(1), 6754. https://doi.org/10.1038/s41467-021-27049-2

Smargiassi, A., Sidi, E. A. L., Robert, L.-E., Plante, C., Haddad, M., Gamache, P., Burnett, R., Goudreau, S., Liu, L., Fournier, M., Pelletier, E., & Yankoty, I. (2020). Exposure to ambient air pollutants and the onset of dementia in Québec, Canada. Environmental Research, 190, 109870. https://doi.org/https://doi.org/10.1016/j.envres.2020.109870

Steenland, K., Zhao, L., John, S. E., Goldstein, F. C., Levey, A., & Alvaro, A. (2018). A 'Framingham-like' Algorithm for Predicting 4-Year Risk of Progression to Amnestic Mild Cognitive Impairment or Alzheimer's Disease Using Multidomain Information. J Alzheimers Dis, 63(4), 1383-1393. https://doi.org/10.3233/jad-170769

Wang, J., Li, T., Lv, Y., Kraus, V. B., Zhang, Y., Mao, C., Yin, Z., Shi, W., Zhou, J., Zheng, T., Kinney, P. L., Ji, J., Tang, S., & Shi, X. (2020). Fine Particulate Matter and Poor Cognitive Function among Chinese Older Adults: Evidence from a Community-Based, 12-Year Prospective Cohort Study. Environmental Health Perspectives, 128(6), 067013. https://doi.org/doi:10.1289/EHP5304

Weuve, J., Puett, R. C., Schwartz, J., Yanosky, J. D., Laden, F., & Grodstein, F. (2012). Exposure to particulate air pollution and cognitive decline in older women. Arch Intern Med, 172(3), 219-227. https://doi.org/10.1001/archinternmed.2011.683

Yao, Y., Lv, X., Qiu, C., Li, J., Wu, X., Zhang, H., Yue, D., Liu, K., Eshak, E. S., Lorenz, T., Anstey, K. J., Livingston, G., Xue, T., Zhang, J., Wang, H., & Zeng, Y. (2022). The effect of China's Clean Air Act on cognitive function in older adults: a population-based, quasi-experimental study. The Lancet Healthy Longevity, 3(2), e98-e108. https://doi.org/10.1016/S2666-7568(22)00004-6

Zare Sakhvidi, M. J., Yang, J., Lequy, E., Chen, J., de Hoogh, K., Letellier, N., Mortamais, M., Ozguler, A., Vienneau, D., Zins, M., Goldberg, M., Berr, C., & Jacquemin, B. (2022). Outdoor air pollution exposure and cognitive performance: findings from the enrolment phase of the CONSTANCES cohort. The Lancet Planetary Health, 6(3), e219-e229. https://doi.org/10.1016/S2542-5196(22)00001-8

Zeng, Y., Vaupel, J., Xiao, Z., Liu, Y., & Zhang, C. (2017). Chinese Longitudinal Healthy Longevity Survey (CLHLS), 1998-2014 Inter-university Consortium for Political and Social Research [distributor]. https://doi.org/10.3886/ICPSR36692.v1

Zeng, Y., & Vaupel, J. W. (2002). Functional Capacity and Self–Evaluation of Health and Life of Oldest Old in China [https://doi.org/10.1111/1540-4560.00287]. Journal of Social Issues, 58(4), 733-748. https://doi.org/https://doi.org/10.1111/1540-4560.00287

Zhu, Q., Bi, J., Liu, X., Li, S., Wang, W., Zhao, Y., & Liu, Y. (2022). Satellite-Based Long-Term Spatiotemporal Patterns of Surface Ozone Concentrations in China: 2005-2013;2019. Environmental Health Perspectives, 130(2), 027004. https://doi.org/doi:10.1289/EHP9406

3.8. Tables and Figures

Table 3-1 Sociodemographic characteristics of the CLHLS participants

	Baseline (N=3887)	First follow-up (N=2882)	Second follow-up (N=1362)	Third follow-up (N=521)
Age (years)				
Mean (SD)	80.0 ± 11.3	81.6 ± 10.9	79.7 ± 8.54	80.7 ± 6.63
Gender				
Male	2088 (53.7%)	1464 (50.8%)	724 (53.2%)	276 (53.0%)
Female	1799 (46.3%)	1418 (49.2%)	638 (46.8%)	245 (47.0%)
BMI				
Mean (SD)	22.0 ± 29.4	22.3 ± 7.14	23.0 ± 12.4	23.1 ± 7.59
Ethnic group				
Han	3480 (89.5%)	2539 (88.1%)	1200 (88.1%)	324 (62.2%)
Zhuang	112 (2.9%)	94 (3.3%)	48 (3.5%)	12 (2.3%)
Others	295 (7.6%)	249 (8.6%)	114 (8.4%)	185 (35.5%)
Education (years)				
Mean (SD)	3.09 ± 3.88	3.13 ± 3.88	3.62 ± 4.02	2.90 ± 4.04
Living area				
Rural	2642 (68.0%)	1802 (62.5%)	830 (60.9%)	336 (64.5%)
Urban	1245 (32.0%)	1080 (37.5%)	532 (39.1%)	185 (35.5%)
Cognitive impairment				
Normal cognitive function	3887 (100%)	2130 (73.9%)	1233 (90.5%)	471 (90.4%)
Yes	0 (0%)	752 (26.1%)	129 (9.5%)	50 (9.6%)
Alcohol drinking				
Current drinker	834 (21.5%)	556 (19.3%)	251 (18.4%)	103 (19.8%)
Former drinker	490 (12.6%)	451 (15.6%)	176 (12.9%)	63 (12.1%)
Never drinker	2563 (65.9%)	1875 (65.1%)	935 (68.6%)	355 (68.1%)
Tobacco smoking				
Current smoker	881 (22.7%)	603 (20.9%)	298 (21.9%)	94 (18.0%)
Former smoker	605 (15.6%)	521 (18.1%)	243 (17.8%)	94 (18.0%)
Never smoker	2401 (61.8%)	1758 (61.0%)	821 (60.3%)	333 (63.9%)
Exercise				
Yes	1419 (36.5%)	1254 (43.5%)	587 (43.1%)	232 (44.5%)
No	2468 (63.5%)	1628 (56.5%)	775 (56.9%)	289 (55.5%)

	Baseline (N=3887)	First follow-up (N=2882)	Second follow-up (N=1362)	Third follow-up (N=521)
Heart diseases				
Yes	401 (10.3%)	392 (13.6%)	221 (16.2%)	105 (20.2%)
No	3486 (89.7%)	2490 (86.4%)	1141 (83.8%)	416 (79.8%)
High blood pressure				
Yes	951 (24.5%)	880 (30.5%)	532 (39.1%)	236 (45.3%)
No	2936 (75.5%)	2002 (69.5%)	830 (60.9%)	285 (54.7%)
Diabetes				
Yes	154 (4.0%)	185 (6.4%)	117 (8.6%)	55 (10.6%)
No	3733 (96.0%)	2697 (93.6%)	1245 (91.4%)	466 (89.4%)

Table 3-2. The association between model covariates and cognitive impairment

Covariates	OR (95% CI)	P-value
Age (yr)	1.007 (1.004, 1.010)	<0.001*
BMI (kg/m^2)	1.000 (0.999, 1.000)	0.948
Time since enrollment (yr)	1.010 (1.008,1.012)	<0.001*
Sex		
Male	-	-
Female	1.040 (1.004, 1.075)	<0.001*
Ethnic group		
Han	-	-
Zhuang	1.020 (0.982, 1.059)	0.339
Others	0.983 (0.954, 1.012)	0.145
Living area		
Rural	-	-
Urban	0.980 (0.963, 0.996)	0.018*
Education (yr)	0.997 (0.995, 0.999)	0.003*
Tobacco smoking		
Never smoker	-	-
Former smoker	1.017 (0.997, 1.036)	0.104
Current smoker	1.026 (1.006, 1.045)	0.008*
Alcohol drinking		
Never drinker	-	-
Former drinker	1.024 (1.005, 1.042)	0.012*
Current drinker	1.006 (0.986, 1.026)	0.571
Exercise		
No	-	-
Yes	0.966 (0.952, 0.980)	<0.001*
Heart disease		
No	-	-
Yes	1.010 (0.991, 1.030)	0.304
High blood pressure		
No	-	-
Yes	1.008 (0.993, 1.023)	0.252
Diabetes		
No	-	-
Yes	1.002 (0.975, 1.028)	0.924

Notes: OR (95% CI) and P-value were from the multi-pollutant model. *: $p < 0.05$.

Table 3-3 Exposure levels to O_3, $PM_{2.5}$, and NO_2 ($\mu g/m^3$)

	Baseline (N=3887)	First follow-up (N=2882)	Second follow-up (N=1362)	Third follow-up (N=521)	Overall (N=8652)	P-value
Warm season O_3						
Mean (SD)	106 ± 12.2	107 ± 13.1	108 ± 14.7	113 ± 18.9	107 ± 13.5	<0.001*
Annual average O_3						
Mean (SD)	89.2 ± 5.82	89.0 ± 6.45	89.4 ± 7.53	93.2 ± 8.86	89.4 ± 6.61	<0.001*
Annual average $PM_{2.5}$						
Mean (SD)	62.5 ± 14.3	62.6 ± 16.0	61.1 ± 18.7	47.5 ± 11.1	61.4 ± 15.9	<0.001*
Annual average NO_2						
Mean (SD)	29.1 ± 11.7	32.2 ± 12.4	31.7 ± 12.8	28.5 ± 11.5	30.5 ± 12.2	<0.001*

*: $p < 0.05$

Table 3-4. The association between air pollution and cognitive impairment

Air pollutants	IQR ($\mu g/m^3$)	OR (95% CI)[1]	P-value[1]	OR (95% CI)[2]	P-value[2]
$PM_{2.5}$ (yearly)	18.34	1.009 (1.001,1.016)	0.034*	1.001 (0.992,1.010)	0.721
O_3 (yearly)	8.54	1.006 (0.997,1.014)	0.192	1.000 (0.991,1.009)	0.889
O_3 (warm season)	20.98	1.011 (1.000,1.022)	0.033*	1.007 (0.989,1.024)	0.452
NO_2 (yearly)	18.20	1.019 (1.007,1.031)	0.001*	1.018 (1.002,1.033)	0.033*

Notes: 1, OR (95% CI) and P-value from the single pollutant model; 2, OR (95% CI) and P-value from the multi-pollutant models. Multiple air pollutants were included based on the temporal range, i.e., the effect of warm season O_3 was adjusted for warm season $PM_{2.5}$ and NO_2, while yearly average air pollutants were evaluated simultaneously in a separate model. The OR values are per IQR increase of the air pollutants. *: $p < 0.05$

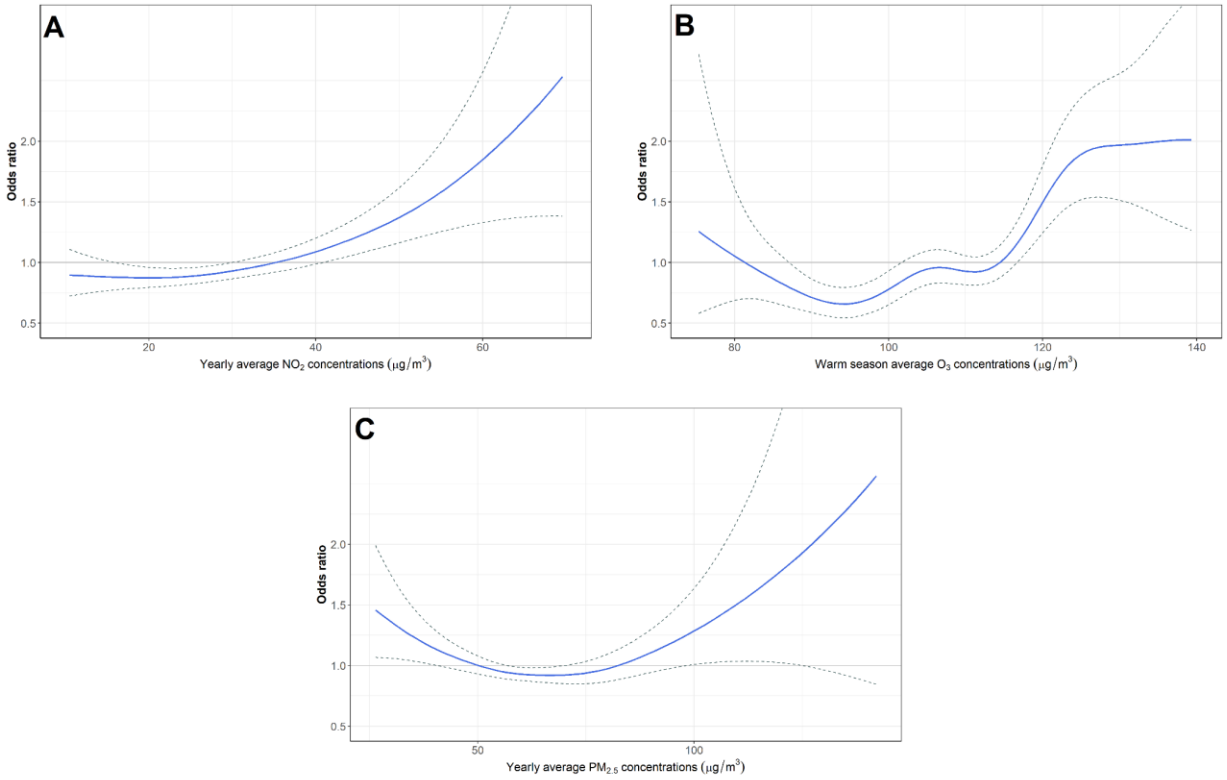

Fig. 3-1. Concentration-response relationship between air pollutants and cognitive impairment. A: yearly average NO_2; B: Warm-season (April-September) average O_3; C: yearly average $PM_{2.5}$.

4. The Association between Wildfire and Emergency Department (ED) Visits for Anxiety Disorders in the Western United States

[Manuscript 3]

Qingyang Zhu, Danlu Zhang, Wenhao Wang, Rohan Richard D'Souza, Haisu Zhang, Kyle Steenland, Noah Scovronick, Stefanie Ebelt, Howard H. Chang, and Yang Liu

4.1. Abstract

Background: Wildfires and anxiety are both growing threats to the global economy and public health. Nevertheless, the association between wildfire-related exposures and anxiety disorders remains largely unclear.

Objectives: We aimed to examine the association between wildfire-related exposures and emergency department (ED) visits for anxiety disorders in the Western United States.

Methods: We used a case-crossover design for the present study. Records of ED visits were obtained from five different Western US states, including Arizona, California, Nevada, Oregon, and Utah. Anxiety disorders were defined as ICD-10 codes F40-F48 and their corresponding ICD-9 codes. Exposure to wildfire smoke $PM_{2.5}$ and background $PM_{2.5}$ was evaluated with an ensemble learning method. We used a conditional logistic regression to evaluate the association between wildfire smoke $PM_{2.5}$ and ED visits for anxiety disorders.

Results: A total of 1,897,865 cases from 2007-2018 were included in this study. We found that a 10 ug/m^3 increase in wildfire smoke $PM_{2.5}$ was associated with a 0.6% (OR = 1.006 [1.001,1.012], p = 0.029) increase in the risk of ED visits for anxiety disorders. Age- and sex-stratified analysis showed that females (OR per 10 ug/m^3 = 1.011 [1.002,1.021], p = 0.020) and the elderly population (OR per 10 ug/m^3 = 1.035 [1.017, 1.054], p < 0.001) were more

vulnerable to wildfire smoke $PM_{2.5}$ regarding anxiety disorders. Additionally, an extreme smoke event (defined as smoke PM2.5 contributed to >= 75% of the total $PM_{2.5}$ in the past 48 hours) was also associated with an increase in the risk of ED visits for anxiety disorders (OR = 1.063 [1.015, 1.113], p = 0.009).

Conclusion: Our results suggest that wildfires are associated with an increased risk of ED visits for anxiety disorders. Females and the elderly are more vulnerable to the anxiety disorders associated with wildfire-related exposures.

4.2. Introduction

Attributable to anthropogenic climate change repercussions, wildfire has become a growing threat to the global economy and public health (Ellis et al., 2022; Jones et al., 2022). Over the past 20 years, rising temperatures and shifting drying patterns have substantially escalated global fire potential (Ellis et al., 2022), resulting in expanded burned areas and prolonged fire seasons (Jolly et al., 2015; Richardson et al., 2022). The impact of wildfires, however, is not uniformly distributed across the globe, with variations stemming from differences in climatology and geographical conditions. The Western United States has long been identified as a major fire-prone region, predominantly due to the recurrent presence of fire weather conditions, increasing droughts, and the abundance of fuel resources (Gannon & Steinberg, 2021; Jones et al., 2022; Zhang et al., 2020). The widespread occurrence of wildfires in the Western US has caused a surge in smoke emissions. In recent years, it was estimated that wildfire smoke accounted for around 40% of the total $PM_{2.5}$ across the whole Western US and even 50% in the Northwestern region, exacerbated substantially from the 15-20% contribution in the early 2000s (Burke et al., 2021). Previous epidemiological studies have linked wildfire smoke exposure to a variety of adverse health outcomes, particularly those affecting the respiratory system (Reid Colleen et al., 2016).

Mental health disorders, including anxiety disorders, have been another expanding threat to global public health in the past decades. According to the global burden of diseases (GBD) study, mental health disorders contributed to a total of 125.3 million (95% uncertainty interval (UI) = [93.0 – 163.2]) disability-adjusted life-years (DALYs) in 2019, increased substantially from 80.8 million (95% UI = [59.5 – 105.9]) in 1990. Anxiety disorders, in particular, were the most prevalent mental health condition that affected 970.1 (95% UI = [990.9 - 1044.4]) per

million individuals in 2019 (GBD Collaborators, 2022). The GBD 2019 revealed that anxiety disorders ranked among the top 25 leading contributors to the global DALYs for all populations and were among the top 10 contributors for females and adolescents (Murray et al., 2020). Regions with high socio-demographic indices, including Western Europe, Australia, and high-income North America, exhibited the highest age-standardized incidence rates of anxiety disorders (Yang et al., 2021).

The coupled increasing trend of wildfire activities and the prevalence of anxiety disorders has highlighted the need to investigate the mental health consequences associated with wildfires. Although a handful of studies have established the link between ambient $PM_{2.5}$ and anxiety disorders in the US (Power et al., 2015; Pun et al., 2017), China (Shi et al., 2020; Zhao et al., 2022), and the UK (Hao et al., 2022), evidence concerning wildfire smoke exposure remains inconclusive (Eisenman & Galway, 2022). For example, Mirabelli et al. reported that the prevalence of being unable to stop or control worrying more than half the time during the past 14 days elevated by 30% (prevalence ratio = 1.30, 95% CI = [1.03 – 1.65]) among adults exposed to medium or heavy smoke for six weeks or more in the past year in Oregon, US (Mirabelli et al., 2022). Similarly, Humphreys et al. found that wildfire smoke events were associated with heightened anxiety and depression in the rural Washington State community (Humphreys et al., 2022). However, the absence of high-performance quantitative measurements of wildfire smoke $PM_{2.5}$ has limited the potential for large-scale population studies that feature higher statistical power and validity.

In addition to the inhalation of smoke $PM_{2.5}$, wildfire itself may have adverse psychological effects that ultimately result in anxiety disorders. For example, a case study in Canada showed a positive association between to prevalence of generalized anxiety disorders and witnessing

homes being destroyed by the wildfire or living in a different home among survivors of the 2016 Fort McMurray wildfire (Agyapong et al., 2018). As reviewed by To et al., trauma-related factors, such as property loss or fearing the loss of loved ones, could increase the risk of anxiety disorders following wildfire events (To et al., 2021). However, those studies were limited in scope and did not quantify the magnitude of risk associated with wildfire exposure. Furthermore, it remains unclear whether certain population groups are more susceptible to anxiety disorders due to wildfire-related exposures since some individuals, such as women, are considerably more vulnerable to anxiety and stress-related disorders (Li & Graham, 2017; Yang et al., 2021).

Therefore, the present study aimed to investigate the impact of wildfires on emergency department (ED) visits for anxiety disorders in the Western United States using a satellite-driven exposure dataset. The association between wildfires and anxiety disorders was explored through two potential pathways: 1) the inhalation of wildfire smoke $PM_{2.5}$, and 2) the psychological effects of wildfire smoke events and visible fire points. Additionally, we also evaluated whether the association between wildfire and anxiety disorders differed among distinct sex, age, and ethnic groups. The findings of this study will enhance our mutual understanding of the mental health impact of wildfires and promote environmental justice by benefiting vulnerable populations.

4.3. Methods

4.3.1. ED visits for anxiety disorders

We obtained ED visits data from five different Western US states, including Arizona (2010-2018), California (2007-2018), Nevada (2009-2016), Oregon (2014-2018), and Utah (2007-

2016). Anxiety disorders were defined as the International Classification of Disease, Tenth Revision (ICD-10) codes F40-F48 and the corresponding ICD-9 codes (300, 308, 309.0, 309.1, 309.24, 309.28, 309.29, 309.3, 309.4, 309.8, and 309.9) were applied for records before Oct 1, 2015. We only included patients whose primary reason for the ED visit was anxiety disorders.

4.3.2. Exposure assessments

Exposure to wildfire smoke $PM_{2.5}$ was assessed with a one km satellite-driven model. In brief, we considered two different scenarios of $PM_{2.5}$ pollution: total $PM_{2.5}$ and background $PM_{2.5}$ (non-smoke $PM_{2.5}$). The total $PM_{2.5}$ model was trained with the data from regions that were affected by wildfire smoke. The background $PM_{2.5}$ model was trained with data from the smoke-free regions (i.e., regions that were not affected by wildfire smoke). We then use both models to predict $PM_{2.5}$ concentrations under different scenarios and subtract the background $PM_{2.5}$ from the total $PM_{2.5}$ to get wildfire smoke $PM_{2.5}$. The detailed description of this model has been documented elsewhere (manuscript in preparation). We further aggregated wildfire smoke $PM_{2.5}$ and background $PM_{2.5}$ to the zip-code level to match the ED visits data. We did a vaguer aggregation (aggregate by the first four digits of the zip codes) for all patients in Nevada, given that the full zip codes were not available for this state.

Daily active wildfire points from 2007-2018 were obtained from the Fire Information for Resource Management System (FIRMS) data archive (https://firms.modaps.eosdis.nasa.gov/download/). We considered two proxies of exposure to wildfire: the number of active wildfire points within a given zip code and the cumulative fire radiative power (FRP) for all those fire points. The state of Nevada was excluded from this specific analysis, given that the complete zip code information was unavailable.

4.3.3. Meteorological data

Daily maximum and minimum temperature in degrees Celsius and vapor pressure in pascals at 1 km resolution from 2007-2018 were obtained from Daymet (https://daymet.ornl.gov/). We further calculated the daily mean temperature by averaging the daily maximum and minimum temperatures. Relative humidity was calculated using Magnus' formula (Lawrence, 2005). Similar to wildfire smoke $PM_{2.5}$, we also aggregated the Daymet meteorological data to the zip code level to align with ED visits records.

4.3.4. Statistical analysis

We used a case-crossover design to investigate the association between wildfire exposure and ED visits for anxiety disorders. Specifically, if an ED visit occurred on day X, we use all the other dates within the same month that fell on the same day of the week as day X to serve as self-control days. The exposures of interest included: 1) two-day average wildfire smoke $PM_{2.5}$ (the day of the ED visits and the previous day); 2) the occurrence of a wildfire smoke event (defined as wildfire smoke $PM_{2.5}$ contributed to $\geq$ 25% of the total $PM_{2.5}$ in the past two days); 3) the occurrence of a major wildfire smoke event (defined as wildfire smoke $PM_{2.5}$ contributed to $\geq$ 75% of the total $PM_{2.5}$ in the past two days); 4) The total number of active wildfire points within a given zip code in the past two days; and 5) The cumulative FRP of all the wildfire points within a given zip code in the past two days.

We employed a two-stage conditional logistic regression model to examine the association between the exposures of interest and ED visits for anxiety disorders. Stage one (model 1) considered only the effects of the exposures of interest, while stage two (model 2) controlled for background $PM_{2.5}$. Common covariates for both models included federal holiday indicators and

natural splines for the day of year (DOY), mean temperature, and relative humidity (RH). The degrees of freedom were four for DOY and six for temperature and RH. The detailed model specification is shown as eq. 1 below.

$$Logit\ P(Y) = \beta_0 + \beta_1\ exposures\ of\ interest + \beta_2 background\ PM_{2.5} + \beta_3 holidays + ns(DOY) + ns(temp) + ns(RH) \quad \text{(eq. 1)}$$

Where exposures of interest included 2-day average smoke $PM_{2.5}$, smoke events, major smoke events, the total number of active fire points within a 2-day period, and their cumulative FRP, each exposure of interest was analyzed independently. Model 1 incorporated the exposures of interest and other covariates, while Model 2 further adjusted for background $PM_{2.5}$ levels.

Although an advantage of a case-crossover study is that the individual-level time-invariant variables (e.g., age, sex, race) are automatically controlled for in the design stage, we conducted multiple stratified analyses to determine if the association between wildfire-related exposures and ED visits for anxiety disorders varied across different population groups. Specifically, we evaluated whether the association varied across different sex (males/females), age groups (adolescents aged 5-17, adults aged 18-64, and the elderly aged 65 and above), races (white/black/Asian/others) as well as ethnicities (Hispanic/non-Hispanic).

We also conducted some sensitivity analyses to see if the results were stable under different model settings. First, we explored various lagged effects of smoke $PM_{2.5}$, ranging from the same-day exposure of the ED visits (day 0) to the five-day moving average (day 0 plus four previous days). Second, we investigated the effects of different degrees of freedom for DOY (4-8), temperature (4-6), and RH (4-6).

All analyses were performed with R (version 4.0.5). Package *survival* was used to run the conditional logistic regression models.

4.4. Results

4.4.1. Study population

This study analyzed 1,897,865 emergency department (ED) visits for anxiety disorders (Table 4-1). The majority of cases (1,513,553, 79.8%) originated from California, while Arizona, Nevada, Oregon, and Utah contributed 184,772 (9.7%), 63,643 (3.4%), 67,953 (3.6%), and 67,944 (3.6%) cases, respectively. Among all participants, 60.5% (1,148,133) were female, with the percentage of females varying between 59.0% and 61.8% across different states. Adults accounted for 83.0% (1,575,972) of the total ED visits, while children and adolescents made up 8.0% (152,465), and elderly individuals accounted for 8.9% (169,448). Out of all the participants, 1,181,866 participants were non-Hispanic. The highest proportion of Hispanic participants was observed in California (580,410, 38.3%), while the lowest proportion was found in Oregon (8,264, 12.2%). A total of 1,228,284 (64.7%) participants were white, while black, Asian, and other racial groups accounted for 8.1% (154,493), 4.0% (76,312), and 23.1% (438,766), respectively.

As illustrated in Table 4-2, the averaged 48-h exposure to smoke $PM_{2.5}$ and background $PM_{2.5}$ was 0.93 ± 3.18 $\mu g/m^3$ and 9.91 ± 4.42 $\mu g/m^3$, respectively. A total of 629,622 smoke events occurred during the study period, including 142,436 that occurred on case days and 486,186 that occurred on control days. Additionally, we also identified 11,931 extreme wildfire smoke events, with 2,809 took place on case days and 9,122 on the control days.

A total of 4,264 cases occurred on days with active wildfire points in the same zip code (Nevada was excluded). On case days with active fire points, the mean fire count was 3.16 ± 8.34, with an average cumulative FRP of 415 ± 821. We also identified 14,574 control days with active fire points. The average fire count and cumulative FPR were 2.92 ± 7.48, and 211 ± 814, respectively (Table 4-2).

4.4.2. The effects of wildfire smoke $PM_{2.5}$

We found that a 10 μg/m^3 increase in 48-h exposure to smoke $PM_{2.5}$ was associated with a 0.6% increase in the risk of ED visits for anxiety disorders (OR = 1.006 [1.000,1.012], p = 0.040) in model 1 (Table 4-3). The OR for smoke $PM_{2.5}$ in the model adjusted for background $PM_{2.5}$ was 1.003 (95% CI = [0.998,1.010], p = 0.169).

As illustrated in Fig. 4-1, a 10 μg/m^3 increase in smoke $PM_{2.5}$ was associated with a 1.8% increase in the risk of ED visits for anxiety disorders among females in model 1 (OR = 1.011, 95% CI = [1.002, 1.021], p = 0.020). Smoke $PM_{2.5}$ was also a significant risk factor for ED visits for anxiety disorders in elderly males (OR per 10 μg/m^3 = 1.033 [1.011, 1.056], p = 0.003), elderly females (OR per 10 μg/m^3 = 1.040 [1.006, 1.074], p = 0.027), and female adults (OR per 10 μg/m^3 = 1.012 [1.001,1.022], p = 0.027). No significant association between smoke $PM_{2.5}$ and ED visits for anxiety disorders was observed for children and adolescents, regardless of sex.

The race and ethnicity stratified analysis (supplemental Fig. S2-1) demonstrated that 48-h exposure to smoke $PM_{2.5}$ was associated with the risk of ED visits for anxiety disorders in white females (OR = 1.012 [1.000, 1.024], p = 0.045). We also observed marginally significant associations in other females (OR = 1.021 [0.998, 1.044], p = 0.068) and Hispanic females (OR = 1.017 [0.997, 1.036], p = 0.073).

4.4.3. The effects of smoke events

We found that a smoke event was not significantly associated with the risk of ED visits for anxiety disorders in the general population, regardless of the adjustment for background $PM_{2.5}$ (Table 4-3). Nevertheless, as demonstrated in Fig. 4-2, the age- and sex-stratified analysis revealed the association between smoke events in the past 48 hours and an elevated risk of ED visits for anxiety disorders among all females (OR = 1.013 [1.001, 1.025], p = 0.035), and female adults (OR = 1.015 [1.002, 1.029], p = 0.021). Both associations remained significant after adjusting for background $PM_{2.5}$ (OR = 1.012 [1.000, 1.029], p = 0.044 for all females and OR = 1.015 [1.002, 1.028], p = 0.026 for female adults). We found no significant association between smoke events and ED visits for anxiety disorders in males among all age groups.

Furthermore, our results (Table 4-3) showed that a major smoke event was associated with an increased risk of ED visits for anxiety disorders in the general population (OR = 1.063 [1.015, 1.113], p = 0.009), even adjusting for background $PM_{2.5}$ (OR = 1.056 [1.009, 1.106], p = 0.019). While this association was not observed in females (Fig. 4-3), we found significant impacts of major smoke events on both adult males (OR = 1.082 [1.013, 1.158], p = 0.018) and elderly males (OR = 1.235 [1.052, 1.452], p = 0.010). However, we also found that major smoke events were negatively associated with ED visits for anxiety disorders in all female children and adolescents (OR = 0.812 [0.684,0.964], p = 0.008 and OR = 0.636 [0.474, 0.852], p = 0.002, respectively).

4.4.4. The effects of active fire points and FRP

As shown in Table 4-3, we found a marginally significant association between the number of visible fire points and ED visits for anxiety disorders in the general population (OR per fire point

= 1.002 [0.999, 1.005], p = 0.066). No association was observed for the cumulative FRP (OR per 67.75 W = 1.000 [0.999, 1.001], p = 0.200). However, the age- and sex-stratified analysis (Fig. 4-4) showed that an active fire point is associated with a 1.1% increase in the risk of ED visits for anxiety disorders among the elderlies (OR = 1.011 [1.000, 1.022], p = 0.042). Additionally, per IQR increase (67.75) in the cumulative fire radiative power is also associated with an increased risk of ED visits for anxiety disorders in all elderlies (OR = 1.003 [1.001, 1.005], p = 0.008) and elderly males (OR = 1.003 [1.001, 1.006], p = 0.020) (supplemental Fig. S2-2). Adjusting for background $PM_{2.5}$ did not change the associations for both fire counts and FRP.

4.4.5. Sensitivity analyses

As shown in supplemental Fig. S2-3, we found that the same day and 48-h average exposure to wildfire smoke $PM_{2.5}$ were positively associated with ED visits for anxiety disorders. The ORs for same-day and 48-h average smoke $PM_{2.5}$ were 1.006 (95% CI = [1.001,1.012], p = 0.030) and 1.006 (95% CI = [1.000,1.012], p = 0.040), respectively. However, exposures with an extended temporal coverage showed no association with anxiety disorders. The different degrees of freedom for temperature and RH did not significantly alter the association between smoke $PM_{2.5}$ and ED visits for anxiety disorders (supplemental Figsf. S2-4 and S2-5)

4.5. Discussion

The present study investigated the association between wildfire-related exposures and ED visits for anxiety disorders in the Western US from 2007-2018. Our findings suggest that wildfire is associated with an increased risk of anxiety disorders through multiple pathways. First, we identified a positive link between wildfire smoke $PM_{2.5}$ and ED visits for anxiety disorders. While previous epidemiological evidence is inconclusive on this specific association, the mental health impact of ambient $PM_{2.5}$ has been widely documented. For example, Hao et al. found that

per 10 μg/m^3 increase in $PM_{2.5}$ was associated with an OR of 2.31 (95% CI = [2.15, 2.50]) for symptoms of nerves, anxiety, tension, or depression from UK Biobank data (Hao et al., 2022). Shi et al. further revealed that certain $PM_{2.5}$ constituents, including organic carbon (OC) and elemental carbon (EC), were associated with anxiety and depression symptoms (Shi et al., 2020). The impact of ambient $PM_{2.5}$ on the nervous system has also been supported by multiple toxicological studies (Chu et al., 2019; Ferreira et al., 2022). Wildfire smoke $PM_{2.5}$ may also trigger neuroinflammation and thus exhibit neurotoxicity through a similar mechanism, given that the effect of wildfire smoke $PM_{2.5}$ is not completely independent from ambient $PM_{2.5}$ in this study (Fig. 4-1).

In addition to the inhalation of smoke $PM_{2.5}$, our findings also suggest that wildfire has a direct psychological impact that increases the risk of anxiety disorders. Specifically, we found that a major smoke event (in which smoke $PM_{2.5}$ contributed to ≥ 75% of the total $PM_{2.5}$) was associated with a 6.3% increase in the risk of ED visits for anxiety disorders in the general population (OR = 1.063 [1.015, 1.113], p = 0.009). During such major smoke events, the average wildfire smoke $PM_{2.5}$ concentration was 53.56 ± 30.14 μg/m^3. This concentration only corresponds to a cumulative OR of 1.030 [1.000, 1.061] if we assume a linear concentration-response relationship for smoke $PM_{2.5}$. The discrepancy between these two ORs suggests that major smoke events may be associated with ED visits not solely through the neurotoxicity of $PM_{2.5}$. Additionally, adjusting for background $PM_{2.5}$ slightly modified but did not change the significance of major smoke events, highlighting that the effect of major smoke events is partially independent of background $PM_{2.5}$. Furthermore, we also identified that the number of active fire spots and FRP were associated with ED visits for anxiety disorders among the elderly, and these effects were completely independent of background $PM_{2.5}$. Taken together, our

findings suggest that the direct psychological impact of wildfires also contributed to their association with anxiety disorders.

Our stratified analyses further suggest that females are more susceptible to wildfire-related exposures with regard to anxiety disorders. Specifically, significant associations between smoke $PM_{2.5}$ and anxiety disorders were only observed among female adults and all the elderly. Besides, a smoke event is positively associated with anxiety disorders in all females, while only major smoke events are linked to anxiety disorders among males. The sex disparity is possibly attributable to sex hormones, as previous literature reported that oestradiol and progesterone are associated with increased vulnerability to anxiety, trauma, and stress-related disorders in females (Andréen et al., 2009; Li & Graham, 2017). Such vulnerability not only results in an increased prevalence of anxiety disorders but also exacerbates the severity of anxiety symptoms and the overall burden of diseases in females (GBD Collaborators, 2022; Yang et al., 2021). The comprehensive impact of wildfires on females needs to be emphasized since they are also more susceptible to the respiratory outcomes associated with wildfires (Kondo et al., 2019),

The elderly population is also disproportionately affected by wildfires, especially in the Western US. A study by Masri et al. reported that regions in California that experience significant wildfire effects tend to have a higher concentration of elderly residents (Masri et al., 2021). Factors such as household wealth, insurance coverage, and health conditions may hinder the ability of older individuals to adapt and recover from the adverse effects of wildfires (Wibbenmeyer & Robertson, 2022). Our findings indicate that, compared to other age groups, the elderly are more vulnerable to the anxiety disorders associated with wildfire-related exposures. Living with anxiety is associated with higher outpatient and inpatient costs among the elderly population. It is estimated that the excess annual adjusted healthcare costs of anxiety and

comorbid of anxiety and depression reached $80.0 and $119.8 million per 1 million elderly population in Canada (Vasiliadis et al., 2013). The total burden of disease attributable to wildfires is expected to grow among the elderly population, given the population aging and the continuous exacerbation of climate change in the US.

Our study has several advantages. First, our study comprises 1,897,865 ED visits from five Western US states from 2007-2018. To our best knowledge, this is currently the largest and the most comprehensive research on the association between wildfire-related exposures and anxiety disorders, while previous studies typically focused on a small region with several hundred subjects. Second, we used high-performance satellite-driven exposure datasets to quantify wildfire-related exposures. With this advance, we were able to identify multiple pathways through which wildfires are associated with an increased risk of anxiety disorders.

The present study also has some limitations. To begin with, all the ED visits data were at the zip code level. That might increase the risk of exposure misclassification due to the inability to ascertain precise residential addresses for all participants. Additionally, using active fire points within a certain zip code does not fully represent the visible fire points that might have psychological impacts on an individual since some fire points that fell out of this zip code may actually be closer to this individual's living address. Moreover, our study used ED visits for anxiety disorders as the outcome of interest. Nevertheless, only a small portion of patients with anxiety symptoms will visit the emergency department. Under such a circumstance, we were not able to identify the association between wildfire-related exposures and milder anxiety symptoms. This may ultimately result in an underestimation of the mental health impact associated with wildfires.

4.6. Conclusions

In this study, we used satellite-driven exposure datasets to examine the association between wildfire-related exposures and ED visits for anxiety disorders in the Western US from 2007-2018. Our results suggest that wildfires are associated with an increased risk of anxiety disorders through two different pathways, including the inhalation of smoke $PM_{2.5}$ and the direct psychological impact of smoke events and active fire points. The age- and sex-stratified analysis further revealed that females and the elderly population are more susceptible to anxiety disorders associated with wildfire-related exposures. Our findings highlight the need to protect vulnerable populations from the continuous exacerbation of global climate change.

4.7. References

Agyapong, V. I. O., Hrabok, M., Juhas, M., Omeje, J., Denga, E., Nwaka, B., Akinjise, I., Corbett, S. E., Moosavi, S., Brown, M., Chue, P., Greenshaw, A. J., & Li, X. M. (2018). Prevalence Rates and Predictors of Generalized Anxiety Disorder Symptoms in Residents of Fort McMurray Six Months After a Wildfire. Front Psychiatry, 9, 345. https://doi.org/10.3389/fpsyt.2018.00345

Andréen, L., Nyberg, S., Turkmen, S., van Wingen, G., Fernández, G., & Bäckström, T. (2009). Sex steroid induced negative mood may be explained by the paradoxical effect mediated by GABAA modulators. Psychoneuroendocrinology, 34(8), 1121-1132. https://doi.org/10.1016/j.psyneuen.2009.02.003

Burke, M., Driscoll, A., Heft-Neal, S., Xue, J., Burney, J., & Wara, M. (2021). The changing risk and burden of wildfire in the United States. Proceedings of the National Academy of Sciences, 118(2), e2011048118. https://doi.org/10.1073/pnas.2011048118

Chu, C., Zhang, H., Cui, S., Han, B., Zhou, L., Zhang, N., Su, X., Niu, Y., Chen, W., Chen, R., Zhang, R., & Zheng, Y. (2019). Ambient PM2.5 caused depressive-like responses through Nrf2/NLRP3 signaling pathway modulating inflammation. Journal of Hazardous Materials, 369, 180-190. https://doi.org/https://doi.org/10.1016/j.jhazmat.2019.02.026

Collaborators, G. M. D. (2022). Global, regional, and national burden of 12 mental disorders in 204 countries and territories, 1990-2019: a systematic analysis for the Global Burden of Disease Study 2019. The Lancet Psychiatry, 9(2), 137-150. https://doi.org/10.1016/S2215-0366(21)00395-3

Eisenman, D. P., & Galway, L. P. (2022). The mental health and well-being effects of wildfire smoke: a scoping review. BMC Public Health, 22(1), 2274. https://doi.org/10.1186/s12889-022-14662-z

Ellis, T. M., Bowman, D. M. J. S., Jain, P., Flannigan, M. D., & Williamson, G. J. (2022). Global increase in wildfire risk due to climate-driven declines in fuel moisture [https://doi.org/10.1111/gcb.16006]. Global Change Biology, 28(4), 1544-1559. https://doi.org/https://doi.org/10.1111/gcb.16006

Ferreira, A. P. S., Ramos, J. M. O., Gamaro, G. D., Gioda, A., Gioda, C. R., & Souza, I. C. C. (2022). Experimental rodent models exposed to fine particulate matter (PM2.5) highlighting the injuries in the central nervous system: A systematic review. Atmospheric Pollution Research, 13(5), 101407. https://doi.org/https://doi.org/10.1016/j.apr.2022.101407

Gannon, C. S., & Steinberg, N. C. (2021). A global assessment of wildfire potential under climate change utilizing Keetch-Byram drought index and land cover classifications. Environmental Research Communications, 3(3), 035002. https://doi.org/10.1088/2515-7620/abd836

Hao, G., Zuo, L., Xiong, P., Chen, L., Liang, X., & Jing, C. (2022). Associations of PM2.5 and road traffic noise with mental health: Evidence from UK Biobank. Environmental Research, 207, 112221. https://doi.org/https://doi.org/10.1016/j.envres.2021.112221

Humphreys, A., Walker, E. G., Bratman, G. N., & Errett, N. A. (2022). What can we do when the smoke rolls in? An exploratory qualitative analysis of the impacts of rural wildfire smoke on mental health and wellbeing, and opportunities for adaptation. BMC Public Health, 22(1), 41. https://doi.org/10.1186/s12889-021-12411-2

Jolly, W. M., Cochrane, M. A., Freeborn, P. H., Holden, Z. A., Brown, T. J., Williamson, G. J., & Bowman, D. M. J. S. (2015). Climate-induced variations in global wildfire danger from 1979 to 2013. Nature Communications, 6(1), 7537. https://doi.org/10.1038/ncomms8537

Jones, M. W., Abatzoglou, J. T., Veraverbeke, S., Andela, N., Lasslop, G., Forkel, M., Smith, A. J. P., Burton, C., Betts, R. A., van der Werf, G. R., Sitch, S., Canadell, J. G., Santín, C., Kolden, C., Doerr, S. H., & Le Quéré, C. (2022). Global and Regional Trends and Drivers of Fire Under Climate Change [https://doi.org/10.1029/2020RG000726]. Reviews of Geophysics, 60(3), e2020RG000726. https://doi.org/https://doi.org/10.1029/2020RG000726

Kondo, M. C., De Roos, A. J., White, L. S., Heilman, W. E., Mockrin, M. H., Gross-Davis, C. A., & Burstyn, I. (2019). Meta-Analysis of Heterogeneity in the Effects of Wildfire Smoke Exposure on Respiratory Health in North America. International Journal of Environmental Research and Public Health, 16(6), 960. https://www.mdpi.com/1660-4601/16/6/960

Lawrence, M. G. (2005). The relationship between relative humidity and the dewpoint temperature in moist air: A simple conversion and applications. Bulletin of the American Meteorological Society, 86(2), 225-234.

Li, S. H., & Graham, B. M. (2017). Why are women so vulnerable to anxiety, trauma-related and stress-related disorders? The potential role of sex hormones. Lancet Psychiatry, 4(1), 73-82. https://doi.org/10.1016/s2215-0366(16)30358-3

Masri, S., Scaduto, E., Jin, Y., & Wu, J. (2021). Disproportionate Impacts of Wildfires among Elderly and Low-Income Communities in California from 2000–2020. International Journal of Environmental Research and Public Health, 18(8), 3921. https://www.mdpi.com/1660-4601/18/8/3921

Mirabelli, M. C., Vaidyanathan, A., Pennington, A. F., Ye, D., & Trenga, C. A. (2022). Wildfire smoke and symptoms affecting mental health among adults in the US state of Oregon. Preventive Medicine, 164, 107333. https://doi.org/https://doi.org/10.1016/j.ypmed.2022.107333

Murray, C. J. L., Aravkin, A. Y., Zheng, P., Abbafati, C., Abbas, K. M., Abbasi-Kangevari, M., Abd-Allah, F., Abdelalim, A., Abdollahi, M., Abdollahpour, I., Abegaz, K. H., Abolhassani, H., Aboyans, V., Abreu, L. G., Abrigo, M. R. M., Abualhasan, A., Abu-Raddad, L. J., Abushouk, A. I., Adabi, M., Adekanmbi, V., Adeoye, A. M., Adetokunboh, O. O., Adham, D., Advani, S. M., Agarwal, G., Aghamir, S. M. K., Agrawal, A., Ahmad, T., Ahmadi, K., Ahmadi, M., Ahmadieh, H., Ahmed, M. B., Akalu, T. Y., Akinyemi, R. O., Akinyemiju, T., Akombi, B., Akunna, C. J., Alahdab, F., Al-Aly, Z., Alam, K., Alam, S., Alam, T., Alanezi, F. M., Alanzi, T. M., Alemu, B. w., Alhabib, K. F., Ali, M., Ali, S., Alicandro, G., Alinia, C., Alipour, V., Alizade, H., Aljunid, S. M., Alla, F., Allebeck, P., Almasi-Hashiani, A., Al-Mekhlafi, H. M., Alonso, J., Altirkawi, K. A., Amini-Rarani, M., Amiri, F., Amugsi, D. A., Ancuceanu, R., Anderlini, D., Anderson, J. A., Andrei, C. L., Andrei, T., Angus, C., Anjomshoa, M., Ansari, F., Ansari-Moghaddam, A., Antonazzo, I. C., Antonio, C. A. T., Antony, C. M., Antriyandarti, E., Anvari, D., Anwer, R., Appiah, S. C. Y., Arabloo, J., Arab-Zozani, M., Ariani, F., Armoon, B., Ärnlöv, J., Arzani, A., Asadi-Aliabadi, M., Asadi-Pooya, A. A., Ashbaugh, C., Assmus, M., Atafar, Z., Atnafu, D. D., Atout, M. M. d. W., Ausloos, F., Ausloos, M., Ayala Quintanilla, B. P., Ayano, G., Ayanore, M. A., Azari, S., Azarian, G., Azene, Z. N., Badawi, A., Badiye, A. D., Bahrami, M. A., Bakhshaei, M. H., Bakhtiari, A., Bakkannavar, S. M., Baldasseroni, A., Ball, K., Ballew, S. H., Balzi, D., Banach, M., Banerjee, S. K., Bante, A. B., Baraki, A. G., Barker-Collo, S. L., Bärnighausen, T. W., Barrero, L. H., Barthelemy, C. M., Barua, L., Basu, S., Baune, B. T., Bayati, M., Becker, J. S., Bedi, N., Beghi, E., Béjot, Y., Bell, M. L., Bennitt, F. B., Bensenor, I. M., Berhe, K., Berman, A. E., Bhagavathula, A. S., Bhageerathy, R., Bhala, N., Bhandari, D., Bhattacharyya, K., Bhutta, Z. A., Bijani, A., Bikbov, B., Bin Sayeed, M. S., Biondi, A., Birihane, B. M., Bisignano, C., Biswas, R. K., Bitew, H., Bohlouli, S., Bohluli, M., Boon-Dooley, A. S., Borges, G., Borzì, A. M., Borzouei, S., Bosetti, C., Boufous, S., Braithwaite, D., Breitborde, N. J. K., Breitner, S., Brenner, H., Briant, P. S., Briko, A. N., Briko, N. I., Britton, G. B., Bryazka, D., Bumgarner, B. R., Burkart, K., Burnett, R. T., Burugina Nagaraja, S., Butt, Z. A., Caetano dos Santos, F. L., Cahill, L. E., Cámera, L. L. A. A., Campos-Nonato, I. R., Cárdenas, R., Carreras, G., Carrero, J. J., Carvalho, F., Castaldelli-Maia, J. M., Castañeda-Orjuela, C. A., Castelpietra, G., Castro, F., Causey, K., Cederroth, C. R., Cercy, K. M., Cerin, E., Chandan, J. S., Chang, K.-L., Charlson, F. J., Chattu, V. K., Chaturvedi, S., Cherbuin, N., Chimed-Ochir, O., Cho, D. Y., Choi, J.-Y. J., Christensen, H., Chu, D.-T., Chung, M. T., Chung, S.-C., Cicuttini, F. M., Ciobanu, L. G., Cirillo, M., Classen, T. K. D., Cohen, A. J., Compton, K., Cooper, O. R., Costa, V. M., Cousin, E., Cowden, R. G., Cross, D. H., Cruz, J. A., Dahlawi, S. M. A., Damasceno, A. A. M., Damiani, G., Dandona, L., Dandona, R., Dangel, W. J., Danielsson, A.-K., Dargan, P. I., Darwesh, A. M., Daryani, A., Das, J. K., Das Gupta, R., das Neves, J., Dávila-Cervantes, C. A., Davitoiu, D. V., De Leo, D., Degenhardt, L., DeLang, M., Dellavalle, R. P., Demeke, F. M., Demoz, G. T., Demsie, D. G., Denova-Gutiérrez, E., Dervenis, N., Dhungana, G. P., Dianatinasab, M., Dias da Silva, D., Diaz, D., Dibaji Forooshani, Z. S., Djalalinia, S., Do, H. T., Dokova, K., Dorostkar, F., Doshmangir, L., Driscoll, T. R., Duncan, B. B., Duraes, A. R., Eagan, A. W., Edvardsson, D., El Nahas, N., El Sayed, I., El Tantawi, M., Elbarazi, I., Elgendy, I. Y., El-Jaafary, S. I., Elyazar, I. R. F., Emmons-Bell, S., Erskine, H. E., Eskandarieh, S., Esmaeilnejad, S., Esteghamati, A., Estep, K., Etemadi, A., Etisso, A. E., Fanzo, J., Farahmand, M., Fareed, M., Faridnia,

R., Farioli, A., Faro, A., Faruque, M., Farzadfar, F., Fattahi, N., Fazlzadeh, M., Feigin, V. L., Feldman, R., Fereshtehnejad, S.-M., Fernandes, E., Ferrara, G., Ferrari, A. J., Ferreira, M. L., Filip, I., Fischer, F., Fisher, J. L., Flor, L. S., Foigt, N. A., Folayan, M. O., Fomenkov, A. A., Force, L. M., Foroutan, M., Franklin, R. C., Freitas, M., Fu, W., Fukumoto, T., Furtado, J. M., Gad, M. M., Gakidou, E., Gallus, S., Garcia-Basteiro, A. L., Gardner, W. M., Geberemariyam, B. S., Gebreslassie, A. A. A. A., Geremew, A., Gershberg Hayoon, A., Gething, P. W., Ghadimi, M., Ghadiri, K., Ghaffarifar, F., Ghafourifard, M., Ghamari, F., Ghashghaee, A., Ghiasvand, H., Ghith, N., Gholamian, A., Ghosh, R., Gill, P. S., Ginindza, T. G. G., Giussani, G., Gnedovskaya, E. V., Goharinezhad, S., Gopalani, S. V., Gorini, G., Goudarzi, H., Goulart, A. C., Greaves, F., Grivna, M., Grosso, G., Gubari, M. I. M., Gugnani, H. C., Guimarães, R. A., Guled, R. A., Guo, G., Guo, Y., Gupta, R., Gupta, T., Haddock, B., Hafezi-Nejad, N., Hafiz, A., Haj-Mirzaian, A., Haj-Mirzaian, A., Hall, B. J., Halvaei, I., Hamadeh, R. R., Hamidi, S., Hammer, M. S., Hankey, G. J., Haririan, H., Haro, J. M., Hasaballah, A. I., Hasan, M. M., Hasanpoor, E., Hashi, A., Hassanipour, S., Hassankhani, H., Havmoeller, R. J., Hay, S. I., Hayat, K., Heidari, G., Heidari-Soureshjani, R., Henrikson, H. J., Herbert, M. E., Herteliu, C., Heydarpour, F., Hird, T. R., Hoek, H. W., Holla, R., Hoogar, P., Hosgood, H. D., Hossain, N., Hosseini, M., Hosseinzadeh, M., Hostiuc, M., Hostiuc, S., Househ, M., Hsairi, M., Hsieh, V. C.-r., Hu, G., Hu, K., Huda, T. M., Humayun, A., Huynh, C. K., Hwang, B.-F., Iannucci, V. C., Ibitoye, S. E., Ikeda, N., Ikuta, K. S., Ilesanmi, O. S., Ilic, I. M., Ilic, M. D., Inbaraj, L. R., Ippolito, H., Iqbal, U., Irvani, S. S. N., Irvine, C. M. S., Islam, M. M., Islam, S. M. S., Iso, H., Ivers, R. Q., Iwu, C. C. D., Iwu, C. J., Iyamu, I. O., Jaafari, J., Jacobsen, K. H., Jafari, H., Jafarinia, M., Jahani, M. A., Jakovljevic, M., Jalilian, F., James, S. L., Janjani, H., Javaheri, T., Javidnia, J., Jeemon, P., Jenabi, E., Jha, R. P., Jha, V., Ji, J. S., Johansson, L., John, O., John-Akinola, Y. O., Johnson, C. O., Jonas, J. B., Joukar, F., Jozwiak, J. J., Jürisson, M., Kabir, A., Kabir, Z., Kalani, H., Kalani, R., Kalankesh, L. R., Kalhor, R., Kanchan, T., Kapoor, N., Karami Matin, B., Karch, A., Karim, M. A., Kassa, G. M., Katikireddi, S. V., Kayode, G. A., Kazemi Karyani, A., Keiyoro, P. N., Keller, C., Kemmer, L., Kendrick, P. J., Khalid, N., Khammarnia, M., Khan, E. A., Khan, M., Khatab, K., Khater, M. M., Khatib, M. N., Khayamzadeh, M., Khazaei, S., Kieling, C., Kim, Y. J., Kimokoti, R. W., Kisa, A., Kisa, S., Kivimäki, M., Knibbs, L. D., Knudsen, A. K. S., Kocarnik, J. M., Kochhar, S., Kopec, J. A., Korshunov, V. A., Koul, P. A., Koyanagi, A., Kraemer, M. U. G., Krishan, K., Krohn, K. J., Kromhout, H., Kuate Defo, B., Kumar, G. A., Kumar, V., Kurmi, O. P., Kusuma, D., La Vecchia, C., Lacey, B., Lal, D. K., Lalloo, R., Lallukka, T., Lami, F. H., Landires, I., Lang, J. J., Langan, S. M., Larsson, A. O., Lasrado, S., Lauriola, P., Lazarus, J. V., Lee, P. H., Lee, S. W. H., LeGrand, K. E., Leigh, J., Leonardi, M., Lescinsky, H., Leung, J., Levi, M., Li, S., Lim, L.-L., Linn, S., Liu, S., Liu, S., Liu, Y., Lo, J., Lopez, A. D., Lopez, J. C. F., Lopukhov, P. D., Lorkowski, S., Lotufo, P. A., Lu, A., Lugo, A., Maddison, E. R., Mahasha, P. W., Mahdavi, M. M., Mahmoudi, M., Majeed, A., Maleki, A., Maleki, S., Malekzadeh, R., Malta, D. C., Mamun, A. A., Manda, A. L., Manguerra, H., Mansour-Ghanaei, F., Mansouri, B., Mansournia, M. A., Mantilla Herrera, A. M., Maravilla, J. C., Marks, A., Martin, R. V., Martini, S., Martins-Melo, F. R., Masaka, A., Masoumi, S. Z., Mathur, M. R., Matsushita, K., Maulik, P. K., McAlinden, C., McGrath, J. J., McKee, M., Mehndiratta, M. M., Mehri, F., Mehta, K. M., Memish, Z. A., Mendoza, W., Menezes, R. G., Mengesha, E. W., Mereke, A., Mereta, S. T., Meretoja,

A., Meretoja, T. J., Mestrovic, T., Miazgowski, B., Miazgowski, T., Michalek, I. M., Miller, T. R., Mills, E. J., Mini, G. K., Miri, M., Mirica, A., Mirrakhimov, E. M., Mirzaei, H., Mirzaei, M., Mirzaei, R., Mirzaei-Alavijeh, M., Misganaw, A. T., Mithra, P., Moazen, B., Mohammad, D. K., Mohammad, Y., Mohammad Gholi Mezerji, N., Mohammadian-Hafshejani, A., Mohammadifard, N., Mohammadpourhodki, R., Mohammed, A. S., Mohammed, H., Mohammed, J. A., Mohammed, S., Mokdad, A. H., Molokhia, M., Monasta, L., Mooney, M. D., Moradi, G., Moradi, M., Moradi-Lakeh, M., Moradzadeh, R., Moraga, P., Morawska, L., Morgado-da-Costa, J., Morrison, S. D., Mosapour, A., Mosser, J. F., Mouodi, S., Mousavi, S. M., Mousavi Khaneghah, A., Mueller, U. O., Mukhopadhyay, S., Mullany, E. C., Musa, K. I., Muthupandian, S., Nabhan, A. F., Naderi, M., Nagarajan, A. J., Nagel, G., Naghavi, M., Naghshtabrizi, B., Naimzada, M. D., Najafi, F., Nangia, V., Nansseu, J. R., Naserbakht, M., Nayak, V. C., Negoi, I., Ngunjiri, J. W., Nguyen, C. T., Nguyen, H. L. T., Nguyen, M., Nigatu, Y. T., Nikbakhsh, R., Nixon, M. R., Nnaji, C. A., Nomura, S., Norrving, B., Noubiap, J. J., Nowak, C., Nunez-Samudio, V., Oţoiu, A., Oancea, B., Odell, C. M., Ogbo, F. A., Oh, I.-H., Okunga, E. W., Oladnabi, M., Olagunju, A. T., Olusanya, B. O., Olusanya, J. O., Omer, M. O., Ong, K. L., Onwujekwe, O. E., Orpana, H. M., Ortiz, A., Osarenotor, O., Osei, F. B., Ostroff, S. M., Otstavnov, N., Otstavnov, S. S., Øverland, S., Owolabi, M. O., P A, M., Padubidri, J. R., Palladino, R., Panda-Jonas, S., Pandey, A., Parry, C. D. H., Pasovic, M., Pasupula, D. K., Patel, S. K., Pathak, M., Patten, S. B., Patton, G. C., Pazoki Toroudi, H., Peden, A. E., Pennini, A., Pepito, V. C. F., Peprah, E. K., Pereira, D. M., Pesudovs, K., Pham, H. Q., Phillips, M. R., Piccinelli, C., Pilz, T. M., Piradov, M. A., Pirsaheb, M., Plass, D., Polinder, S., Polkinghorne, K. R., Pond, C. D., Postma, M. J., Pourjafar, H., Pourmalek, F., Poznańska, A., Prada, S. I., Prakash, V., Pribadi, D. R. A., Pupillo, E., Quazi Syed, Z., Rabiee, M., Rabiee, N., Radfar, A., Rafiee, A., Raggi, A., Rahman, M. A., Rajabpour-Sanati, A., Rajati, F., Rakovac, I., Ram, P., Ramezanzadeh, K., Ranabhat, C. L., Rao, P. C., Rao, S. J., Rashedi, V., Rathi, P., Rawaf, D. L., Rawaf, S., Rawal, L., Rawassizadeh, R., Rawat, R., Razo, C., Redford, S. B., Reiner, R. C., Jr., Reitsma, M. B., Remuzzi, G., Renjith, V., Renzaho, A. M. N., Resnikoff, S., Rezaei, N., Rezaei, N., Rezapour, A., Rhinehart, P.-A., Riahi, S. M., Ribeiro, D. C., Ribeiro, D., Rickard, J., Rivera, J. A., Roberts, N. L. S., Rodríguez-Ramírez, S., Roever, L., Ronfani, L., Room, R., Roshandel, G., Roth, G. A., Rothenbacher, D., Rubagotti, E., Rwegerera, G. M., Sabour, S., Sachdev, P. S., Saddik, B., Sadeghi, E., Sadeghi, M., Saeedi, R., Saeedi Moghaddam, S., Safari, Y., Safi, S., Safiri, S., Sagar, R., Sahebkar, A., Sajadi, S. M., Salam, N., Salamati, P., Salem, H., Salem, M. R. R., Salimzadeh, H., Salman, O. M., Salomon, J. A., Samad, Z., Samadi Kafil, H., Sambala, E. Z., Samy, A. M., Sanabria, J., Sánchez-Pimienta, T. G., Santomauro, D. F., Santos, I. S., Santos, J. V., Santric-Milicevic, M. M., Saraswathy, S. Y. I., Sarmiento-Suárez, R., Sarrafzadegan, N., Sartorius, B., Sarveazad, A., Sathian, B., Sathish, T., Sattin, D., Saxena, S., Schaeffer, L. E., Schiavolin, S., Schlaich, M. P., Schmidt, M. I., Schutte, A. E., Schwebel, D. C., Schwendicke, F., Senbeta, A. M., Senthilkumaran, S., Sepanlou, S. G., Serdar, B., Serre, M. L., Shadid, J., Shafaat, O., Shahabi, S., Shaheen, A. A., Shaikh, M. A., Shalash, A. S., Shams-Beyranvand, M., Shamsizadeh, M., Sharafi, K., Sheikh, A., Sheikhtaheri, A., Shibuya, K., Shield, K. D., Shigematsu, M., Shin, J. I., Shin, M.-J., Shiri, R., Shirkoohi, R., Shuval, K., Siabani, S., Sierpinski, R., Sigfusdottir, I. D., Sigurvinsdottir, R., Silva, J. P., Simpson, K. E., Singh, J. A., Singh, P., Skiadaresi, E., Skou, S. T., Skryabin, V. Y.,

Smith, E. U. R., Soheili, A., Soltani, S., Soofi, M., Sorensen, R. J. D., Soriano, J. B., Sorrie, M. B., Soshnikov, S., Soyiri, I. N., Spencer, C. N., Spotin, A., Sreeramareddy, C. T., Srinivasan, V., Stanaway, J. D., Stein, C., Stein, D. J., Steiner, C., Stockfelt, L., Stokes, M. A., Straif, K., Stubbs, J. L., Sufiyan, M. a. B., Suleria, H. A. R., Suliankatchi Abdulkader, R., Sulo, G., Sultan, I., Szumowski, Ł., Tabarés-Seisdedos, R., Tabb, K. M., Tabuchi, T., Taherkhani, A., Tajdini, M., Takahashi, K., Takala, J. S., Tamiru, A. T., Taveira, N., Tehrani-Banihashemi, A., Temsah, M.-H., Tesema, G. A., Tessema, Z. T., Thurston, G. D., Titova, M. V., Tohidinik, H. R., Tonelli, M., Topor-Madry, R., Topouzis, F., Torre, A. E., Touvier, M., Tovani-Palone, M. R. R., Tran, B. X., Travillian, R., Tsatsakis, A., Tudor Car, L., Tyrovolas, S., Uddin, R., Umeokonkwo, C. D., Unnikrishnan, B., Upadhyay, E., Vacante, M., Valdez, P. R., van Donkelaar, A., Vasankari, T. J., Vasseghian, Y., Veisani, Y., Venketasubramanian, N., Violante, F. S., Vlassov, V., Vollset, S. E., Vos, T., Vukovic, R., Waheed, Y., Wallin, M. T., Wang, Y., Wang, Y.-P., Watson, A., Wei, J., Wei, M. Y. W., Weintraub, R. G., Weiss, J., Werdecker, A., West, J. J., Westerman, R., Whisnant, J. L., Whiteford, H. A., Wiens, K. E., Wolfe, C. D. A., Wozniak, S. S., Wu, A.-M., Wu, J., Wulf Hanson, S., Xu, G., Xu, R., Yadgir, S., Yahyazadeh Jabbari, S. H., Yamagishi, K., Yaminfirooz, M., Yano, Y., Yaya, S., Yazdi-Feyzabadi, V., Yeheyis, T. Y., Yilgwan, C. S., Yilma, M. T., Yip, P., Yonemoto, N., Younis, M. Z., Younker, T. P., Yousefi, B., Yousefi, Z., Yousefinezhadi, T., Yousuf, A. Y., Yu, C., Yusefzadeh, H., Zahirian Moghadam, T., Zamani, M., Zamanian, M., Zandian, H., Zastrozhin, M. S., Zhang, Y., Zhang, Z.-J., Zhao, J. T., Zhao, X.-J. G., Zhao, Y., Zhou, M., Ziapour, A., Zimsen, S. R. M., Brauer, M., Afshin, A., & Lim, S. S. (2020). Global burden of 87 risk factors in 204 countries and territories, 1990-2013;2019: a systematic analysis for the Global Burden of Disease Study 2019. The Lancet, 396(10258), 1223-1249. https://doi.org/10.1016/S0140-6736(20)30752-2

Power, M. C., Kioumourtzoglou, M.-A., Hart, J. E., Okereke, O. I., Laden, F., & Weisskopf, M. G. (2015). The relation between past exposure to fine particulate air pollution and prevalent anxiety: observational cohort study. BMJ : British Medical Journal, 350, h1111. https://doi.org/10.1136/bmj.h1111

Pun, V. C., Manjourides, J., & Suh, H. (2017). Association of Ambient Air Pollution with Depressive and Anxiety Symptoms in Older Adults: Results from the NSHAP Study. Environmental Health Perspectives, 125(3), 342-348. https://doi.org/doi:10.1289/EHP494

Reid Colleen, E., Brauer, M., Johnston Fay, H., Jerrett, M., Balmes John, R., & Elliott Catherine, T. (2016). Critical Review of Health Impacts of Wildfire Smoke Exposure. Environmental Health Perspectives, 124(9), 1334-1343. https://doi.org/10.1289/ehp.1409277

Richardson, D., Black, A. S., Irving, D., Matear, R. J., Monselesan, D. P., Risbey, J. S., Squire, D. T., & Tozer, C. R. (2022). Global increase in wildfire potential from compound fire weather and drought. npj Climate and Atmospheric Science, 5(1), 23. https://doi.org/10.1038/s41612-022-00248-4

Shi, W., Li, T., Zhang, Y., Sun, Q., Chen, C., Wang, J., Fang, J., Zhao, F., Du, P., & Shi, X. (2020). Depression and Anxiety Associated with Exposure to Fine Particulate Matter Constituents: A Cross-Sectional Study in North China. Environmental Science & Technology, 54(24), 16006-16016. https://doi.org/10.1021/acs.est.0c05331

To, P., Eboreime, E., & Agyapong, V. I. O. (2021). The Impact of Wildfires on Mental Health: A Scoping Review. Behavioral Sciences, 11(9), 126. https://www.mdpi.com/2076-328X/11/9/126

Vasiliadis, H. M., Dionne, P. A., Préville, M., Gentil, L., Berbiche, D., & Latimer, E. (2013). The excess healthcare costs associated with depression and anxiety in elderly living in the community. Am J Geriatr Psychiatry, 21(6), 536-548. https://doi.org/10.1016/j.jagp.2012.12.016

Wibbenmeyer, M., & Robertson, M. (2022). The distributional incidence of wildfire hazard in the western United States. Environmental Research Letters, 17(6), 064031. https://doi.org/10.1088/1748-9326/ac60d7

Yang, X., Fang, Y., Chen, H., Zhang, T., Yin, X., Man, J., Yang, L., & Lu, M. (2021). Global, regional and national burden of anxiety disorders from 1990 to 2019: results from the Global Burden of Disease Study 2019. Epidemiol Psychiatr Sci, 30, e36. https://doi.org/10.1017/s2045796021000275

Zhang, L., Lau, W., Tao, W., & Li, Z. (2020). Large Wildfires in the Western United States Exacerbated by Tropospheric Drying Linked to a Multi-Decadal Trend in the Expansion of the Hadley Circulation [https://doi.org/10.1029/2020GL087911]. Geophysical Research Letters, 47(16), e2020GL087911. https://doi.org/https://doi.org/10.1029/2020GL087911

Zhao, W., Zhao, Y., Wang, P., Zhou, Y., Meng, X., Ma, W., Li, J., & Zhang, Y. (2022). PM2.5 exposure associated with prenatal anxiety and depression in pregnant women. Ecotoxicology and Environmental Safety, 248, 114284. https://doi.org/https://doi.org/10.1016/j.ecoenv.2022.114284

4.8. Tables and Figures

Table 4-1. Study population

	Arizona	California	Nevada	Oregon	Utah	Overall
N	184,772	1,513,553	63,643	67,953	67,944	1,897,865
SEX						
Males	75,710 (41.0%)	594,981 (39.3%)	25,697 (40.4%)	27,372 (40.3%)	25,972 (38.2%)	749,732 (39.5%)
Females	109,062 (59.0%)	918,572 (60.7%)	37,946 (59.6%)	40,581 (59.7%)	41,972 (61.8%)	1,148,133 (60.5%)
Age groups						
5-17	14,797 (8.0%)	120,235 (7.9%)	4,718 (7.4%)	6,232 (9.2%)	6,423 (9.5%)	152,405 (8.0%)
18-64	152,477 (82.5%)	1,258,049 (83.1%)	53,879 (84.7%)	54,913 (80.8%)	56,654 (83.4%)	1,575,972 (83.0%)
65+	17,498 (9.5%)	135,269 (8.9%)	5,046 (7.9%)	6,808 (10.0%)	4,867 (7.2%)	169,488 (8.9%)
Ethnicity						
Non-Hispanic	132,933 (71.9%)	893,532 (59.0%)	51,800 (81.4%)	60,348 (88.8%)	43,253 (63.7%)	1,181,866 (62.3%)
Hispanic	50,398 (27.3%)	580,410 (38.3%)	10,744 (16.9%)	6,371 (9.4%)	8,264 (12.2%)	656,187 (34.6%)
Missing	1,441 (0.8%)	39,611 (2.6%)	1,099 (1.7%)	1,234 (1.8%)	16,427 (24.2%)	59,812 (3.2%)
Race						
White	114,490 (62.0%)	959,218 (63.4%)	38,497 (60.5%)	56,605 (83.3%)	59,474 (87.5%)	1,228,284 (64.7%)
Black	10,623 (5.7%)	132,832 (8.8%)	7,905 (12.4%)	2,089 (3.1%)	1,044 (1.5%)	154,493 (8.1%)
Asian	2,110 (1.1%)	70,372 (4.6%)	1,823 (2.9%)	1,004 (1.5%)	1,003 (1.5%)	76,312 (4.0%)
Others	57,549 (31.1%)	351,131 (23.2%)	15,418 (24.2%)	8,255 (12.1%)	6,423 (9.5%)	438,776 (23.1%)

Table 4-2. Wildfire-related exposures

	Control days (N = 6,452,523)	Case days (N = 1,897,865)	Overall (N = 8,350,546)
Smoke $PM_{2.5}$			
Mean (SD)	0.930 (3.17)	0.935 (3.20)	0.931 (3.18)
Background $PM_{2.5}$			
Mean (SD)	9.90 (4.42)	9.91 (4.41)	9.91 (4.42)
Smoke events	486,186	142,436	629,622
Major smoke events	9,122	2,809	11,931
	Control days (N = 14,574)	**Case days (N = 4,264)**	**Overall (N = 18,838)**
Active fire points[#]			
Mean (SD)	2.92 (7.48)	3.16 (8.34)	2.97 (7.68)
Cumulative FRP[#]			
Mean (SD)	211 (814)	415 (821)	362 (816)

[#]: We only included days with active fire points for these statistics. Nevada was excluded from the analyses for fire points due to insufficient zip code information.

Table 4-3. The associations between wildfire-related exposures and ED visits for anxiety disorders

Exposures	Model 1		Model 2	
	OR (95% CI)	P-value	OR (95% CI)	P-value
Smoke $PM_{2.5}$[1]	1.006 (1.000,1.012)	0.029*	1.003 (0.998,1.010)	0.169
Smoke events	1.005 (0.998,1.013)	0.183	1.005 (0.997,1.012)	0.230
Major smoke events	1.063 (1.015,1.113)	0.009*	1.056 (1.009,1.106)	0.019*
Fire points	1.002 (0.999,1.005)	0.066	1.002 (0.999,1.005)	0.068
Cumulative FRP[2]	1.000 (0.999,1.001)	0.200	1.000 (0.999,1.001)	0.205

*: $p < 0.05$. Model 1 only included wildfire-related exposures and the covariates, while Model 2 also adjusted for background $PM_{2.5}$. 1: The OR was for a 10 $\mu g/m^3$ increase in 48-h smoke $PM_{2.5}$. 2: The OR was for an IQR (67.75 W) increase in the cumulative FRP.

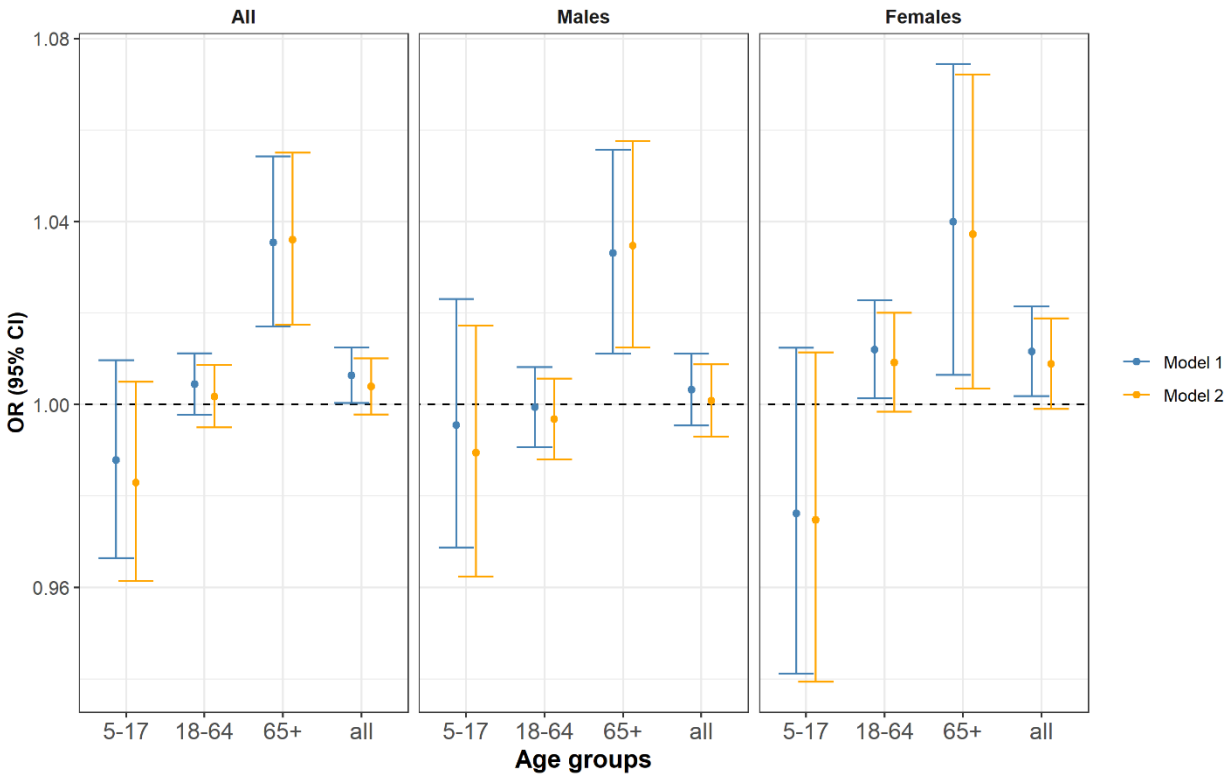

Fig. 4-1. The age- and sex-stratified analysis for 48-h smoke $PM_{2.5}$. Model 1 only included 48-h smoke $PM_{2.5}$ and the covariates. Model 2 also adjusted for background $PM_{2.5}$. The ORs are for a 10 $\mu g/m^3$ increase in smoke $PM_{2.5}$.

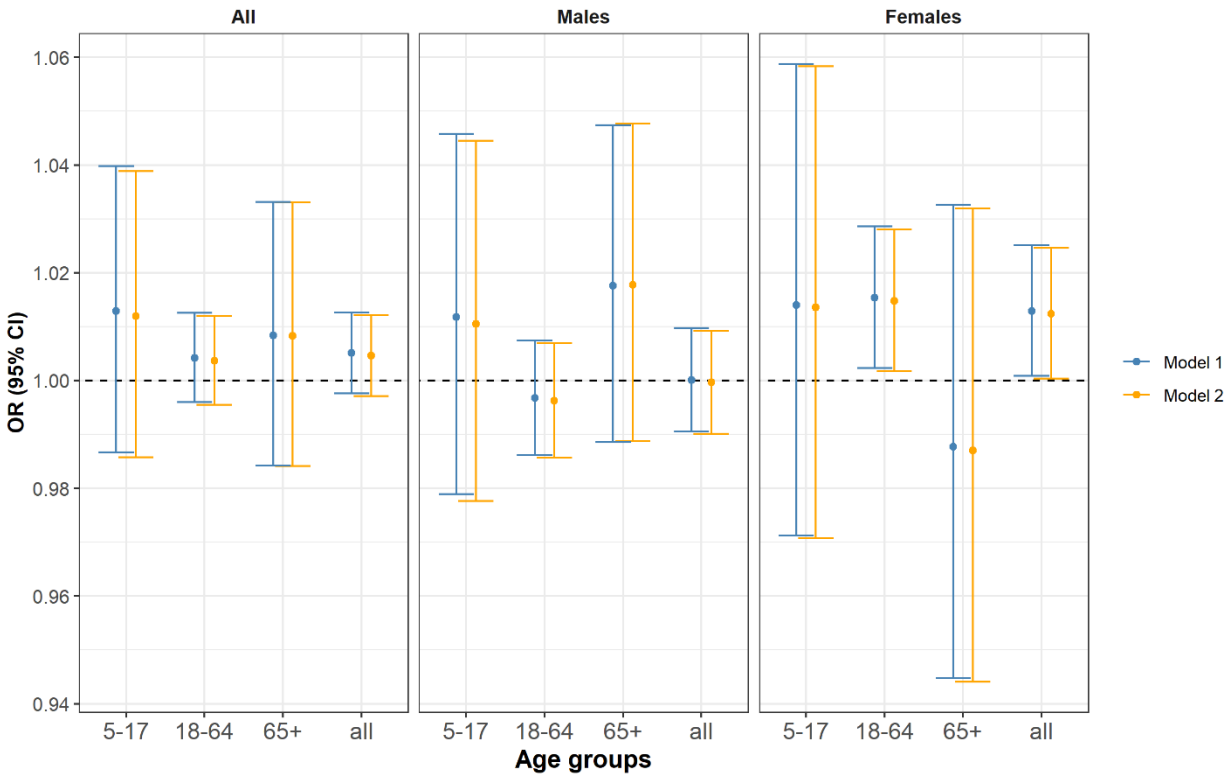

Fig. 4-2. The age- and sex-stratified analysis for smoke events. Model 1 only included smoke events and other covariates. Model 2 also adjusted for background $PM_{2.5}$.

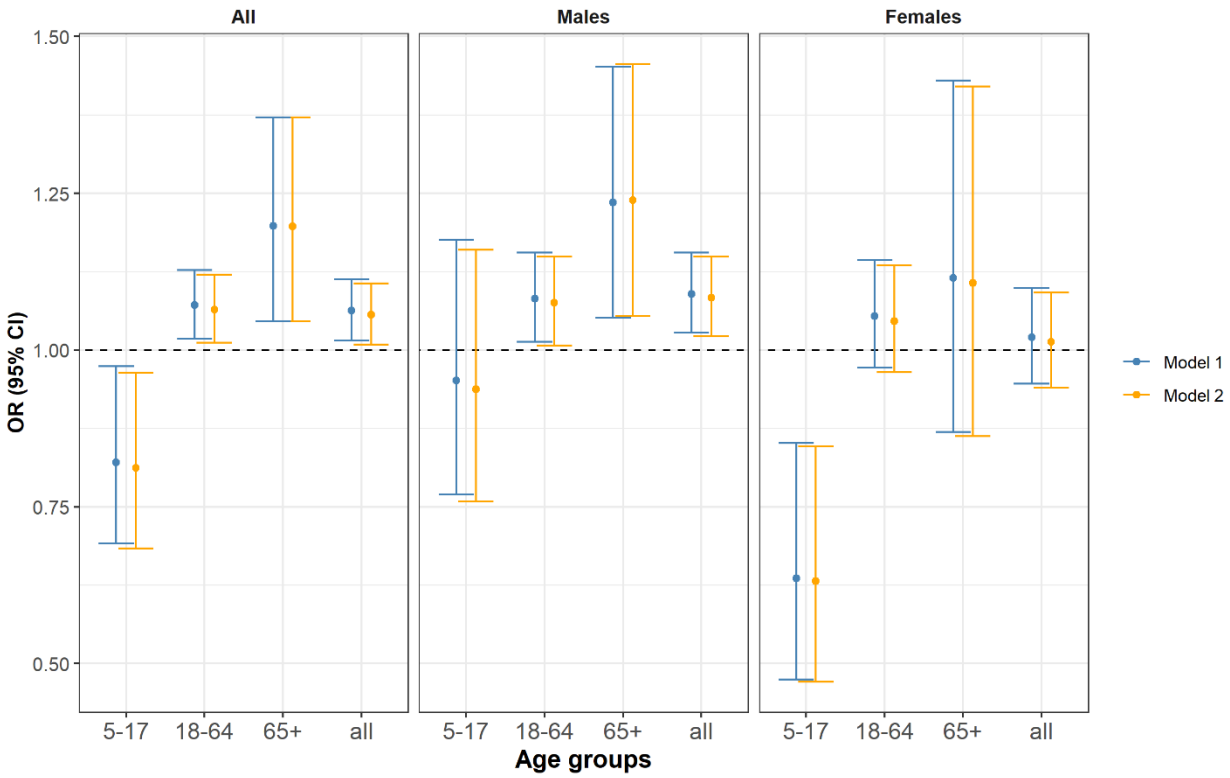

Fig. 4-3. The age- and sex-stratified analysis for major smoke events. Model 1 only included major smoke events and other covariates. Model 2 also adjusted for background $PM_{2.5}$.

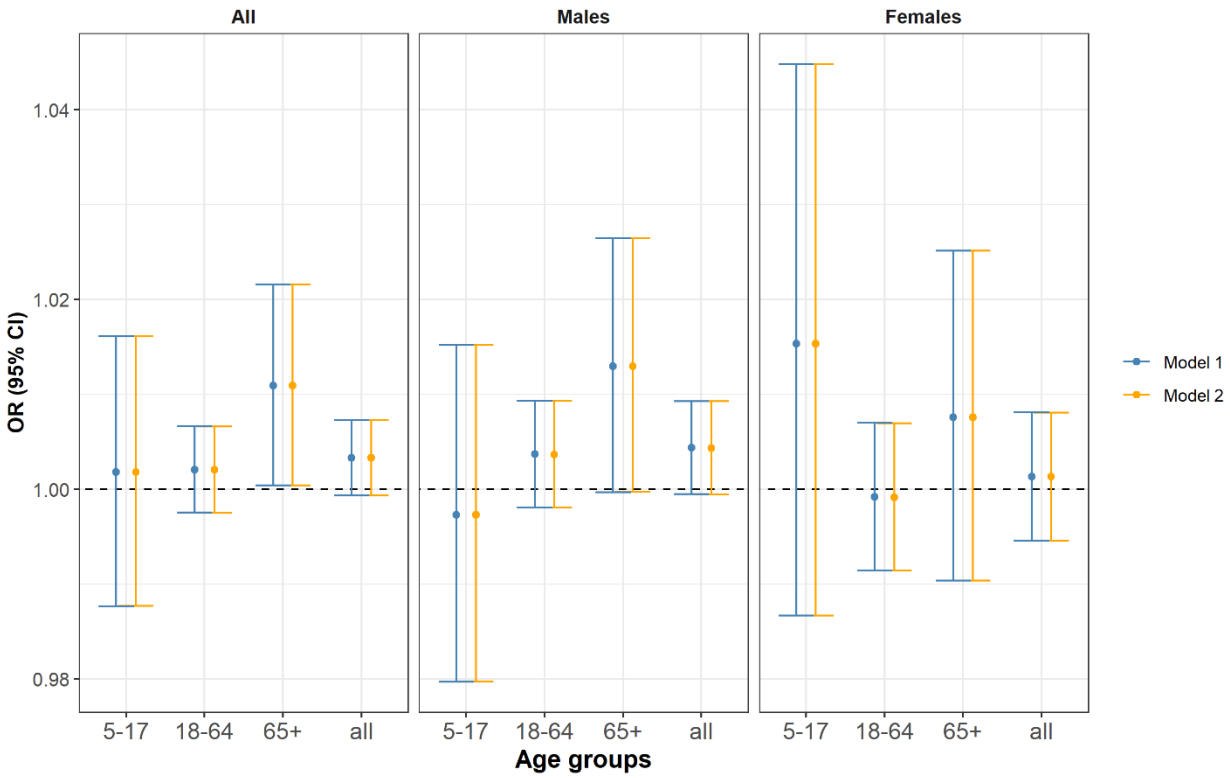

Fig. 4-4. The age- and sex-stratified analysis for active fire points. Model 1 only included the total number of active fire points in the past 48h and other covariates. Model 2 also adjusted for background $PM_{2.5}$.

5. Conclusions

Aim 1 of this dissertation used satellite remote sensing to establish a high-performance model for ground-level O_3 pollution from 2005-2018 in China. Our model considered two potential pathways through which surface-level O_3 pollution can be produced. Compared to existing models, our model improved the spatial resolution to 0.05° and agreed well with the CNEMC monitoring data and the TOAR historical O_3 concentrations. With this advance, we were able to identify the seasonal and spatial variation of O_3 pollution in China, especially in the major city clusters like the NCP, the YRD, and the PRD. Our model would greatly benefit future epidemiological studies that aim to investigate the health impact of O_3, especially the historical cohort studies established before 2013. Furthermore, our findings highlighted that ground-level O_3 pollution is controlled by the concentrations of both NOx and VOCs. Under such a circumstance, only controlling for NOx is insufficient to mitigate O_3 pollution in China. The next round of the APPCAP in China should prioritize VOCs control as well.

Combining the O_3 model with other satellite-driven exposure datasets. The aim 2 of this dissertation investigated the impact of ambient air pollution on the cognitive health among the Chinese elderly population using the CLHLS. The CLHLS comprises six rounds of survey that took place in 1998, 2000, 2002, 2005, 2008, 2014, and 2018, respectively. With the advance of the satellite-driven exposure model, we were able to use all the CLHLS data after 2005 to study the long-term impact of air pollution. Our results highlighted that annual mean $PM_{2.5}$ and NO_2 concentrations were both positively associated with cognitive impairment in the single pollutant model. While the annual mean MDA8 O_3 did not exhibit a positive correlation with cognitive impairment, our findings indicate that the average MDA8 O_3 during the warm season (defined as April to September) significantly contributes to the risk of this adverse outcome, suggesting that

warm-season O_3 is potentially a better exposure metric. Furthermore, the role of NO_2 need to be emphasized since it was the only air pollutant that remained positively associated with cognitive impairment in the multi-pollutant model.

In addition to anthropogenic air pollution, aim 3 of this dissertation investigated the mental health impact of air pollution and other related exposures caused by wildfires. Our study was the largest and most comprehensive investigation on the association between wildfire-related exposures and anxiety disorders. The findings of this study suggest that wildfires are associated with an increased risk of ED visits for anxiety disorders through two potential pathways, i.e., the inhalation of wildfire smoke $PM_{2.5}$ and the direct psychological impacts of wildfire smoke events and active fire points. Furthermore, we found that women and the elderly population are more susceptible to the anxiety disorders associated with wildfire-related exposures. Our study was the first to quantify the magnitude of the association between wildfire-related exposures and ED visits for anxiety disorders. Given the continuous exacerbation of global climate change, the mental health consequences associated with wildfires warrant further investigation.

6. Appendix A. Supplemental materials for manuscript 1

Table S1-1. List of the input variables

Abbreviation	name	Source
DISPH	Zero plane displacement height	MERRA-2
PBLH	Planetary boundary layer height	MERRA-2
ALBEDO	Surface albedo	MERRA-2
EFLUX	Total latent energy flux	MERRA-2
T10M	10 meter air temperature	MERRA-2
USTAR	Surface velocity scale	MERRA-2
PRECTOT	Total precipitation	MERRA-2
SWGDN	Surface incoming shortwave flux	MERRA-2
RH	Relative humidity	MERRA-2
U	Eastward wind	MERRA-2
V	Northward wind	MERRA-2
PS	Surface pressure	MERRA-2
QV	Specific humidity	MERRA-2
T	Air temperature	MERRA-2
OMEGA	Vertical pressure velocity	MERRA-2
TROPPT	Tropopause pressure based on thermal estimate	MERRA-2
RH_C	Relative humidity	MERRA-2
U_C	Eastward wind	MERRA-2
V_C	Northward wind	MERRA-2
OMEGA_C	Vertical pressure velocity	MERRA-2
PS_C	Surface pressure	MERRA-2
QV_C	Specific humidity	MERRA-2
T_C	Air temperature	MERRA-2
PV_C	Ertels potential vorticity	MERRA-2
Boundary-layer O3	Gap-filled boundary-layer column ozone	OMPROFOZ
Elevation	Elevation	ASTER GDEM
LANDUSE_10	Cropland, rainfed	ESA CCI
LANDUSE_11	Herbaceous cover	ESA CCI
LANDUSE_12	Tree or shrub cover	ESA CCI
LANDUSE_20	Cropland, irrigated or post flooding	ESA CCI
LANDUSE_30	Mosaic cropland (>50%) / natural vegetation (tree, shrub, herbaceous cover) (<50%)	ESA CCI
LANDUSE_40	Mosaic natural vegetation (tree, shrub, herbaceous cover) (>50%) / cropland (<50%)	ESA CCI
LANDUSE_50	Tree cover, broadleaved, evergreen, closed to open (>15%)	ESA CCI
LANDUSE_60	Tree cover, broadleaved, deciduous, closed to open (>15%)	ESA CCI
LANDUSE_61	Tree cover, broadleaved, deciduous, closed (>40%)	ESA CCI
LANDUSE_62	Tree cover, broadleaved, deciduous, open (15•]40%)	ESA CCI

LANDUSE_70	Tree cover, needleleaved, evergreen, closed to open (>15%)	ESA CCI
LANDUSE_71	Tree cover, needleleaved, evergreen, closed (>40%)	ESA CCI
LANDUSE_72	Tree cover, needleleaved, evergreen, open (15•]40%)	ESA CCI
LANDUSE_80	Tree cover, needleleaved, deciduous, closed to open (>15%)	ESA CCI
LANDUSE_81	Tree cover, needleleaved, deciduous, closed (>40%)	ESA CCI
LANDUSE_90	Tree cover, mixed leaf type (broadleaved and needleleaved)	ESA CCI
LANDUSE_100	Mosaic tree and shrub (>50%) / herbaceous cover (<50%)	ESA CCI
LANDUSE_110	Mosaic herbaceous cover (>50%) / tree and shrub (<50%)	ESA CCI
LANDUSE_120	Shrubland	ESA CCI
LANDUSE_121	Evergreen shrubland	ESA CCI
LANDUSE_122	Deciduous shrubland	ESA CCI
LANDUSE_130	Grassland	ESA CCI
LANDUSE_140	Lichens and mosses	ESA CCI
LANDUSE_150	Sparse vegetation (tree, shrub, herbaceous cover) (<15%)	ESA CCI
LANDUSE_152	Sparse shrub (<15%)	ESA CCI
LANDUSE_153	Sparse herbaceous cover (<15%)	ESA CCI
LANDUSE_160	Tree cover, flooded, fresh or brakish water	ESA CCI
LANDUSE_170	Tree cover, flooded, saline water	ESA CCI
LANDUSE_180	Shrub or herbaceous cover, flooded, fresh/saline/brakish water	ESA CCI
LANDUSE_190	Urban areas	ESA CCI
LANDUSE_200	Bare areas	ESA CCI
LANDUSE_201	Consolidated bare areas	ESA CCI
LANDUSE_202	Unconsolidated bare areas	ESA CCI
LANDUSE_210	Water bodies	ESA CCI
LANDUSE_220	Permanent snow and ice	ESA CCI
ROAD_LENGTH	Total road length	gROADs
NO2	OMI tropospheric column Nitrogen dioxide	OMI
Population	Population	Landscan
FLASH	Lightning activity	GEOS-Chem
FRP*	Fire radiative power	MODIS
A priori L22_24 *	Gap-filled a priori L22-L24 partial column ozone	OMPROFOZ
A priori L24 *	Gap-filled a priori L24 partial column ozone	OMPROFOZ
OMI L22_L24*	Gap-filled retrieved L22-L24 partial column ozone	OMPROFOZ

* Variables not included in the original model but used for parameter comparison.

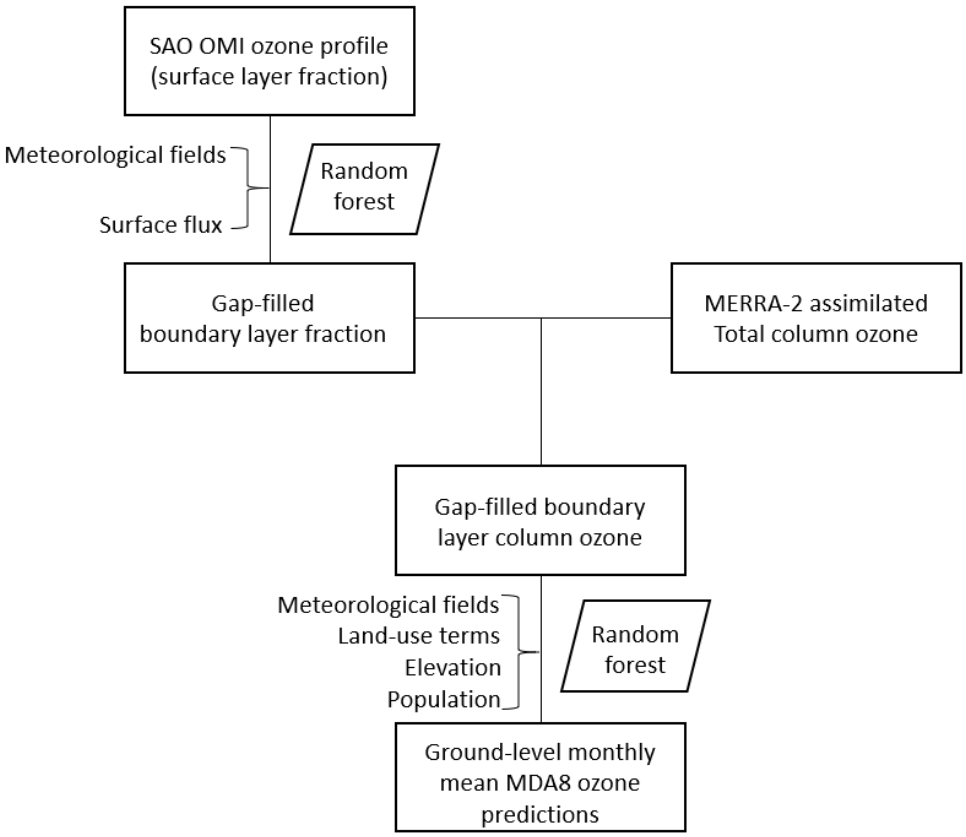

Fig.S1-1. Study workflow Abbreviations: SAO, Smithsonian Astrophysical Observatory; OMI, Ozone Monitoring Instrument; MERRA-2, the Modern-Era Retrospective analysis for Research and Applications, Version 2.

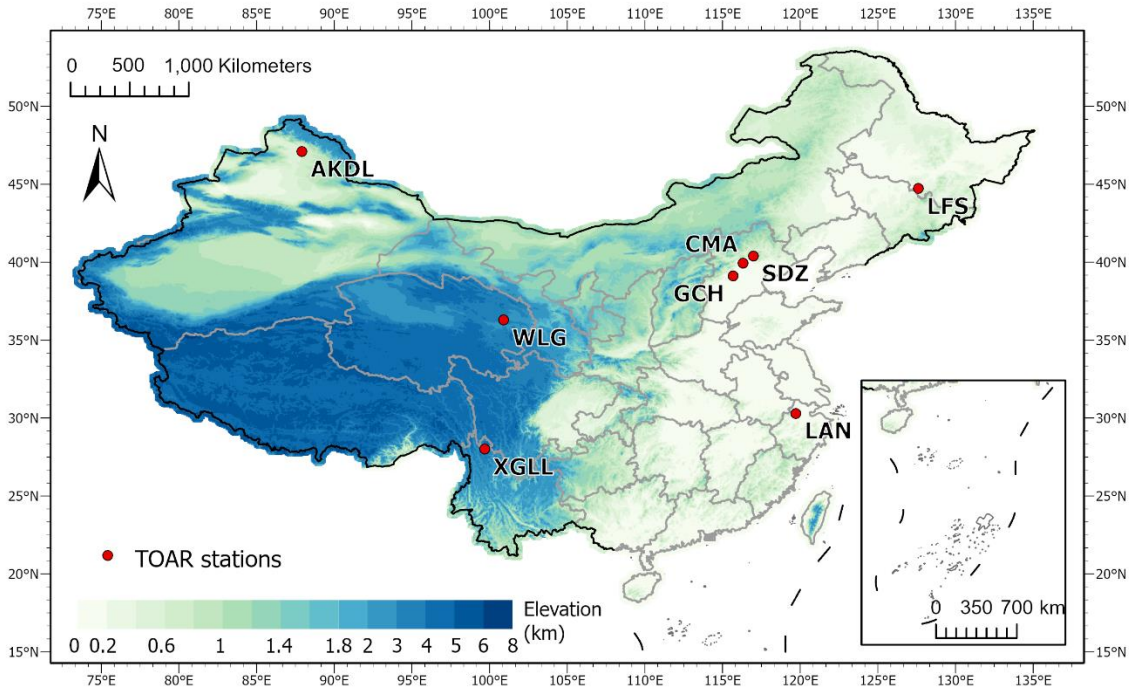

Fig. S1-2. Distribution of the Tropospheric Ozone Assessment Report (TOAR) monitoring stations. Red circle dots with black outlines represent the location of TOAR monitoring stations. Abbreviations: WLG, Mt. Waliguan; SDZ, Shandianzi; LAN, Lin'an; LFS, Longfengshan; XGLL, Xianggelila; AKDL, Akedala; GCH, Gucheng, CMA. China Meteorological Administration; TOAR: Tropospheric Ozone Assessment Report.

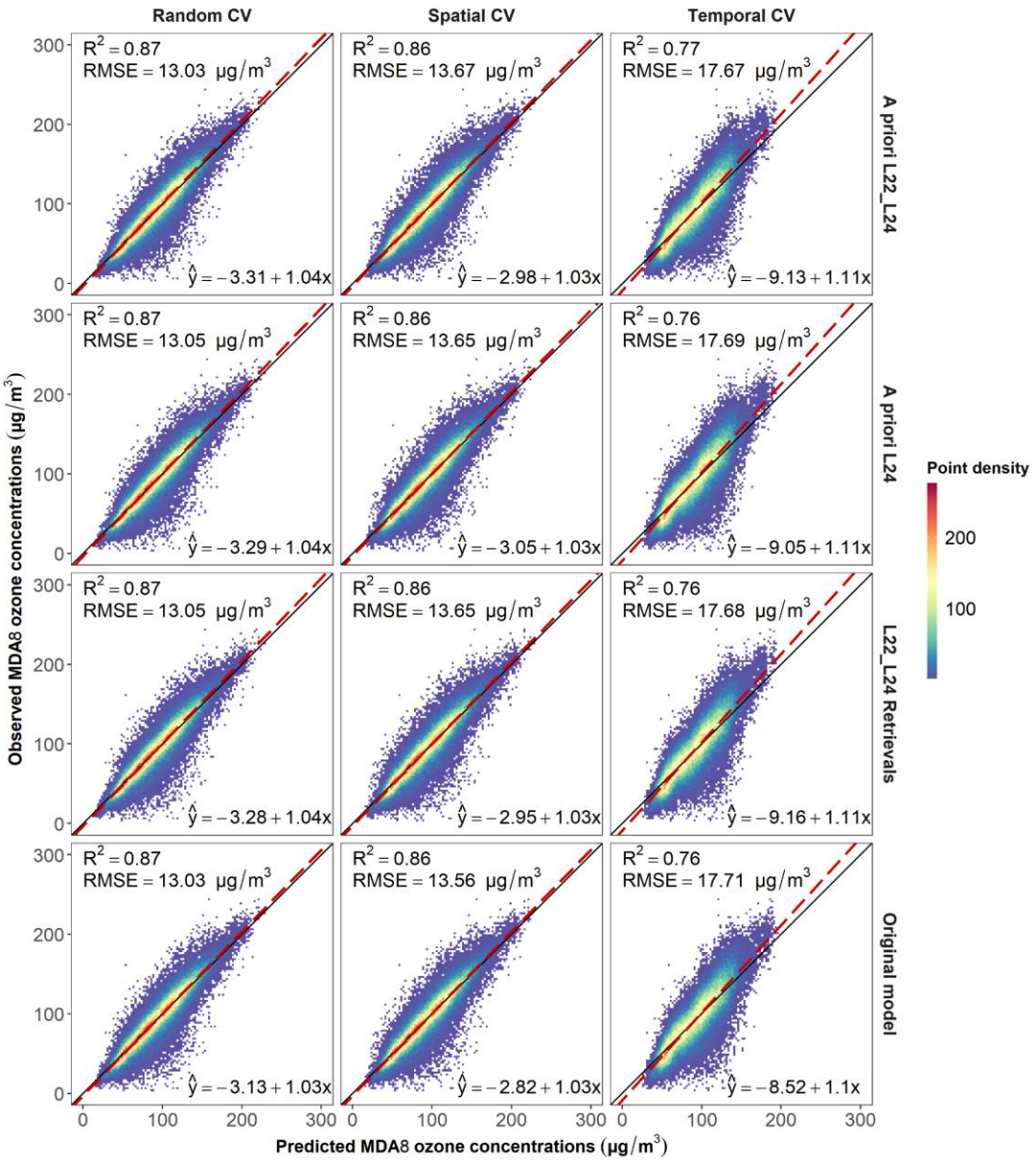

Fig. S1-3. Comparison of model performance on the training dataset (2014-2019) with different OMI-derived partial column ozone (original model). Left column: random CV; middle column: spatial CV; right column: temporal CV. Top row: model with a priori ozone profile L22-L24; second row (from top to bottom): model with a priori ozone profile L24; third row: model with L22-L24 retrievals; bottom row: the original model with retrieved ozone profile L24. The functions on the bottom-right corners are the regression functions between the predicted and observed monthly mean MDA8 ozone concentrations. Red dashed lines: the regression line between the predictions and observations; black solid lines: the x = y line; The color scale represents the density of the points. Abbreviations: MDA8, daily maximum 8-hour average; OMI, Ozone Monitoring Instrument.

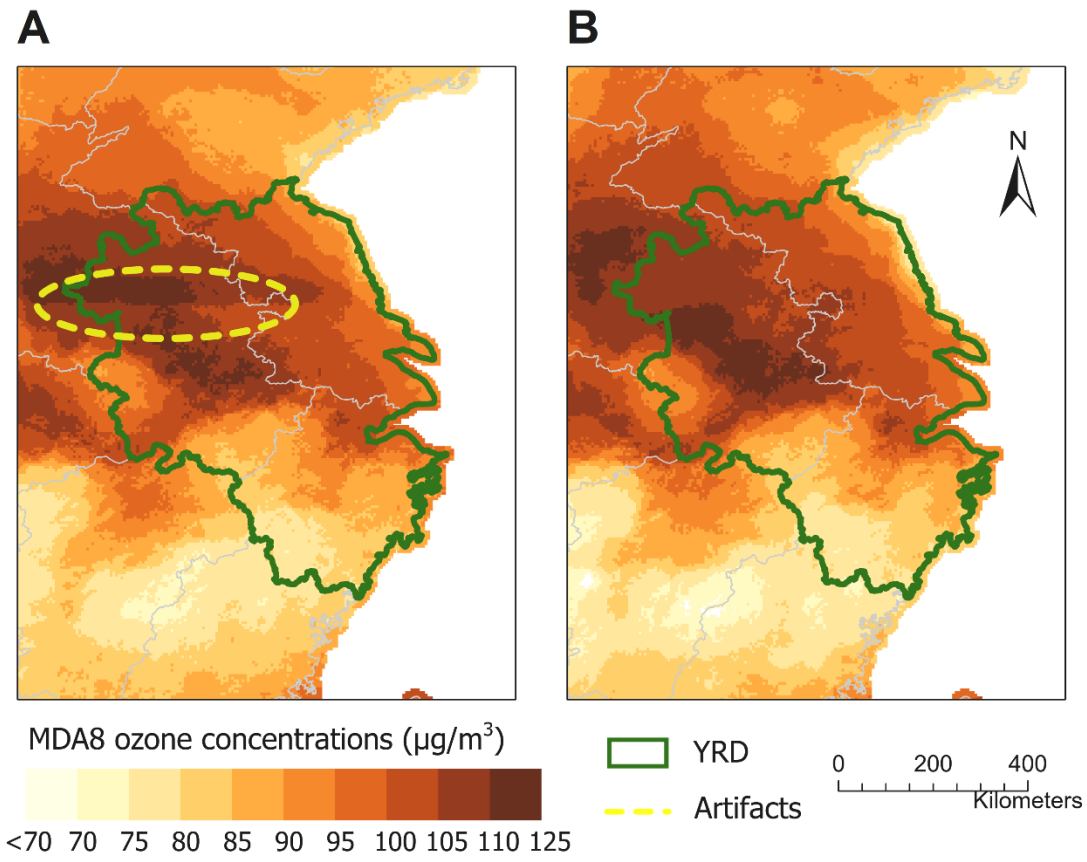

Fig. S1-4. An example of the spatial artifacts in the predicted monthly mean MDA8 ozone concentrations in the YRD (April 2019). Panel A was generated from the model with a priori ozone profile L22-L24; panel B was generated from the original model with OMI L24 retrieval. The green box represents YRD, and the yellow dashed line encircles an example of the spatial artifacts (the hard horizontal gap in predicted ozone concentrations). Abbreviations: MDA8, daily maximum 8-hour average; OMI, Ozone Monitoring Instrument; YRD, Yangtze River Delta.

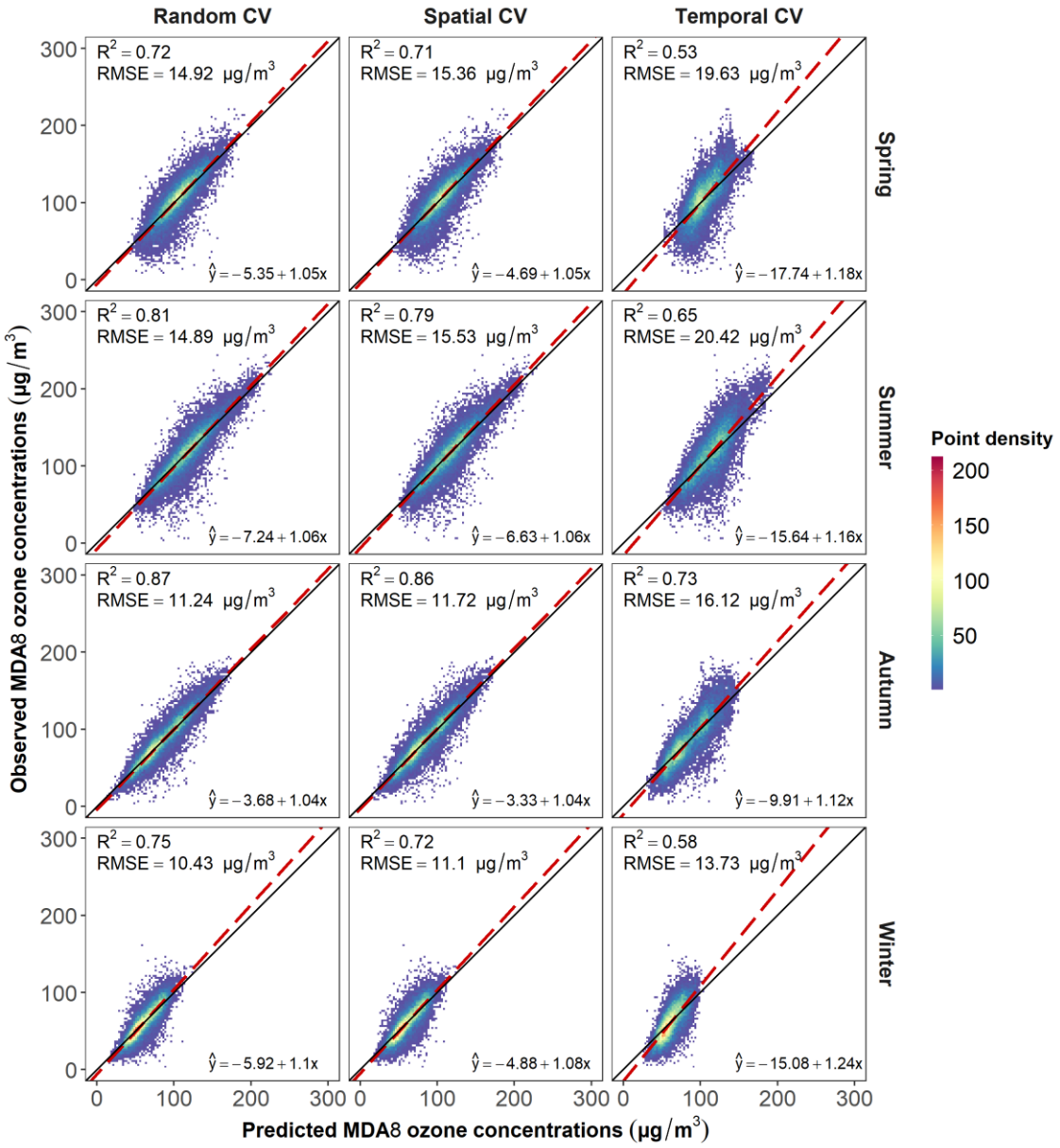

Fig.S1-5. Season-specific cross-validation results for the original model with OMI L24 retrieval. Left column: random CV; middle column: spatial CV; right column: temporal CV. Top row: spring (March-April-May); second row (from top to bottom): summer (June-July-August); third row: autumn (September, October, November); bottom row: winter (December-January-February). The functions on the bottom-right corners are the regression functions between the predicted and observed MDA8 ozone concentrations. Red dashed lines: the regression line between the predictions and observations; black solid lines: the x = y line; The color scale represents the density of the points. Abbreviations: MDA8, daily maximum 8-hour average; OMI, Ozone Monitoring Instrument.

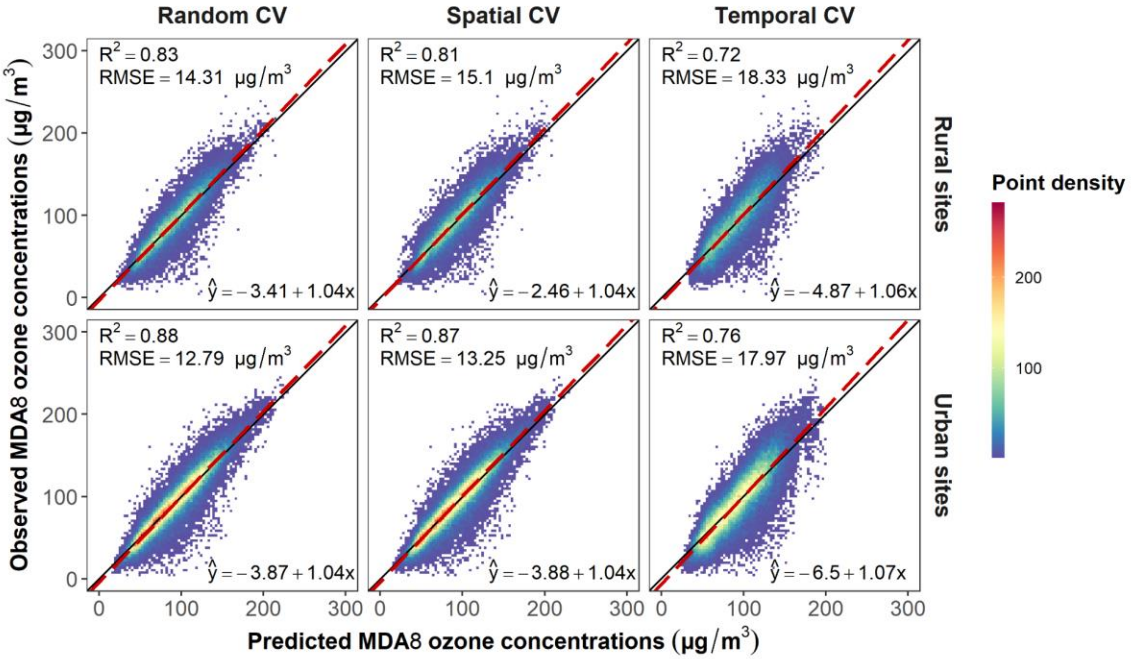

Fig.S1-6. Comparison of model performance in rural/urban areas using OMI L24 retrieval. Left column: random CV; middle column: spatial CV; right column: temporal CV. Upper row: model performance at rural CNEMC sites; Lower row: model performance in urban CNEMC sites. The functions on the bottom-right corners are the regression functions between the predicted and observed MDA8 ozone concentrations. Red dashed lines: the regression line between the predictions and observations; black solid lines: the x = y line; The color scale represents the density of the points. Abbreviations: CNEMC, China National Environmental Monitoring Centre; MDA8, daily maximum 8-hour average; OMI, Ozone Monitoring Instrument.

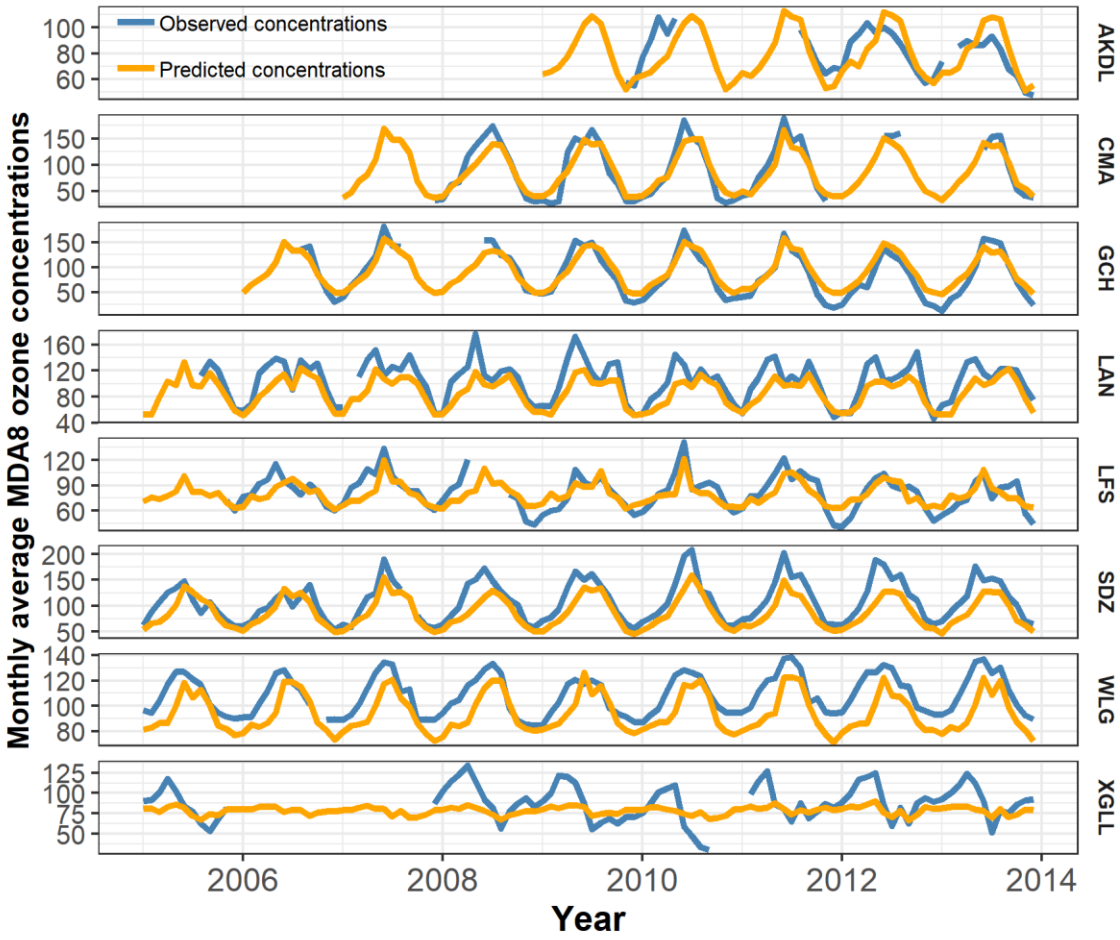

Fig.S1-7. Trend comparison between model predictions and the TOAR historical monitoring data (original model using OMI L24 retrieval). Each row represents a TOAR monitoring site. Blue lines: the observed monthly mean MDA8 ozone concentrations. Orange lines: the model predicted monthly MDA8 ozone concentrations. Abbreviations: MDA8, daily maximum 8-hour average; OMI, Ozone Monitoring Instrument. TOAR, Tropospheric Ozone Assessment Report.

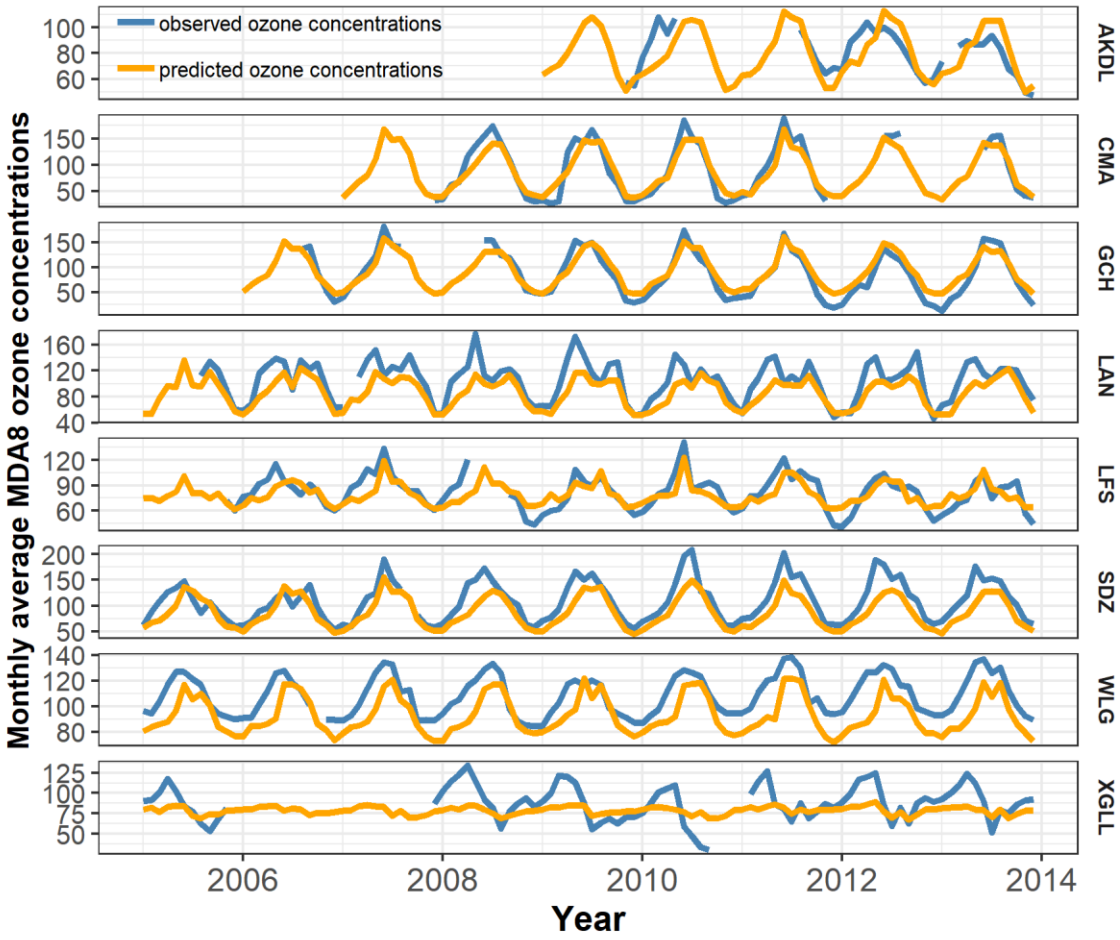

Fig.S1-8. Trend comparison between model predictions and the TOAR historical monitoring data (model trained with OMI L24 retrieval + MODIS FRP). Each row represents a TOAR monitoring site. Blue lines: the observed monthly mean MDA8 ozone concentrations. Orange lines: the model predicted monthly MDA8 ozone concentrations. Abbreviations: FRP, fire radiative power; MDA8, daily maximum 8-hour average; MODIS, Moderate Resolution Imaging Spectrometer; OMI, Ozone Monitoring Instrument. TOAR, Tropospheric Ozone Assessment Report.

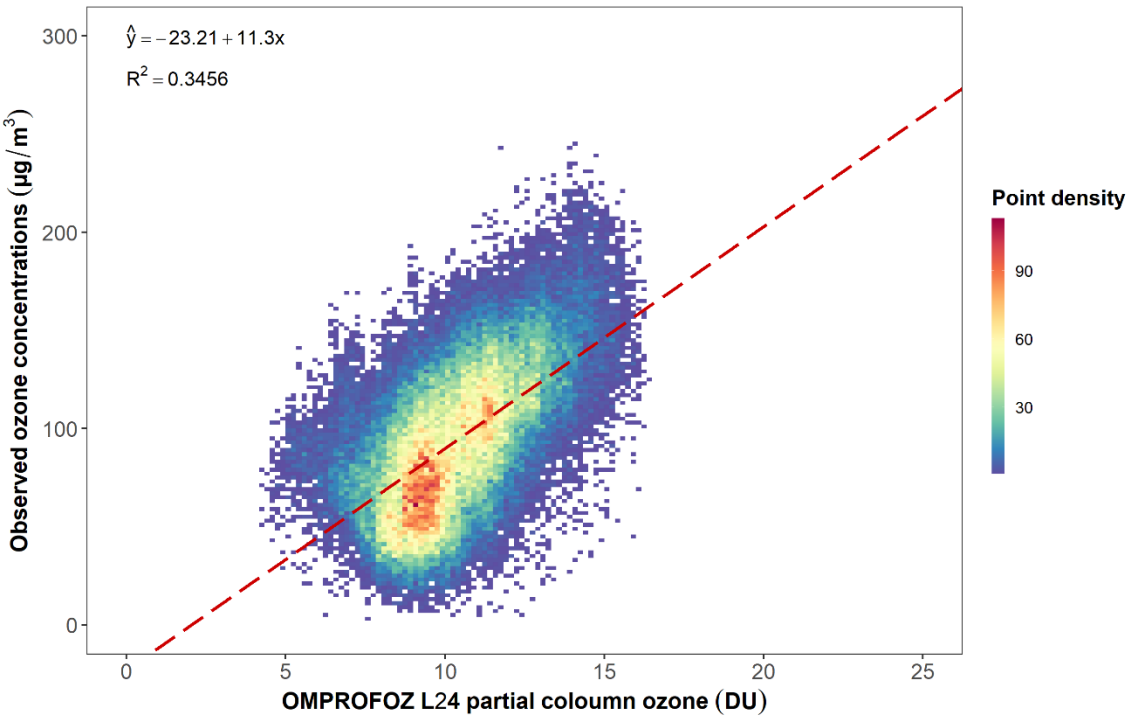

Fig.S1-9. Raw correlation between OMPROFOZ L24 partial column ozone and ground-level monitoring data. The function on the upper-right corner is the regression function between the OMPROFOZ L24 partial column ozone and the CNEMC surface MDA8 ozone concentrations. Red dashed line: the regression line as the regression function represents; black solid line: the x = y line; The color scale represents the density of the points. Abbreviations: CNEMC, China National Environmental Monitoring Centre; MDA8, daily maximum 8-hour average;

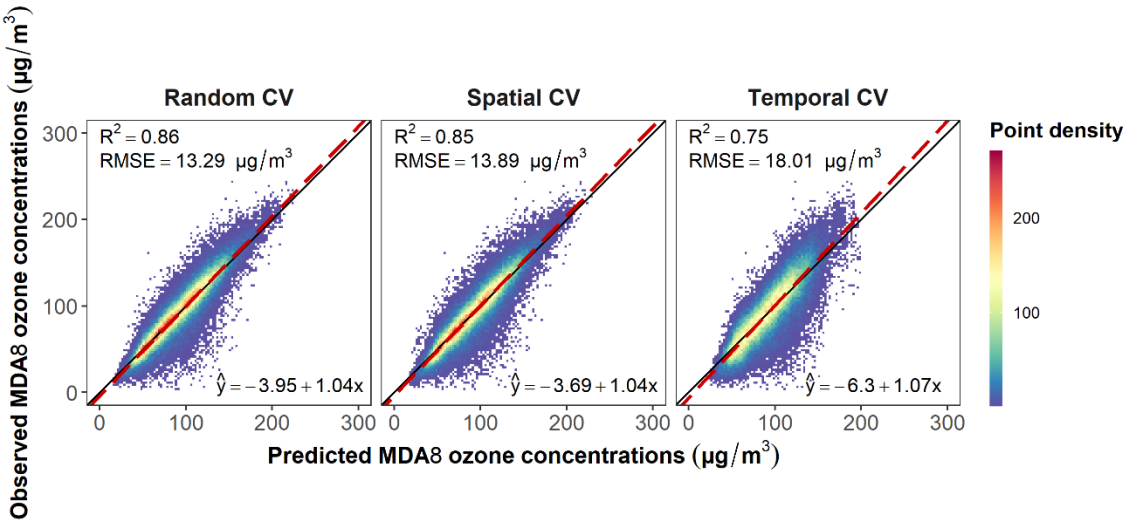

Fig.S1-10. model performance without the OMI L24 retrieval. Left panel: random CV; middle panel: spatial CV; right panel: temporal CV. The functions on the bottom-right corners are the regression functions between the predicted and observed monthly mean MDA8 ozone concentrations. Red dashed lines: the regression line between the predictions and observations; black solid lines: the x = y line; The color scale represents the density of the points. Abbreviations: CV, cross-validation; MDA8, daily maximum 8-hour average;

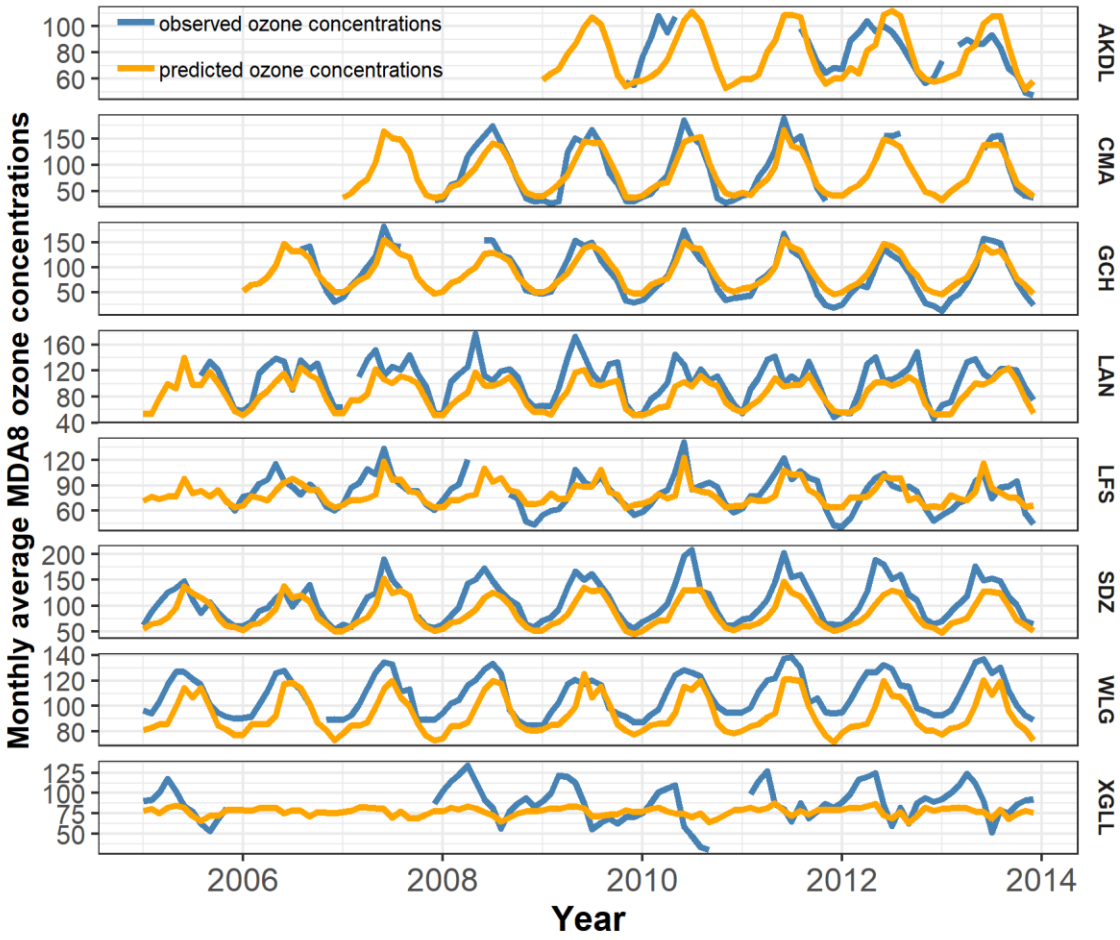

Fig.S1-11. Trend comparison between model predictions and the TOAR historical monitoring data (OMI-excluded model). Each row represents a TOAR monitoring site. Blue lines: the observed monthly mean MDA8 ozone concentrations. Orange lines: the model predicted monthly MDA8 ozone concentrations. Abbreviations: MDA8, daily maximum 8-hour average; OMI, Ozone Monitoring Instrument. TOAR, Tropospheric Ozone Assessment Report.

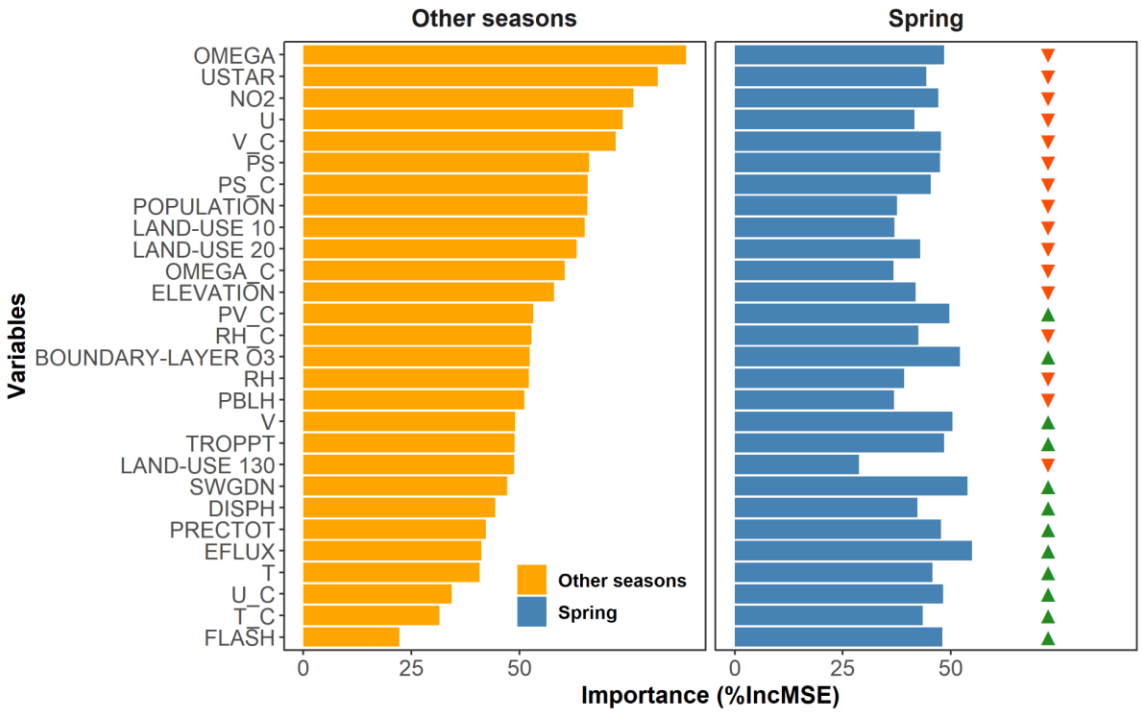

Fig. S1-12. The importance ranking of the input predictors. Orange bars in the left panel: the spring-excluded (all months except for March-April-May) model; blue bars in the right panel: the spring (March-April-May) model. The red downward arrows denoted that the relative ranking of the variable dropped in the spring model compared to other seasons; the blue upward arrows denoted that the relative ranking of a variable increased in spring. Variables' importance was generated with a permutation method.

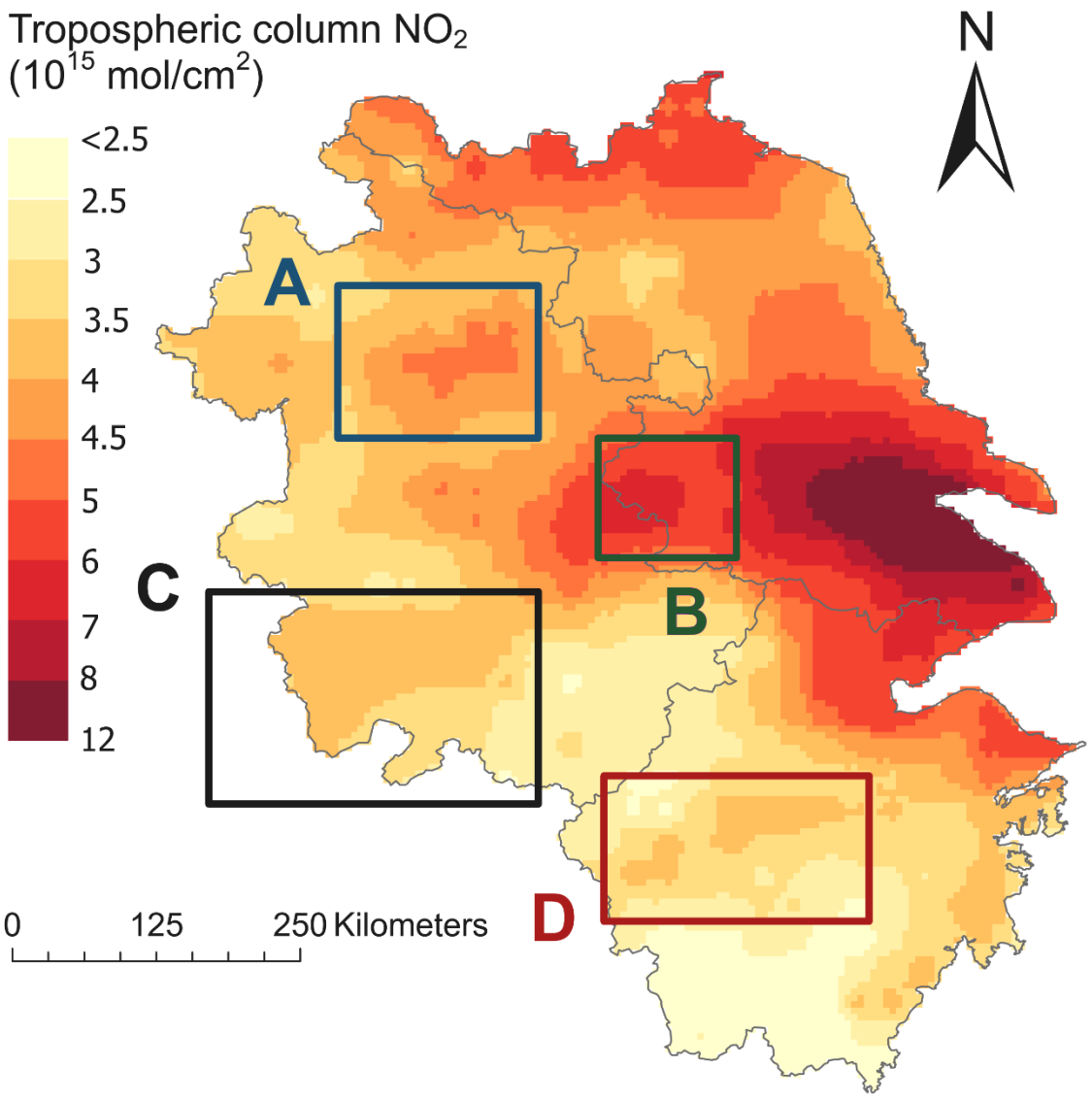

Fig.S1-13. The OMI tropospheric column NO_2 concentrations in the Yangtze River Delta region (August 2019, the marked regions were consistent to Fig. 5) The boxes represent some YRD cities and their surrounding area; A: Bengbu and Huainan City; B: Nanjing Metropolitan Area; C: Anqing and Jinhua City; D: Quzhou City. Abbreviations: MDA8, daily maximum 8-hour average.

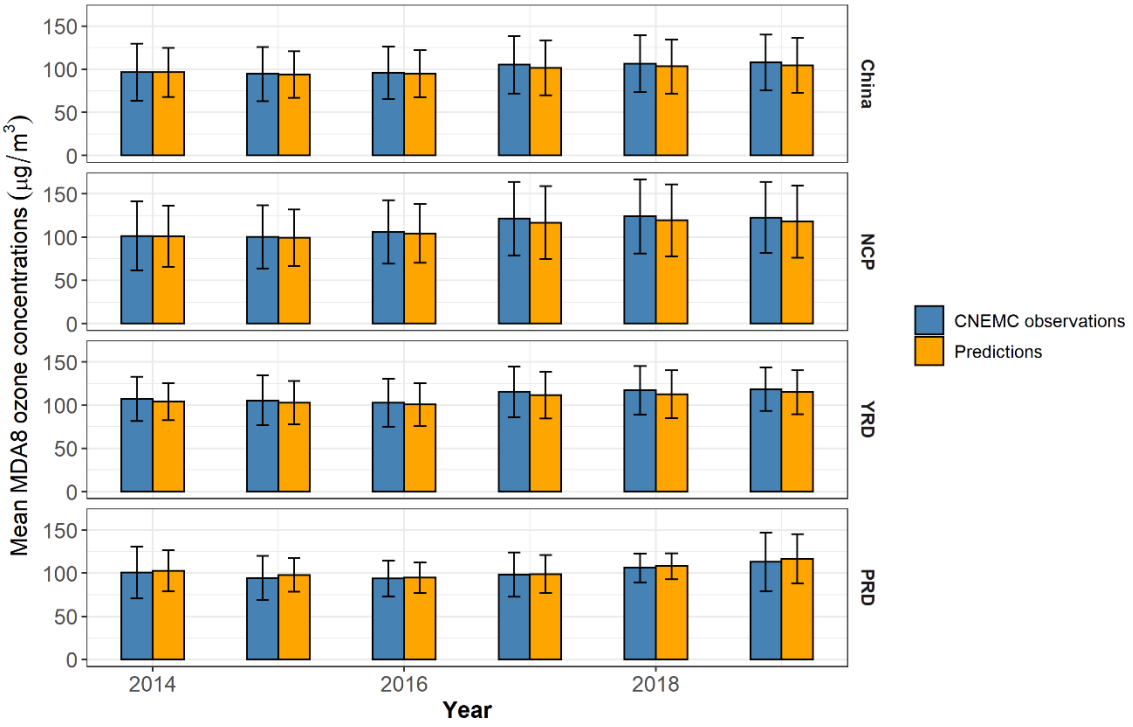

Fig. S1-14. The comparison of the mean ozone season (March-September) MDA8 ozone concentrations between our model predictions and the CNEMC monitoring data over 2014-2019. The blue columns on the left represent the CNEMC observations; the orange column on the right represents our model predictions. The height of the columns and the error bars represent the mean MDA8 ozone concentrations and the standard error. Abbreviations: CNEMC, China National Environmental Monitoring Centre; MDA8, daily maximum 8-hour average; NCP: the North China Plain; PRD: the Pearl River Delta; YRD: the Yangtze River Delta.

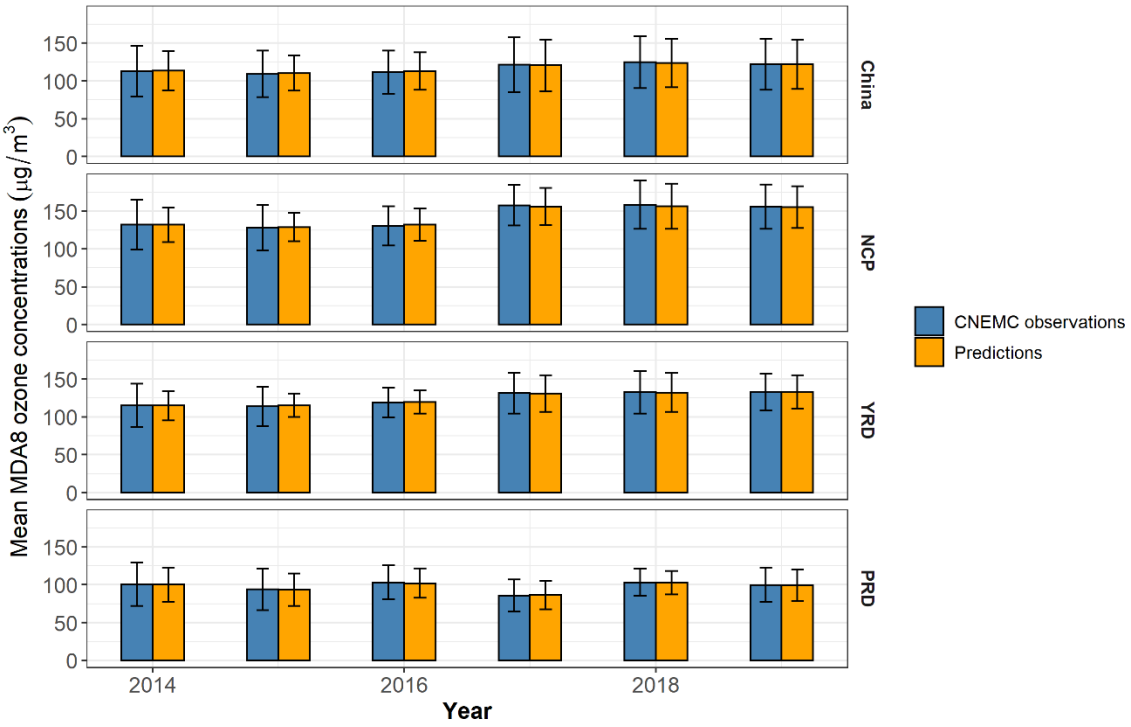

Fig. S1-15. The comparison of the summertime (June-July-August) mean MDA8 ozone concentrations between our model predictions and the CNEMC monitoring data over 2014-2019. The blue columns on the left represent the CNEMC observations; the orange column on the right represents our model predictions. The height of the columns and the error bars represent the mean MDA8 ozone concentrations and the standard error. Abbreviations: CNEMC, China National Environmental Monitoring Centre; MDA8, daily maximum 8-hour average; NCP: the North China Plain; PRD: the Pearl River Delta; YRD: the Yangtze River Delta.

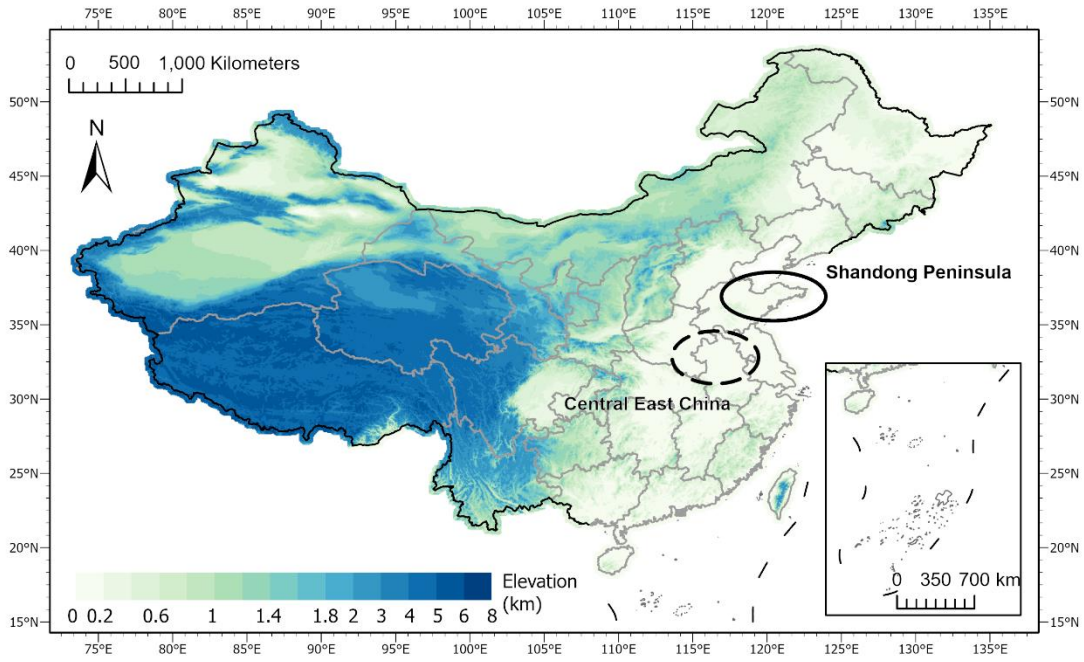

Fig. S1-16 Locations of the Shandong Peninsula and Central East China. The solid line encircles the Shandong Peninsula, while the dashed line encircles the Central East China area.

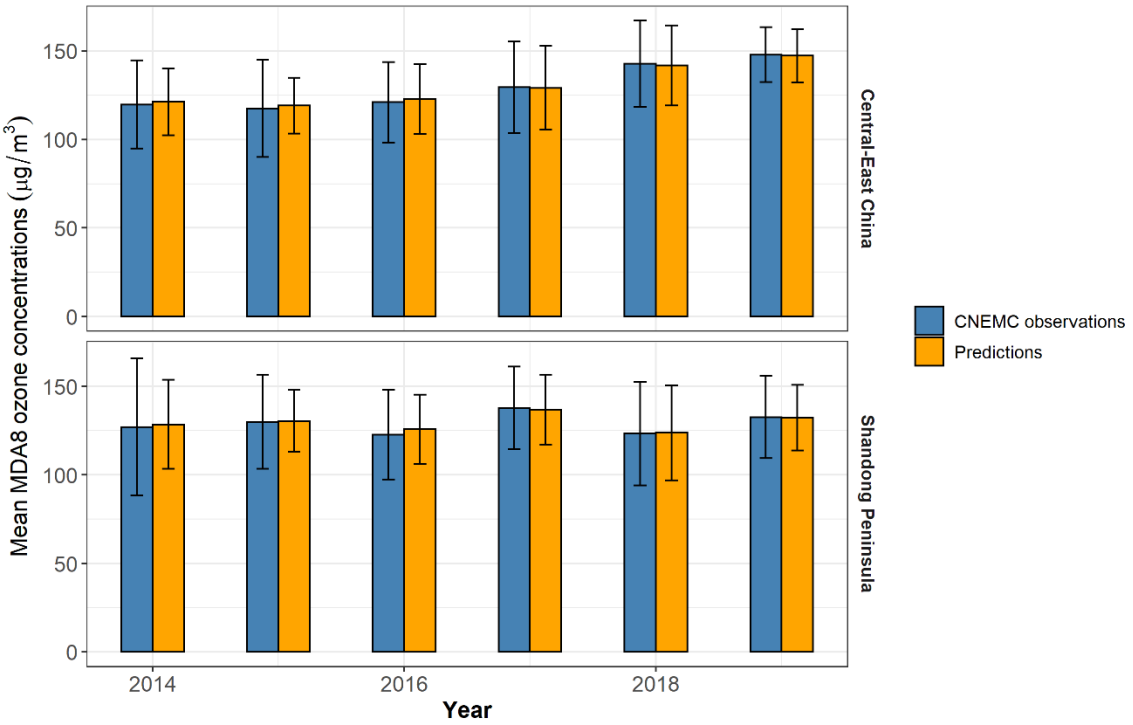

Fig. S1-17. The comparison of the summertime (June-July-August) mean MDA8 ozone concentrations between our model predictions and the CNEMC monitoring data over 2014-2019 for selected regions. Upper panel: Central-East China; Lower panel: the Shandong Peninsula. The blue columns on the left represent the CNEMC observations; the orange column on the right represents our model predictions. The height of the columns and the error bars represent the mean MDA8 ozone concentrations and the standard error. Abbreviations: CNEMC, China National Environmental Monitoring Centre; MDA8, daily maximum 8-hour average; NCP: the North China Plain; PRD: the Pearl River Delta; YRD: the Yangtze River Delta.

7. Appendix B. Supplemental materials for manuscript 3

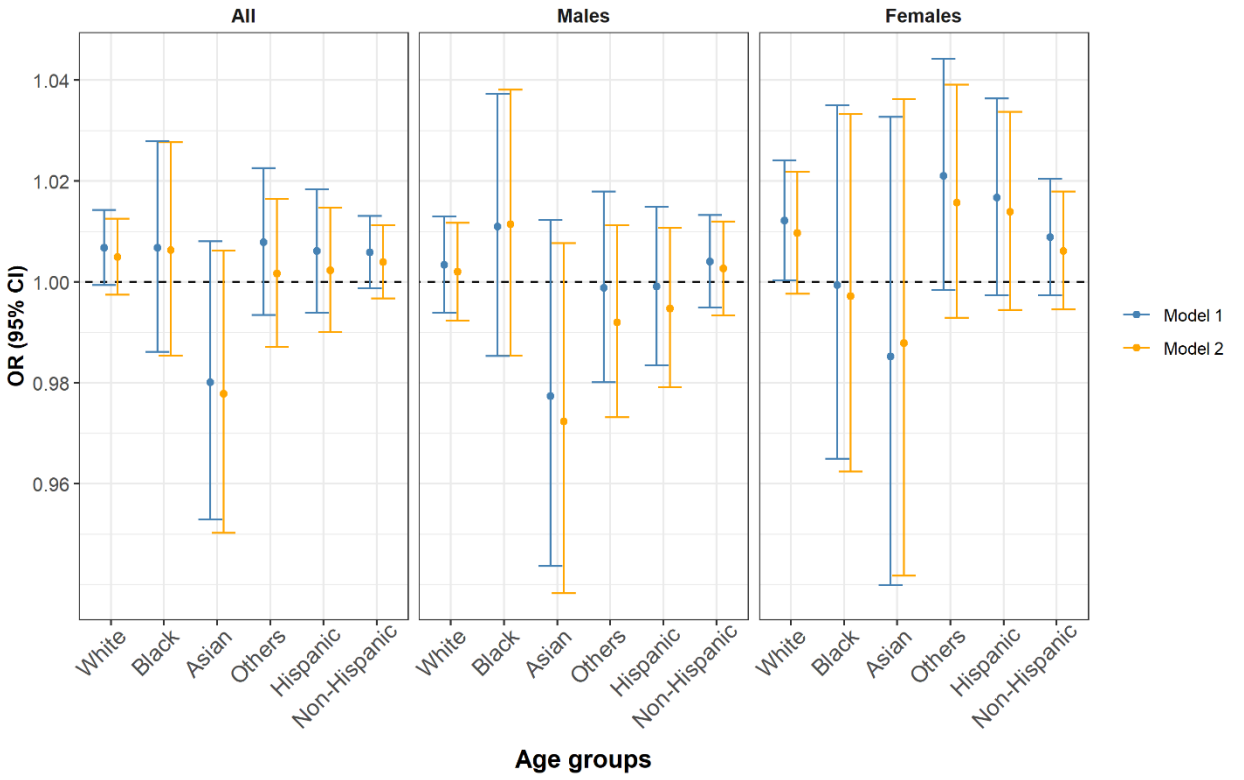

Fig. S2-1. The race- and ethnicity-stratified analysis for 48-h smoke $PM_{2.5}$. Model 1 only included 48-h smoke $PM_{2.5}$ and the covariates. Model 2 also adjusted for background $PM_{2.5}$. The ORs are for a 10 $\mu g/m^3$ increase in smoke $PM_{2.5}$.

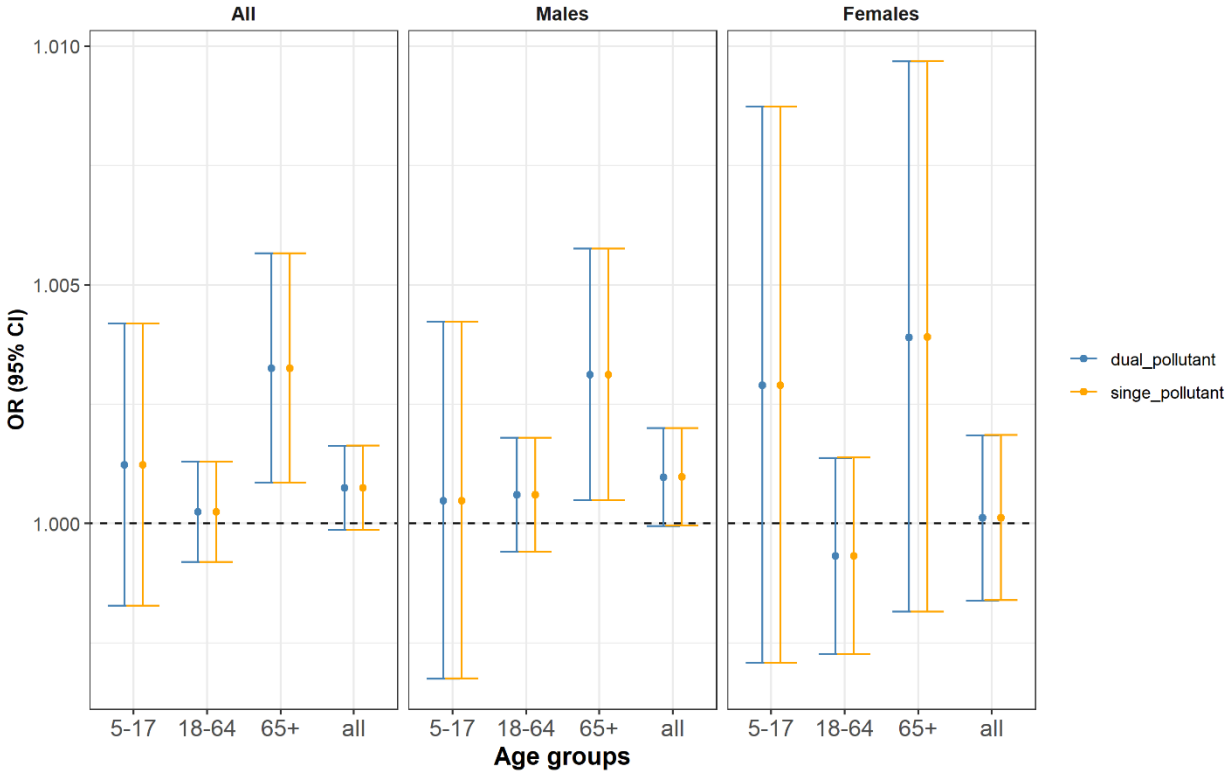

Fig. S2-2. The age- and sex-stratified analysis for cumulative FRP. Model 1 only included FRP and the covariates. Model 2 also adjusted for background $PM_{2.5}$. The ORs are for a 67.75 W increase in the cumulative FRP.

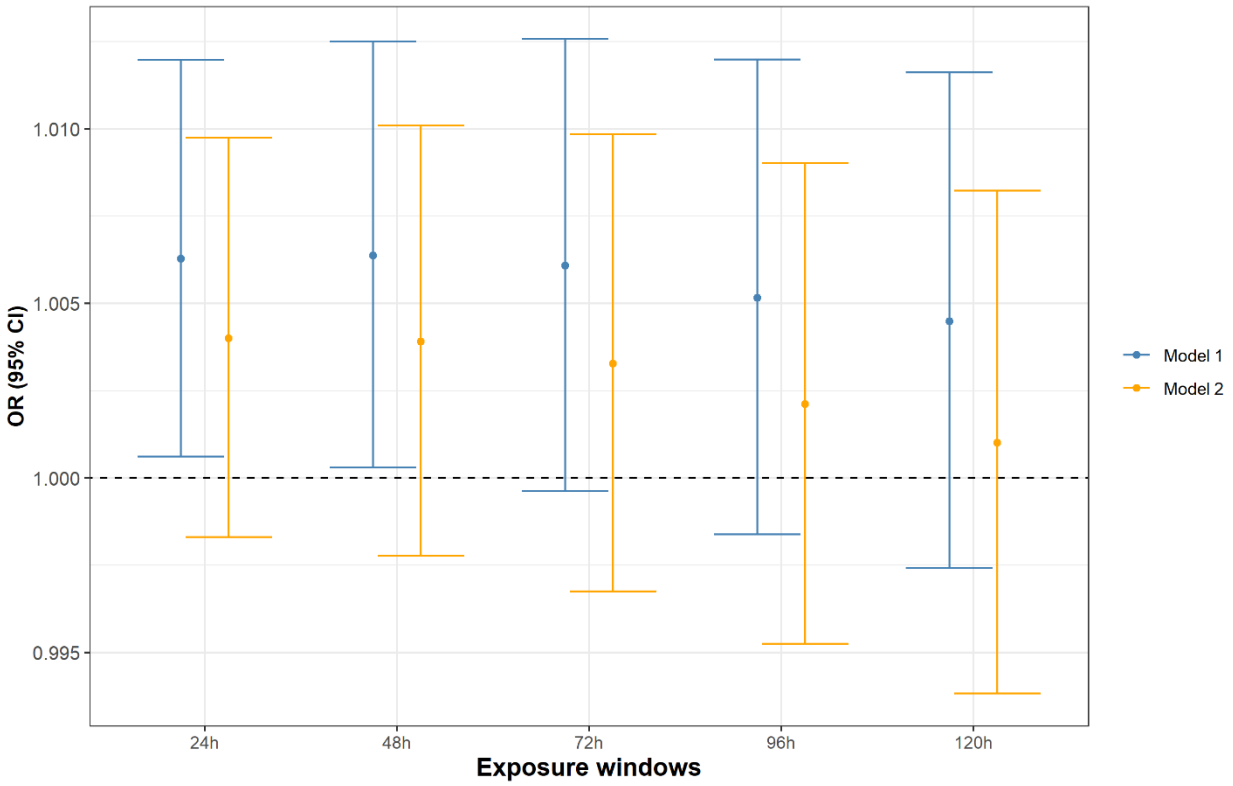

Fig. S2-3. The sensitivity analyses for different exposure time windows. Model 1 only included 48-h smoke $PM_{2.5}$ and the covariates. Model 2 also adjusted for background $PM_{2.5}$. The ORs are for a 10 $\mu g/m^3$ increase in smoke $PM_{2.5}$.

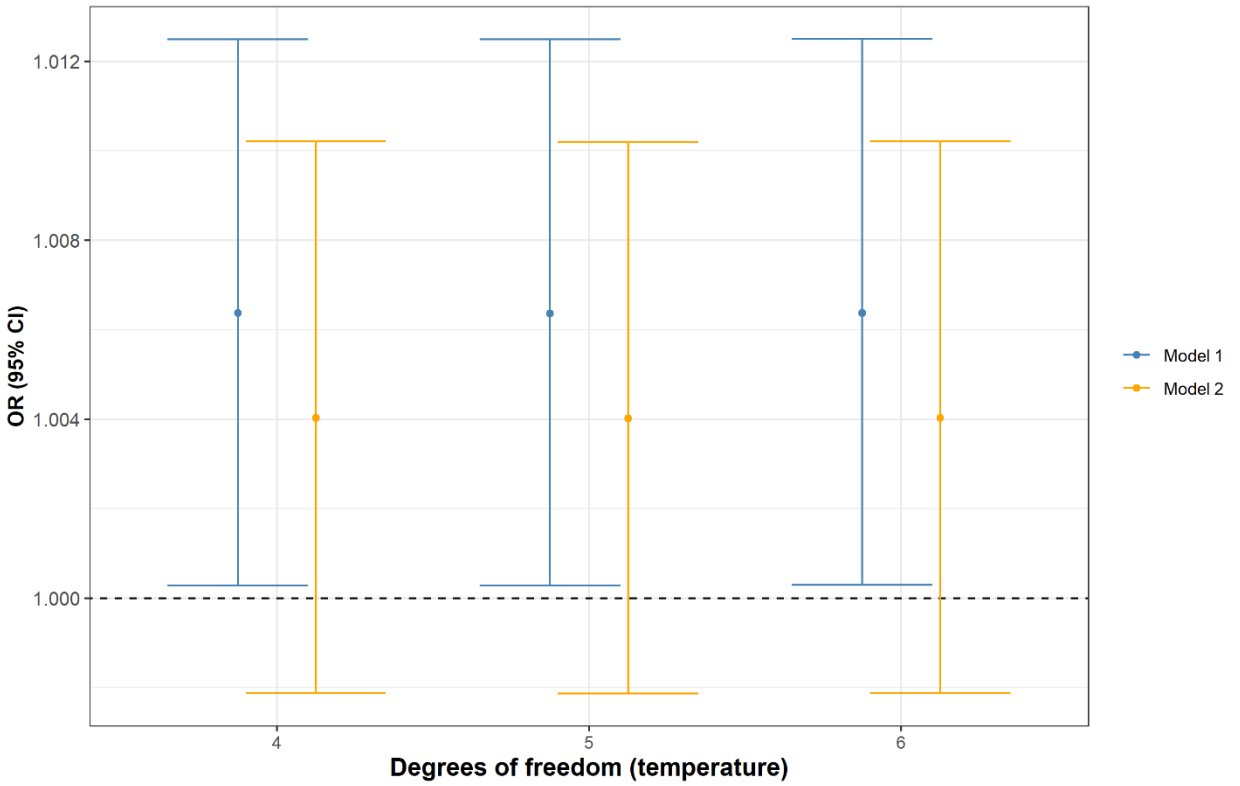

Fig. S2-4. The sensitivity analyses for different degrees of freedom of temperature. Model 1 only included 48-h smoke $PM_{2.5}$ and the covariates. Model 2 also adjusted for background $PM_{2.5}$. The ORs are for a 10 μg/m^3 increase in smoke $PM_{2.5}$.

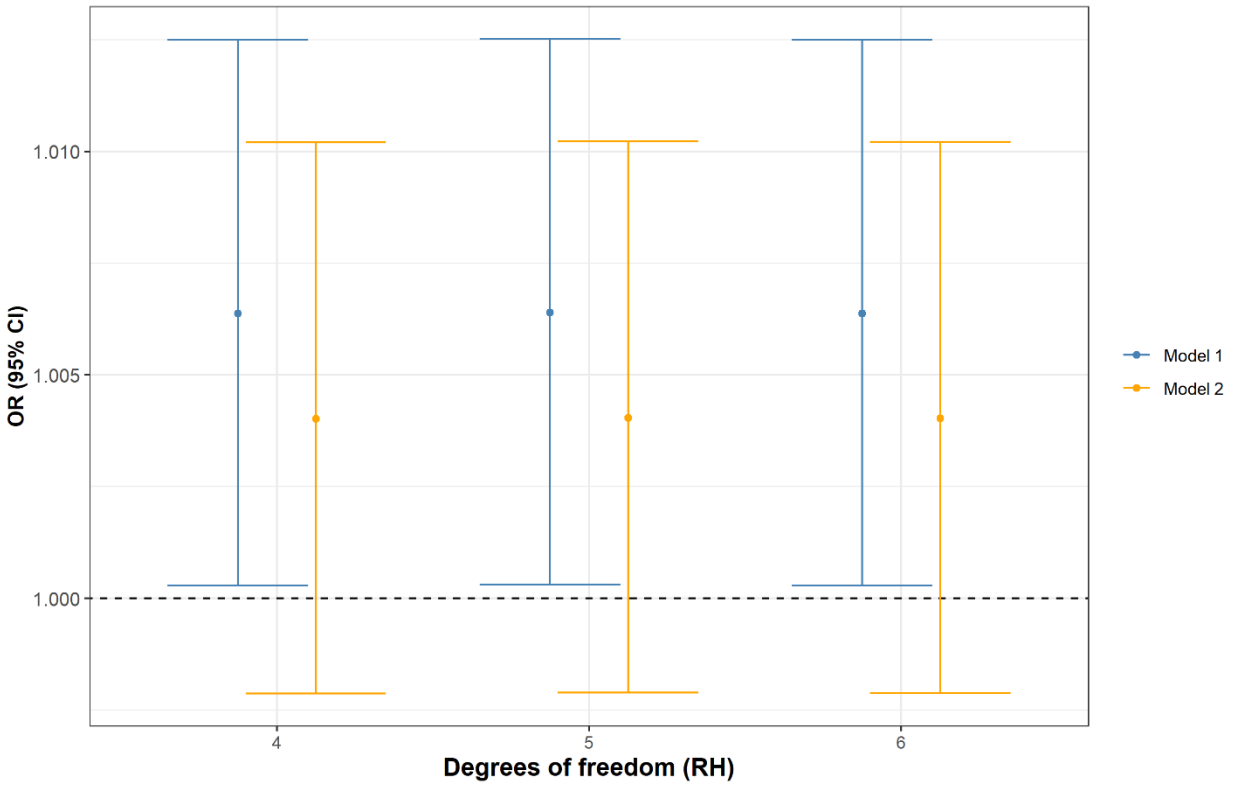

Fig. S2-5. The sensitivity analyses for different degrees of freedom of RH. Model 1 only included 48-h smoke $PM_{2.5}$ and the covariates. Model 2 also adjusted for background $PM_{2.5}$. The ORs are for a 10 $\mu g/m^3$ increase in smoke $PM_{2.5}$.